Co-assembled DNA-protein polymer bottlebrushes

Main-chain stiffening & liquid crystallinity

Ingeborg Maria Storm

Thesis committee

Promotors
Emeritus Prof. Dr M. A. Cohen Stuart
Professor of Physical Chemistry and Colloid Science
Wageningen University

Prof. Dr F. A. M. Leermakers
Personal chair at Physical Chemistry and Soft Matter
Wageningen University

Co-Promotor
Dr R. de Vries
Associate Professor of Physical Chemistry and Soft Matter
Wageningen University

Other members
Emeritus Prof. Dr J. H. S. G. M. de Jong, Wageningen University
Dr S. J. T. van Noort, Leiden University, The Netherlands
Dr O. V. Borisov, University of Pau and Pays de l'Adour, France
Emeritus Prof. Dr G. ten Brinke, University of Groningen, The Netherlands

This research was conducted under the auspices of the Graduate School VLAG (Advanced studies in Food Technology, Agrobiotechnology, Nutrition and Health Sciences).

Co-assembled DNA-protein polymer bottlebrushes

Main-chain stiffening & liquid crystallinity

Ingeborg Maria Storm

Thesis
submitted in fulfillment of the requirements for the degree of doctor
at Wageningen University
by the authority of the Rector Magnificus
Prof. Dr A.P.J. Mol,
in the presence of the
Thesis Committee appointed by the Academic Board
to be defended in public
on Friday 13 May 2016
at 1.30 p.m. in the Aula.

Ingeborg Maria Storm
Co-assembled DNA-protein polymer bottlebrushes: Main-chain stiffening & liquid crystallinity
161 pages.

PhD thesis, Wageningen University, Wageningen, NL (2016)
With references, with summaries in English and Dutch

ISBN: 978-94-6257-746-6

Contents

1 General Introduction

1.1 Bottlebrush Molecules

Molecular bottlebrushes are structures consisting of a backbone molecule onto which side chains are chemically linked.[1–3] Bottlebrushes play an important role in nature. The aggrecan bottlebrush, for example, is part of the synovial fluid acting as a joint lubricant in the cartilage.[4–7] The lubrication properties of aggrecan are based on its ability to hold on to water even under high pressure load, due to its high number of charges on the side chains. An atomic force microscopy (AFM) image of an aggrecan molecule is shown in Figure 1.1(a). The side chains, which are in fact bottlebrushes themselves, follow the contour of the backbone. Neurofilaments, which ensure the mechanical strength of neurons, are another example of bottlebrushes. They are constructed from three types of proteins of different molecular weight. These subunits form a macromolecular bottlebrush with protruding side chains, see Figure 1.1(b).[8,9]

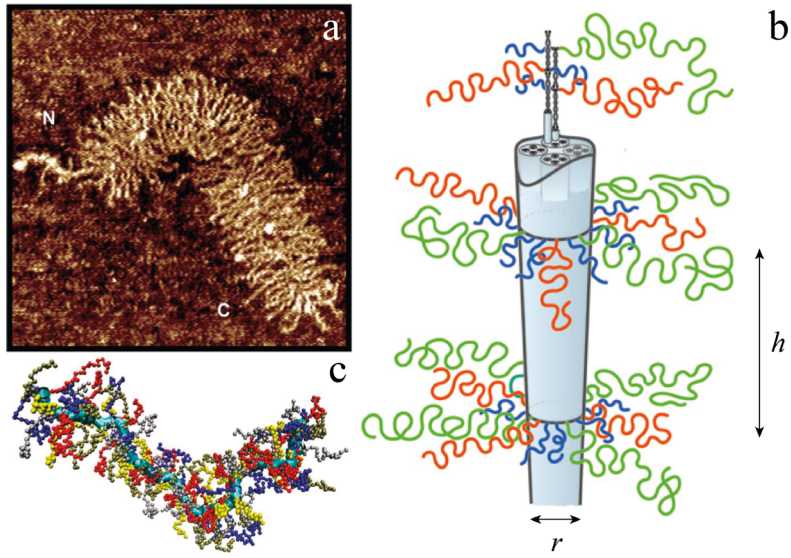

Figure 1.1: *An aggrecan bottlebrush molecule (a); a schematic image of a neurofilament, where h is the measure for the distance between side chains and r is the backbone diameter (b); a snapshot of a bottlebrush from a Monte Carlo simulation (c). These images were reproduced with permission from references.*[10–12]

In the previous century Fredrickson proposed a theory about the stiffness of bottlebrush molecules. He suggested that attaching side chains

to a flexible polymer (backbone) would induce the so-called main-chain stiffening effect.[13] Due to this effect the bottlebrush molecule would behave as a semi-flexible polymer with an increased aspect ratio, l_p/D, where l_p is the persistence length and D the diameter of the brush. The persistence length is defined as the length along the backbone for which the chain can be seen as a rod, while at larger length scales it behaves as a coil. This increased aspect ratio would also make it easier for the system to show liquid crystalline behaviour. In a liquid crystalline phase the molecules (locally) line up in a given direction (director). This alignment occurs when the bottlebrush concentration is high enough, which will be discussed in more detail later. Fredricksons predictions were followed by many experiments,[14–20] simulations[21–27] and theoretical research about bottlebrushes.[28–34] A snapshot from a bottlebrush in a Monte Carlo simulation is shown in Figure 1.1(c). Invariably these works are targeted at better understanding of the physical and biological behaviour of molecular bottlebrushes but it is fair to say that a full understanding has not been reached. Especially the liquid crystalline behaviour of bottlebrushes is not very well understood. From the theory it seems very easy to make an anisotropically aligned bottlebrush system but the absence of good model systems suggests that there have to be some unforeseen problems. The aim of this thesis is to focus specifically on the reason why bottlebrushes experience difficulty in showing liquid crystalline ordering. This thesis contributes to the field by introducing a new supramolecular bottlebrush system which does show liquid crystallinity. We characterised the system, analysed and modeled some of its structural properties.

Despite the above mentioned works, there are very few experimental reports showing the expected liquid crystalline behaviour of bottlebrush molecules.[14,16] Apparently, it is not so easy to develop a molecular bottlebrush architecture which shows macroscopic liquid crystallinity. The fact is that most of the known molecular bottlebrushes behave as flexible macromolecules retaining the coil shape up to the melt state (i.e. far beyond the overlap concentration). Why this happens is virtually unknown. A theoretical onset to clarify this issue has been given by Feuz *et al.*[29] They modelled molecular bottlebrushes by considering the one-dimensional brush, i.e. a homogeneously curved backbone without molecular details, a phantom chain, onto which at regular intervals linear side chains are grafted such that the side chains are laterally interacting and therefore strongly stretched in the radial direction. They showed that attaching side chains to a backbone, in such a way that the distance between the side chains gradually decreases, will initially result in a decrease of the aspect

ratio, l_p/D, because the persistence length is not increasing as fast as the thickness of the brush layer. Nevertheless, at sufficiently high grafting densities and long enough chains, the growth of l_p is predicted to exceed that of D so that again the classical trend of growth of l_p/D is recovered. The theoretical predictions have been carried out in highly idealized situations which are hard to realize experimentally. Therefore, we argue that perhaps the best way to contribute to this discussion is to introduce new routes to form molecular bottlebrushes.

1.2 Self-Assembly and Co-Assembly

In this thesis we use a DNA template to physically bind protein polymers and form a so-called bottlebrush architecture. As is well known, DNA is a negatively charged polyelectrolyte. These negative charges can be used to bind positively charged polymers. In this thesis, we therefore use protein polymers with a positively charged tail. Simply mixing negatively charged DNA with positively charged protein polymers results in the assembly of our DNA-bottlebrushes. For this reason we will first elaborate on self- and co-assembly phenomena.

1.2.1 Molecular Forces that Drive Self-Assembly

On the molecular scale there can be many types of interactions, both between different molecules as well as within the same molecule. For co- and self-assembling behaviour, hydrogen bonds, electrostatic and hydrophobic interactions, are important; they lead to many different types of systems like hydrogels,[35,36] coacervate micelles,[37–39] conjugated polymers,[40] fibers[41,42] and (artificial) viruses.[43–46]

The term "co-assembly" is used when different components bind together to form a larger structure. One famous example is double stranded DNA (dsDNA) which can be seen as a self-assembled molecule consisting of two complementary strands. These single stranded DNA (ssDNA) molecules consist of four types of subunits, the nucleotides. These nucleotides are adenine (A), cytosine (C), guanine (G) and thymine (T). The interaction between two single strands is called base pairing where complementary base pairs interact with one another through hydrogen bonds.[47] The hydrogen bonding interactions are restricted in such a way that adenine only binds to thymine and cytosine only interacts with guanine. Hydrogen bonding is a type of interaction that occurs between a hydrogen atom bound to an electronegative atom of one group/molecule

and an electronegative atom of a second group.[47] The electronegative atoms are oxygen, nitrogen and fluorine.

Electrostatic interactions are based on the attraction between oppositely charged groups or repulsion when the charged groups have the same sign. These charges can often be manipulated by *p*H, and by changing the ionic strength of the solution. Increasing the ionic strength of the solution basically means that, at given *p*H, more charged ions are present in the solution which 'screen' the interaction between the charged molecules of, for example, an assembled system.[48] These charged groups, in that case, simply do not feel each others presence so strongly and eventually attractive electrostatic bonds might be disrupted. On the other hand, a low ionic strength of the solution makes the electrostatic bonding between two oppositely charged molecules a lot stronger since there are not so many ions present that can weaken the interaction. Electrostatic interactions are one of the major driving forces for co-assembly and they are relevant interactions for the DNA-bottlebrush system described in this thesis. In **chapters 2** and **3** a DNA-bottlebrush system will be discussed where the interaction between the backbone molecule (DNA) and the side chains (so-called C_4K_{12} proteins) is predominantly electrostatic. The negative charges of the DNA phosphate groups interact with the 12 positively charged lysines of the C_4K_{12} protein.

In addition to the hydrogen bonds and electrostatic interactions there is another non-covalent interaction that is important for co-assembling behaviour, namely hydrophobic interaction.[48] In proteins, hydrophobic interactions occur because non-polar amino acids tend to favour each others presence above contact with water or with other polar molecules. In **chapter 5** we introduce a protein polymer ($Sso7dC_8$) that binds specifically to DNA by means of electrostatic and hydrophobic interactions as well as hydrogen bonds.[49] Sso7d is a small protein that binds to the minor groove of DNA and thereby significantly widens this minor groove.

1.3 Liquid Crystals

Our finding that the co-assembled DNA bottlebrush system with C_4K_{12} side chains forms anisotropic phases has shaped this thesis in many ways. In this section we first briefly explain the concept of liquid crystals, and we discuss two methods to get information about these liquid crystals.

Large numbers of atoms, molecules or particles that have fixed positions in a (periodic) lattice can be denoted as a crystal. These particles

have long ranged positional and orientational order.[50] The particles or molecules in a liquid, on the other hand, have no predetermined position and can have any orientation with respect to each other.

As depicted in Figure 1.2, liquid crystal phases are somewhere in-between a liquid and a crystal: the particles have a common orientation, but do not have a fixed position in one or more dimensions. There are several of these phases; by changing the concentration of the particles and thereby reducing the available volume per particle, one can obtain different liquid crystalline phases, i.e. nematic, hexagonal or smectic, see Figure 1.2. The nematic phase can be considered as one of the simplest liquid crystalline phases.

An easy method to visualize liquid crystalline phases is to use a crossed polarizer set-up. In short, this set-up works as follows: the first polarizer, polarizes the light in the x direction. The second polarizer, which is turned 90 degrees with respect to the first one, only allows light with a polarization in the y-direction to pass. In such a set-up, no light from the light source will reach the detector when the sample is isotropic. However, when a liquid crystalline sample is placed between the two polarizers, the angle of polarization will change because the light effectively encounters different refractive indices in different directions. Therefore, the polarized light will have a non-zero component in the y-direction, which will pass through the second polarizer and reach the detector. The optical rotation also depends on the wavelength of the light. When white light is passed through a liquid crystalline sample, complex interference results in a colourful picture, see Figure 1.3.

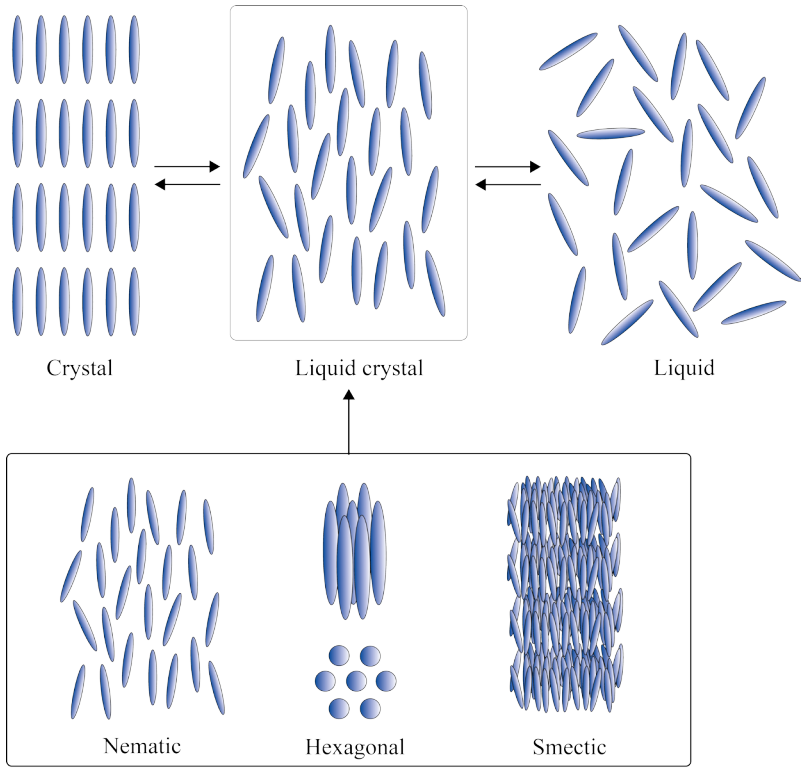

Figure 1.2: *Top row from left to right: particles ordered in a crystal lattice, particles having liquid crystalline ordering and randomly oriented particles, i.e. a liquid. Bottom row: nematic, hexagonal and smectic phase.*

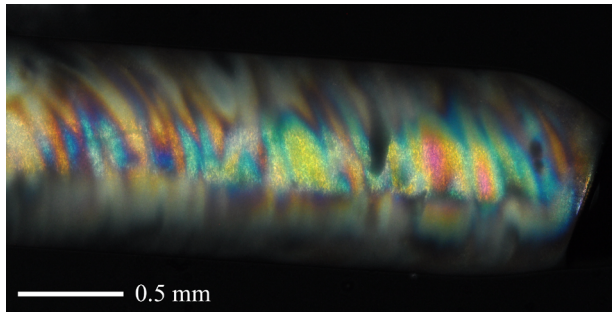

Figure 1.3: *Image of a birefringent liquid crystal between crossed-polarizers. The sample is a DNA-bottlebrush coated with C_4K_{12} protein polymers at stoichiometric amounts.*

Another method to analyse liquid crystals is by using small angle X-ray scattering (SAXS). This method is especially useful since it gives structural information in the size range 1-100 nm. The incoming X-rays interact with the electrons of the sample. The constructive interference of waves coming from the liquid crystal result in a scattering pattern that is characteristic for the liquid crystalline phase. Scattering data are often represented in terms of the scattering intensity, I, as a function of the scattering vector $\vec{q}$. This scattering vector $\vec{q}$ is obtained from

$$\vec{q} = \vec{k} - \vec{k}_0 \tag{1.1}$$

where $\vec{k}_0$ is the incoming wave and $\vec{k}$ the scattered wave. When both $\vec{k}_0$ and $\vec{k}$ equals $2\pi/\vec{\lambda}$, where λ is the wavelength of the X-rays, the scattering vector $\vec{q}$ corresponds to

$$q = \frac{4\pi}{\lambda}\sin\frac{\theta}{2} \tag{1.2}$$

where θ is the scattering angle. A wave vector q probes distances d in the sample according to Bragg's law:

$$d = \frac{n2\pi}{q} \tag{1.3}$$

This can be reformulated to:

$$n\lambda = 2d\sin\frac{\theta}{2} \tag{1.4}$$

where n is an integer number. The constructive interference of the outcoming scattering waves gives rise to characteristic scattering peaks that relate to a specific liquid crystalline phase.[51,52]

1.4 Self Consistent Field Theory

The results of experimental research are not always easy to interpret because quite often systems are also affected by less than ideal parameters like purity, polydispersity or inadvertent admixtures. Computer calculations or simulations might contribute to the understanding of the experimental system simply because they are easier to control.

Ideally, we would prefer carrying out molecular dynamics (MD) simulations to investigate the behaviour of our self-assembled DNA-bottlebrushes. The bottlebrush simulation could be used to predict the behaviour of our DNA-bottlebrushes under specific conditions. By using

MD simulations, information could be obtained about, for example, properties like the persistence length l_p and the brush diameter D. However, calculating bottlebrushes with the MD simulation requires much calculation time. Nevertheless, for chemically grafted brushes this has been done already.[21–27] For co-assembled bottlebrushes, there are additional "degrees of freedom" (complications). For example, in the modeling it must be taken into account that the brush chains have the freedom to move along the DNA template. They can even desorb from and readsorb onto the DNA chain from time to time. That is probably one of the reasons why simulations on co-assembled bottlebrushes have, to our knowledge, not yet been performed. A more computationally efficient way of predicting the behaviour of bottlebrush molecules is by using a different method, the so-called self consistent field (SCF) theory.

The SCF theory uses a field of potentials to calculate the free energy of the bottlebrush macromolecule. We tried to visualize the SCF calculations by the schematic image in figure 1.4. In panel 1.4(a) the backbone chain is visualized from the side. One of the side chains which we call the 'probe' chain, is coloured red. In panel 1.4(b) we see the bottlebrush along the backbone. Now the side chains point out radially. Again the probe chain is labelled in red and the other side chains are blue. In panel 1.4(c) we have the system that is treated by SCF. In this view, only the probe chain remains and the blue chains are replaced by a potential field. The strength of the field is given by the intensity of the blue colour. The intensity is highest near the backbone and is zero far from the backbone. In the SCF approach the probe chain feels the field and adjusts its conformations accordingly. This in turn has an effect on the potentials. In the method the fields are adjusted iteratively until the probe conformations and the field are consistent with each other. When that is the case, the structure corresponds to equilibrium, and we can determine properties such as the thickness of the brush. The persistence length is found by imposing a curvature onto the backbone and analyse the free energy increase due to this curvature. By using this method we are able to both consider chemically grafted as well as co-assembled bottlebrushes.

1.5 Recombinant Protein Polymers

Our DNA-bottlebrushes consist of a DNA backbone; as side chains we use so-called protein polymers that attach in a physical way (so non-covalent) to the backbone molecule. These protein polymers will be briefly introduced

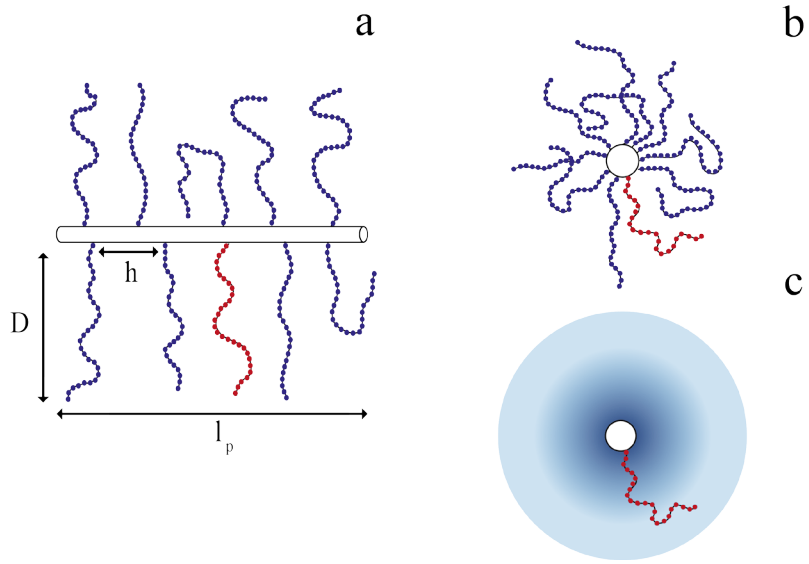

Figure 1.4: *Self consistent field (SCF) representation of a bottlebrush molecule. The bottlebrush (a) shows the brush diameter (D), persistence length (l_p) and average grafting distance (h). A topview of the bottlebrush molecule (b) and the bottlebrush in a self consistent field (c). The red side chain represents the chain that experiences the SCF field (blue).*

in this section.

The field of polymer synthesis has always been struggling to obtain better control over the polymer structure and properties. One of the biggest challenges is regulation of the length and the sequence of the polymer. If one would be able to fully define the sequence of a polymer, the properties of the polymer would be precisely controllable. Over the years more sophisticated methods have been developed which have resulted in very well controlled polymer systems that are fairly monodisperse. However, biopolymers like DNA and proteins are still much better defined than the synthetic ones because each monomer added is precisely controlled according to a precise code.

Developments in molecular biology resulted in a new type of polymers. These so-called "protein polymers" do not face some of the disadvantages of the synthetic polymers. To start with, the protein polymers are built up from amino acids using the genetic code, that is, reading the sequence from DNA. This ensures perfect control over the sequence of the protein polymer and, additionally, this also guarantees an entirely monodisperse batch of

protein polymers.

Evolution and natural selection have already created and optimized many proteins that have interesting properties. With the developments in the field of genetic engineering these proteins can not only be slightly modified, even an entirely new protein can be made by constructing a completely new DNA code, partly using motifs taken from natural proteins. Ferrari and Tirrell pioneered the field of "protein polymers" with the design of silk-like proteins.[53–56] Other well known protein polymers that are used extensively are the elastin and collagen like constructs.[57–61]

After the gene for a newly designed protein polymer has been established it has to be incorporated into a host cell that will produce the protein. In our studies this host is a yeast, *Pichia Pastoris*, that can produce the protein polymer by means of a fermentation process.[58]

1.6 Outline of this Thesis

In this thesis we discuss co-assembled molecular bottlebrushes consisting of a DNA backbone and protein polymer side chains. The first theory for bottlebrushes predicts a main-chain stiffening effect and an accompanying liquid crystalline behaviour.[13] The focus of this thesis is to explain why liquid crystalline bottlebrush systems are difficult to obtain. We will relate self consistent field calculations to our experimental results to investigate the behaviour of our DNA-bottlebrushes.

Many simulations and calculations showed that for molecular bottlebrushes to form liquid crystals, side chains with a high degree of polymerization, N, and a high grafting distance, $\sigma = 1/h$, are required (with h the distance between two grafts along the backbone).[21,24,29,31,32] Only then one can increase the aspect ratio l_p/D of the bottlebrush. An interesting problem, revealed by Feuz *et al.* is that attaching side chains to a backbone would indeed result in a larger brush diameter, D, but the persistence length, l_p, of the backbone would not increase in the same way and would even, initially, become smaller.[29] In **chapter 2** we elaborate on this problem where we present a supramolecular bottlebrush system consisting of DNA as the backbone molecule and the diblock protein polymer C_4K_{12} as the side chains. This is a rather exceptional and interesting model system to illustrate bottlebrush behaviour since it is one of the very few systems that actually does show liquid crystalline behaviour.

The behaviour of biological polymers is often very complicated. Simple

model systems have therefore been used to develop theory that can be used to describe the behaviour of the more complicated types of polymers. Bottlebrushes are in general a type of (supra)molecules that are interesting for lubrication properties due to their ability to withstand relatively high pressure, such as the aggrecan and neurofilaments. Our model system is a relatively simple system that can be used to explain the behaviour of more complicated bottlebrush systems. In **chapter 3** we report on the behaviour of our DNA-bottlebrushes under an external pressure. Our experiments have shown that exerting a pressure on bottlebrushes does not simply improve liquid crystalline behaviour. We noticed that both the osmotic pressure as well as the presence of free polymer make the brush layer collapse, and result in a more flexible bottlebrush molecule. A more flexible bottlebrush in turn is less likely to form a liquid crystalline ordering.

In **chapter 4** we present results from self consistent field (SCF) calculations that explain the persistence length of co-assembled bottlebrushes in the whole range from bare main-chain to fully saturated bottlebrush. In the case of a covalent bottlebrush, where the side chains are attached to the backbone with a covalent bond, the persistence length is mainly affected by the side chain length N and the grafting density, $1/h$. For polyelectrolyte main-chains, that we are dealing with here, the charge density plays a major role when the persistence length is concerned. Attaching side chains to a charged polymer neutralizes some or most of the charges and therefore reduces the contribution from the electrostatic interactions to the persistence length. Completely ignoring the contribution from the charges is, however, not very attractive from a modeling perspective. In **Chapter 4** we try to keep all contributions in the model and see which effect dominates in which regime. **Chapter 4** therefore deals with both the electrostatic and the side chain induced persistence length for our DNA-bottlebrushes.

Apart from the research that focuses on the behaviour of bottlebrushes we also show in **chapter 5** that the bottlebrush architecture shows good promises in preventing the hybridization of DNA. This is especially useful for techniques for sequencing of the genetic code of DNA. These methods rely on the presence of individual single stranded DNA strands. **Chapter 5** uses side chains that are slightly different from the protein polymers used in the previous chapters. Here the binding block is a protein that specifically binds to DNA (Sso7d) and the non-binding C-block side chain consists of 800 amino acids (C_8) instead of the 400 amino acids (C_4) used in the previous chapters. Both the Sso7d binding block as well as the C-block tail prove to be crucial in preventing the hybridization of single stranded

DNA back into double stranded DNA. In **chapter 6** we reflect on the results obtained in this thesis, and discuss options for extending the research.

References

(1) Milner, S. T. *Science* **1991**, *251*, 905–914.

(2) Binder, K.; Milchev, A. *J. Polym. Sci., Part B: Polym. Phys.* **2012**, *50*, 1515–1555.

(3) Ten Brinke, G.; Ikkala, O. *Chem. Rec.* **2004**, *4*, 219–230.

(4) Klein, J.; Perahia, D.; Warburg, S. *Nature* **1991**, *352*, 143–145.

(5) Klein, J. *Polym. Adv. Technol.* **2012**, *23*, 729–735.

(6) Klein, J. *Science* **2009**, *323*, 47–48.

(7) Kiani, C.; Chen, L.; Wu, Y. J.; Yee, A. J.; Yang, B. B. *Cell Res.* **2002**, *12*, 19–32.

(8) Janmey, P. A.; Leterrier, J.-F.; Herrmann, H. *Curr. Opin. Colloid Interface Sci.* **2003**, *8*, 40–47.

(9) Fuchs, E.; Cleveland, D. W. *Science* **1998**, *279*, 514–519.

(10) Ng, L.; Grodzinsky, A. J.; Patwari, P.; Sandy, J.; Plaas, A.; Ortiz, C. *J. Struct. Biol.* **2003**, *143*, 242–257.

(11) Beck, R.; Deek, J.; Jones, J. B.; Safinya, C. R. *Nat. Mater.* **2009**, *9*, 40–46.

(12) Hsu, H.-P.; Paul, W.; Rathgeber, S.; Binder, K. *Macromolecules* **2010**, *43*, 1592–1601.

(13) Fredrickson, G. H. *Macromolecules* **1993**, *26*, 2825–2831.

(14) Wintermantel, M.; Fischer, K.; Gerle, M.; Ries, R.; Schmidt, M.; Kajiwara, K.; Urakawa, H.; Wataoka, I. *Angew. Chem. Int. Ed.* **1995**, *34*, 1472–1474.

(15) Wintermantel, M.; Gerle, M.; Fischer, K.; Schmidt, M.; Wataoka, I.; Urakawa, H.; Kajiwara, K.; Tsukahara, Y. *Macromolecules* **1996**, *29*, 978–983.

(16) Ikkala, O.; Ruokolainen, J.; ten Brinke, G.; Torkkeli, M.; Serimaa, R. *Macromolecules* **1995**, *28*, 7088–7094.

(17) Ruokolainen, J.; Torkkeli, M.; Serimaa, R.; Komanschek, E.; ten Brinke, G.; Ikkala, O. *Macromolecules* **1997**, *30*, 2002–2007.

(18) Ruokolainen, J.; Torkkeli, M.; Serimaa, R.; Vahvaselka, S.; Saariaho, M.; ten Brinke, G.; Ikkala, O. *Macromolecules* **1996**, *29*, 6621–6628.

(19) Ruokolainen, J.; Torkkeli, M.; Serimaa, R.; Komanschek, B. E.; Ikkala, O.; ten Brinke, G. *Phys. Rev. E* **Dec. 1996**, *54*, 6646–6649.

(20) Ruokolainen, J.; ten Brinke, G.; Ikkala, O.; Torkkeli, M.; Serimaa, R. *Macromolecules* **1996**, *29*, 3409–3415.

(21) Saariaho, M.; Ikkala, O.; Szleifer, I.; Erukhimovichm, I.; ten Brinke, G. *J. Chem. Phys.* **1997**, *107*, 3267–3276.

(22) Darinskii, A. A.; Neelov, I. M.; Zarembo, A.; Balabaev, N. K.; Sundholm, F.; Binder, K. *Macromol. Symp.* **2003**, *191*, 191–200.

(23) Grest, G. S.; Murat, M. *Macromolecules* **1993**, *26*, 3108–3117.

(24) Saariaho, M.; Szleifer, I.; Ikkala, O.; ten Brinke, G. *Macromol. Theory Simul.* **1998**, *7*, 211–216.

(25) Hsu, H.-P.; Paul, W.; Binder, K. *Macromolecules* **2014**, *47*, 427–437.

(26) Hsu, H.-P.; Paul, W.; Binder, K. *Macromol. Theory Simul.* **2011**, *20*, 510–525.

(27) Theodorakis, P. E.; Hsu, H.-P.; Paul, W.; Binder, K. *J. Chem. Phys.* **2011**, *135*,

(28) Milner, S. T.; Witten, T. A.; Cates, M. E. *Macromolecules* **1988**, *21*, 2610–2619.

(29) Feuz, L.; Leermakers, F. A. M.; Textor, M.; Borisov, O. V. *Macromolecules* **2005**, *38*, 8891–8901.

(30) Birshtein, T. M.; Borisov, O. V.; Zhulina, Y. B.; Khokhlov, A. R.; Yurasova, T. A. *Polym. Sci. U.S.S.R.* **1987**, *29*, 1293–1300.

(31) Subbotin, A.; Saariaho, M.; Stepanyan, R.; Ikkala, O.; ten Brinke, G. *Macromolecules* **2000**, *33*, 6168–6173.

(32) Rouault, Y.; Borisov, O. V. *Macromolecules* **1996**, *29*, 2605–2611.

(33) Kreer, T.; Balko, S. M. *ACS Macro Lett.* **2013**, *2*, 944–947.

(34) Balko, S. M.; Kreer, T.; Costanzo, P. J.; Patten, T. E.; Johner, A.; Kuhl, T. L.; Marques, C. M. *PLoS ONE* **Mar. 2013**, *8*, e58392.

(35) Martens, A. A.; van der Gucht, J.; Eggink, G.; de Wolf, F. A.; Cohen Stuart, M. A. *Soft Matter* **2009**, *5*, 4191–4197.

(36) Rombouts, W. H.; Colomb-Delsuc, M.; Werten, M. W. T.; Otto, S.; de Wolf, F. A.; van der Gucht, J. *Soft Matter* **2013**, *9*, 6936–6942.

(37) Cohen Stuart, M. A.; Hofs, B.; Voets, I. K.; de Keizer, A. *Curr. Opin. Colloid Interface Sci.* **2005**, *10*, 30–36.

(38) Voets, I. K.; de Vries, R.; Fokkink, R.; Sprakel, J.; May, R. P.; de Keizer, A.; Cohen Stuart, M. A. *Eur. Phys. J. E* **2009**, *30*, 351–359.

(39) Voets, I. K.; de Keizer, A.; Cohen Stuart, M. A. *Adv. Colloid Interface Sci.* **2009**, *147-148*, 300–318.

(40) Cingil, H. E.; Storm, I. M.; Yorulmaz, Y.; te Brake, D.; de Vries, R.; Cohen Stuart, M. A.; Sprakel, J. *J. Am. Chem. Soc.* **2015**.

(41) Beun, L. H.; Beaudoux, X. J.; Kleijn, J. M.; de Wolf, F.; Cohen Stuart, M. A. *ACS Nano* **2012**, *6*, 133–140.

(42) Beun, L. H.; Storm, I. M.; Werten, M. W.; de Wolf, F. A.; Cohen Stuart, M. A.; de Vries, R. *Biomacromolecules* **2014**, *15*, 3349–3357.

(43) Hernandez-Garcia, A.; Kraft, D. J.; Janssen, A. F. J.; Bomans, P. H. H.; Sommerdijk, N. A. J. M.; Thies-Weesie, D. M. E.; Favretto, M. E.; Brock, R.; de Wolf, F. A.; Werten, M. W. T.; van der Schoot, P.; Cohen Stuart, M. A.; de Vries, R. *Nat. Nanotechnol.* **2014**, *9*, 698–702.

(44) Tang, J.; Fraden, S. *Liq. Cryst.* **1995**, *19*, 459–467.

(45) Zlotnick, A. *J. Mol. Biol.* **1994**, *241*, 59–67.

(46) Perlmutter, J. D.; Hagan, M. F. *Annu. Rev. Phys. Chem.* **2015**, *66*, 217–239.

(47) Glowacki, E. D.; Irimia-Vladu, M.; Bauer, S.; Sariciftci, N. S. *J. Mater. Chem. B* **2013**, *1*, 3742–3753.

(48) Jones, R. A. L., *Soft Condesed Matter*; Oxford University Press. New York: 2011, pp 8, 58–60.

(49) Gao, Y.-G.; Su, S.-Y.; Robinson, H.; Padmanabhan, S.; Lim, L.; McCrary, B. S.; Edmondson, S. P.; Shriver, J. W.; Wang, A. H. J. *Nat. Struct. Mol. Biol.* **1998**, *5*, 782–786.

(50) Van der Gucht, J., *Advanced Soft Matter course*; van der Gucht, J., Ed., 2012, pp 191–205.

(51) Bragg, W. H.; Bragg, W. L. *Proc. R. Soc. A* **1913**, *88*, 428–438.

(52) Svensson, A. Phase Equilibria and Structures of Oppositely Charged Polymers and Surfactants in Water., Ph.D. Thesis, Physical Chemistry 1, Lund University, Sweden, 2003.

(53) Cappello, J.; Crissman, J.; Dorman, M.; Mikolajczak, M.; Textor, G.; Marquet, M.; Ferrari, F. *Biotechnol. Prog.* **1990**, *6*, 198–202.

(54) Krejchi, M. T.; Atkins, E. D. T.; Waddon, A. J.; Fournier, M. J.; Mason, T. L.; Tirrell, D. A. *Science* **1994**, *265*, 1427–1432.

(55) Krejchi, M. T.; Atkins, E. D. T.; Fournier, M. J.; Mason, T. L.; Tirrell, D. A. *J. Macromol. Sci., Pure Appl. Chem.* **1996**, *33*, 1389–1398.

(56) Krejchi, M. T.; Cooper, S. J.; Deguchi, Y.; Atkins, E. D. T.; Fournier, M. J.; Mason, T. L.; Tirrell, D. A. *Macromolecules* **1997**, *30*, 5012–5024.

(57) Bracalello, A.; Santopietro, V.; Vassalli, M.; Marletta, G.; Gaudio, R. D.; Bochicchio, B.; Pepe, A. *Biomacromolecules* **2011**, *12*, 2957–2965.

(58) Werten, M. W. T.; Wisselink, W. H.; Jansen-van den Bosch, T. J.; de Bruin, E. C.; de Wolf, F. A. *Protein Eng.* **2001**, *14*, 447–454.

(59) Urry, D. W. *J. Phys. Chem. B* **1997**, *101*, 11007–11028.

(60) Lee, T. A. T.; Cooper, A.; Apkarian, R. P.; Conticello, V. P. *Adv. Mater.* **2000**, *12*, 1105–1110.

(61) MacEwan, S. R.; Chilkoti, A. *Peptide Science* **2010**, *94*, 60–77.

2 Liquid Crystals of Self-Assembled DNA Bottlebrushes

Abstract

Early theories for bottlebrush polymers have suggested that the so-called main-chain stiffening effect caused by the presence of a dense corona of side chains along a central main-chain, should lead to an increased ratio of effective persistence length ($l_{p,eff}$) over the effective thickness (D_{eff}) and hence ultimately to lyotropic liquid crystalline behaviour. More recent theories and simulations suggest that $l_{p,eff} \sim D_{eff}$, such that no liquid crystalline behaviour is induced by bottlebrushes. In this paper we investigate experimentally how lyotropic liquid crystalline behaviour of a semiflexible polymer is affected by a dense coating of side chains. We use semiflexible DNA as the main-chain. A genetically engineered diblock protein polymer C_4K_{12} is used to physically adsorb long side chains on the DNA. The C_4K_{12} protein polymer consists of a positively charged binding block (12 lysines, K_{12}) and a hydrophilic random coil block of 400 amino acids (C_4). From light scattering we find that at low ionic strength (10 mM Tris-HCl), the thickness of the self-assembled DNA bottlebrushes is on the order of 30 nm and the effective grafting density is 1 side chain per 2.7 nm of DNA main-chain. We find these self-assembled DNA bottlebrushes form birefringent lyotropic liquid crystalline phases at DNA concentrations as low as 8 mg/ml, roughly one order of magnitude lower than for bare DNA. Using small angle X-ray scattering we show that at DNA concentrations of 12 mg/ml there is a transition to a hexagonal phase. We also show that while the effective persistence length increases due to the bottlebrush coating, the effective thickness of the bottlebrush increases even more, such that in our case the bottlebrush coating reduces the effective aspect ratio of the DNA. This is in agreement with theoretical estimates that show

that in most cases of practical interest, a bottlebrush coating will lead to a decrease of the effective aspect ratio, while only for bottlebrushes with extremely long side chains at very high grafting densities, a bottlebrush coating may be expected to lead to an increase of the effective aspect ratio.

This chapter is published as: Storm, I. M.; Kornreich, M.; Hernandez-Garcia, A.; Voets, I. K.; Beck, R.; Cohen Stuart, M. A.; Leermakers, F. A. M.; de Vries, R. *The Journal of Physical Chemistry B* **2015**, *119*, 4084–4092.

2.1 Introduction

The bottlebrush polymer architecture, consisting of a main-chain with grafted side chains, has important functions in biology. For example, neurofilaments[1–7] are self-assembled protein filaments, consisting of a compact cylindrical core with charged, unstructured polypeptide side chains that emanate from the core. The neurofilament side chains have complicated interactions that appear to be controlled by phosphorylation at specific sites along the side chains. These interactions regulate the spacing and cohesion of bundles of neurofilaments. Indeed, some mutations in the amino acid sequence of the side chains, lead to incorrect neurofilament bundling, and are linked to neurological disorders.[8,9]

Other naturally occurring bottlebrush polymers are proteoglycans such as aggrecan that consist of a protein core with covalently linked and typically highly charged polysaccharide side chains. Aggrecan (which, to be precise actually has a bottlebrush of a bottlebrush architecture) is a major constituent of the articular cartilage, where it ensures lubrication[10] to prevent wear of joints which might lead to osteoarthritic or even joint breakdown.[11–13] In this case the role of the bottlebrush architecture is to provide for a macromolecular structure with an extreme density of charged groups that is highly swollen and holds on to water even under high load.

Partly inspired by these natural examples, many approaches have been developed to also create synthetic bottlebrush polymers, that show promising applications as biolubricants,[14] and for attaching polymer brushes to surfaces by simple physical adsorption.[15] The different strategies of preparing synthetic bottlebrush polymers are known as 'grafting-from', 'grafting-through' and 'grafting-onto'[16–23] and each has its specific advantages and limitations with respect to the range of main-chain lengths, side chain lengths and side chain grafting densities that are possible. The 'grafting-through' synthesis uses the coupling of macromonomers with predetermined architecture and functionality. In the 'grafting-from' method a backbone molecule with initiator sites is used as a starting material and the side chains are grown from these initiator sites by a polymerization reaction. An especially good control over side chain architecture of the bottlebrush polymer appears to be possible with a click-chemistry-based 'grafting-onto' approach.[24] These and other methods have been used to create a range of exotic bottlebrush polymers varying from brushes with umbrella-like side chains,[20] bottlebrush block copolymers[21] to hydrogel-forming DNA-grafted polypeptide bottlebrushes.[22]

Early theoretical work of Fredrickson directed the attention to the so-called main-chain stiffening effect for bottlebrush polymers.[25] Fredrickson predicted a dramatic stiffening of the main-chain for bottlebrush polymers as a consequence of the presence of a dense corona of side chains. More specifically it was predicted that bottlebrush polymers should behave as semiflexible polymers with a high ratio of the persistence length over their thickness, and hence that they should exhibit lyotropic liquid crystalline behaviour. Although the scaling-behaviour of the effective thickness of cylindrical brushes is well established,[26] conflicting scaling predictions and experimental results exist for the main-chain stiffening effect,[17,25,27–29] such that it is still unclear whether a bottlebrush increases or decreases the effective aspect ratio (the ratio of the effective persistence length over the effective thickness), as compared to that of the main-chain.

Very few examples exist of lyotropic liquid crystalline behaviour for bottlebrushes of flexible main-chains with chemically grafted side chains. One clear example is by Wintermantel *et al.* who showed that flexible polymethacrylate backbones with densely grafted oligostyrene side chains form semiflexible chains that feature lyotropic liquid crystalline behaviour in organic solvents.[30] Fredricksons original paper was developed for self-assembled bottlebrush polymers consisting of polyelectrolytes coated with oppositely charged surfactants. Indeed, complexes of poly(vinylpyridine) with dodecylbenzenesulfonic acid were one of the first examples confirming Fredrickson's prediction that bottlebrush polymers should form lyotropic liquid crystals.[31,32]

Whereas most experiments and theories are for bottlebrushes with flexible main-chains, there are important biological examples of bottlebrush polymers with semiflexible main-chains, in particular neurofilaments. Also, in the context of non-viral gene delivery, a number of authors have demonstrated the possibility of coating single DNA molecules with a dense layer of hydrophilic side chains, thus creating self-assembled DNA bottlebrushes.[33–35] We have previously shown that genetic engineering can be used to create perfectly monodisperse diblock copolypeptides C_4K_{12}, consisting of 12 lysines, K_{12}, and a long hydrophilic corona block, C_4, where C is a 98 amino acid long, net neutral hydrophilic polypeptide domain. When mixed with DNA, these polypeptides coat individual DNA molecules with a dense layer of hydrophilic side chains. At low salt, electrostatic binding is strong enough to overcome the loss in translational entropy and the free energy penalty associated with stretching of the side chains upon binding: at high polypeptide concentrations, complexes are formed that are nearly

electroneutral.[35] This means that for many solution conditions, the grafting density of monodisperse side chains on the DNA can simply be controlled by stoichiometry. The DNA main-chain stiffening effect of C_4K_{12} diblocks copolymers has been exploited in the context of so-called 'optical mapping', a single-molecule DNA sequencing technology that requires stretching of DNA.[36,37] It was shown that the diblock coating of the DNA stiffens it to such an extent that it remains nearly fully stretched in 200 nm × 200 nm nanochannels. The nanopore data was analyzed using Monte-Carlo simulations of confined semiflexible chains and this analysis gave an estimated persistence length of 250 nm for the self-assembled DNA bottlebrush, which was confirmed using analysis of AFM images.[38] The order of magnitude of the main-chain stiffening effect was found to be in approximate agreement with the numerical self-consistent field theory of Feuz *et al.*.[26]

Hence, self-assembled DNA bottlebrushes appear to be excellent model systems for the physical behaviour of bottlebrushes with semiflexible main-chains, such as neurofilaments. As mentioned, neurofilaments readily form liquid crystals[7] and this may be expected to hold more generally for bottlebrushes with semiflexible main-chains. Since in this case the main-chains also form liquid crystals in the absence of side chains the issue is not so much whether the side chains can induce lyotropic liquid crystalline behaviour, but rather how this is changed by the addition of side chains. This is the issue that we wish to address here, by a first exploration of the lyotropic liquid crystalline behaviour of DNA bottlebrushes formed by co-assembly of DNA with the previously mentioned C_4K_{12} diblock copolymers.

2.2 Experimental Methods

2.2.1 DNA

Light scattering experiments were performed using *NoLimits 300 bp DNA Fragments* (Thermo Scientific). For all other experiments, sonicated deoxyribonucleic acid sodium salt from calf thymus, Type I fibers (Sigma) was used. This DNA was first dissolved in 100 ml of 10 mM Tris-HCl *p*H 7.6 to a concentration of 1 mg/ml and sonicated for 10 minutes with a Bandelin Sonopuls GM 70 (power 2/3 and 100% cycle). Sonication decreases the length and thus the molar mass of the DNA fibers. Agarose gel electrophoresis (1.5 wt% of agarose) in TAE/EtBr buffer was used to analyze the progression of the decrease of DNA molar mass, see Figure 2.1,

since smaller objects move faster across the gel. It was found that after 10 min of sonication there was no appreciable further decrease of DNA molar mass, and that final fragments had lengths in the range of 500 to 1000 base pairs (bp). These final fragments were freeze dried.

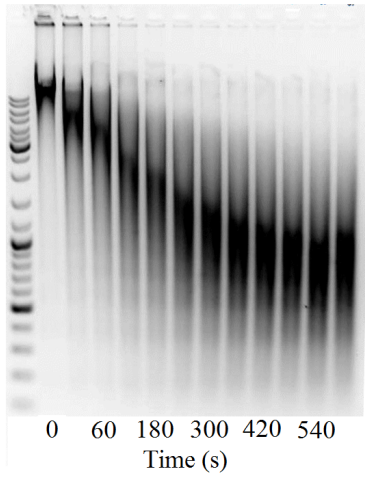

Figure 2.1: *Agarose gel electrophoresis of Calf Thymus DNA for a range of sonication times (1.5 wt% of agarose). The first lane is a DNA ladder, from top to bottom the thick bands are: 3000 bp, 1000 bp and 500 bp. Sonication times (in seconds) for the various lanes are indicated in the figure.*

2.2.2 Fermentation of Protein Polymers

Fermentation of a Pichia Pastoris strain harboring the gene for the secreted expression of the diblock polypeptide C_4K_{12} was performed as described before.[35] In short, a 2.5-L Bioflo3000 fermentor was used for protein biosynthesis. After induction, the fed-batch fermentation was performed for two days at a 0.2% (w/v) methanol content in the broth. During the fermentation the *p*H was kept at *p*H 3 by addition of ammonium hydroxide. After fermentation, the supernatant was separated from the yeast cells by centrifugation at 16000 × *g* for 20 minutes at 20 °C (SLA-1500 rotor). The supernatant was filtered using a 0.2 μm, *AcroPak 200 Capsules with Supor Membrane*, from Pall Corporation.

2.2.3 Purification of Protein Polymers

For purification of the diblock protein polymer, first the medium salts were removed from the filtered supernatant by increasing the *p*H with NaOH to a final *p*H of 8 and centrifugation (16000 × *g*, 30 min, 4 °C, SLA-1500 rotor). The C_4K_{12} protein was separated from the majority of secreted Pichia Pastoris proteins by selective precipitation with ammonium sulphate (45% saturation) for 30 minutes at 4 °C and subsequently centrifuged (16000 × *g*, 30 min). This step was repeated once. Next, the precipitate was resuspended in 0.2 times the original volume of 50 mM NaCl solution and 40% (v/v) acetone. After centrifugation the acetone content of the diblock supernatant was increased to 80% (v/v). After one more wash of the protein precipitate with 80% (v/v) acetone, the precipitate was resuspended in Milli-Q water, extensively dialyzed against Milli-Q water and freeze-dried. The protein purity and molecular weight were determined using dodecylsulfate polyacrylamide gel electrophoresis (SDS-PAGE) and matrix-assisted laser desorption/ionization time-of-flight (MALDI-TOF) respectively. SDS-PAGE and MALDI-TOF results were similar to those obtained before, for the same protein polymer.[35]

2.2.4 Preparation of Concentrated DNA-Protein Mixtures

Concentrated protein-DNA samples were prepared by mixing DNA and protein powders at the required mass ratio, followed by hydration of the powders with the required amount of a Tris-HCl buffer of 10 mM *p*H 7.6 with 0.05% NaN_3 to obtain a DNA concentration of 20 mg/ml. In view of the high viscosity of the resulting samples, adequate mixing was only achieved when centrifuging the samples up and down for many times. To this end, 1.0 ml microcentrifuge tubes were used for the samples, which were enclosed in larger centrifuge tubes. Samples were first centrifuged for 20 minutes at 1000 × g at 4 °C. After 20 minutes, the small microcentrifuge tubes were turned up-side-down and centrifuged again. These steps were repeated for at least 8 hours.

In order to remove excess salt liberated due to the complexation of the diblock polypeptides with the DNA, samples were washed with 10 mM Tris-HCl buffer *p*H 7.6 and 0.05% NaN_3 using centrifugal filters, *Amicon Ultra - 0.5mL 3K Membrane*, at 13000 × g. Samples were washed with roughly 10 times their own volume of buffer solution. UV-spectrophotometry was used to determine the final DNA concentration of the samples (the presence of the protein did not influence this determination since it has negligible

UV absorption at 260 nm). The protein concentration was estimated by assuming that the washing procedure with the centrifugal filters did not affect the mass ratio of protein/DNA due to the small molecular weight cut-off of the centrifugal membranes (3K).

2.2.5 Light Scattering

Light scattering experiments were performed on a *Malvern Instrument*, *zetasizer nanoseries*. Measurements were performed at two scattering angles: 173 ° and 12.8 °. The DNA used for these experiments was short (essentially rod-like) monodisperse DNA of 300 bp in a 10 mM Tris-HCl *p*H 7.6 buffer (NoLimits 300 bp DNA Fragments, Thermo Scientific, used as received). The initial DNA concentration was 0.1 mg/ml. For the light scattering experiments, the protein concentration of the samples was increased by the stepwise addition of small volumes of concentrated protein solution, typically 4 mg/ml in a 10 mM Tris-HCl *p*H 7.6 buffer. Light scattering measurements were performed at a temperature of 25 °C.

Scattering intensities were used to determine the amount of protein bound to DNA, following an approach described earlier by us.[39] In short, we analyze the ratio of the scattering intensity $I_{complex}$ of protein-DNA complexes to the scattering intensity I_{DNA} of the bare DNA:

$$\frac{I_{\text{complex}}}{I_{DNA}} = (1 + \Gamma_{\text{bound}}\zeta)^2 \tag{2.1}$$

where Γ_{bound} is the mass ratio of adsorbed protein over DNA, and ζ is the ratio of the respective refractive index increments of protein and DNA:

$$\zeta = \left(\frac{dn}{dC}\right)_{prot} / \left(\frac{dn}{dC}\right)_{DNA} \tag{2.2}$$

We use $(dn/dc)_{DNA} = 0.165$ and $(dn/dc)_{prot} = 0.18$, such that $\zeta = 1.091$.[40,41] Since adding the protein dilutes the sample, in order to obtain the proper ratio of scattering intensities, the scattering intensity of the bare DNA was corrected by the dilution factor due to the addition of the concentrated protein solution. Assuming the scattering of the free proteins in solution can be neglected compared to the complexes, the mass ratio of bound diblock protein to DNA (Γ_{bound}) is then found to be:

$$\Gamma_{\text{bound}} = \frac{1}{\zeta}\left(\sqrt{\frac{I_{complex}}{I_{DNA}}} - 1\right) \tag{2.3}$$

While strictly speaking this analysis requires the scattering intensities extrapolated to zero scattering angle, we found that intensities at the lowest scattering angle of 12.8 ° were not reproducible enough to perform this analysis. Therefore, instead we have used this analysis on the sattering intensities obtained at a scattering angle of 173 ° to at least obtain a semi-quantitative estimate of the amounts of bound protein.

For estimating the hydrodynamic diameter of the bottlebrush DNA, we have obtained translational diffusion constants D_t using dynamic light scattering (DLS). For each run, intensity weighted average diffusion constants, were obtained using a distribution fit of the autocorrelation function, as performed by the software supplied with the Malvern Instrument, zetasizer nanoseries scattering instrument. Invariably, there was one clear, dominant diffusion peak that was identified as being due to the translational diffusion of the protein-DNA complexes. The intensity-weighted, average diffusion constant corresponding to this peak was used as the average diffusion constant for a single light scattering run. Final averages and standard deviations of the diffusion constant D_t were obtained from values of D_t for a series of 10 or 20 independent runs. For the diffusion constants it was found that values at the lowest scattering angle were still reproducible and reliable, hence for estimating the hydrodynamic diameter of the bottlebrush DNA, we have used data obtained at the 12.8 ° scattering angle.

2.2.6 AFM

For atomic force microscopy (AFM), DNA-protein complexes (DNA concentration 0.1 mg/ml, protein concentration 2.5 mg/ml) were first incubated for 24 hours in a 10 mM Tris-HCl *p*H 7.6 buffer, after which they were deposited on a silica wafer and incubated for 5 min. The wafer was washed with MQ water to remove excess salts and non-adsorbed material, and then dried with N_2(g). A Digital Instruments Nanoscope V was used to analyse the samples. Imaging was performed using a Silicon Tip on a Nitride Lever (Bruker) with a spring constant of 0.4 N/m. The ScanAsyst mode in air was used. A scanning speed of 0.977 Hz and a resolution of 1024 samples/line were used. Nanoscope Analysis 1.4 software was used to process and analyse the images.

2.2.7 Crossed-Polarizer Set-Up

Birefringence of concentrated DNA-protein mixtures was observed with a simple set-up consisting of an analyzer and a polarizer, one being rotated

for 90 °with respect to the other. A white light source (ThorLabs), and a ThorLabs DCx camera were used for imaging. Intensities of birefringence were quantified by averaging the grey scale values of the pixels in an area of the image corresponding to the birefringent sample, for a series of images obtained under identical imaging conditions.

2.2.8 SAXS Data Collection and Processing

The samples were placed in a Hilgenberg quartz capillary with an outside diameter of 2 mm and a wall thickness of 0.01 mm. Initial SAXS experiments were conducted using a SAXS-LAB instrument with a Xenocs GeniX Low Divergence CuKα X-ray source and a Pilatus 300K detector (Dectris, Baden, Switzerland) with a wavelength of 1.54 Å. The sample-detector configuration used were 21, 25, 26 with sample-detector distances of 110 (21), 710 (25), 1510 mm (26). The total q-range reached for these three sample-detector configurations was 0.006 to 2.41 $Å^{-1}$. Acquisition time was typically 3600 seconds for each sample. The 2D images were radially averaged to produce one-dimensional profiles using the data reduction program SAXSGUI. Further measurements were done using a Pilatus 300K detector (Dectris, Baden, Switzerland) and a Xenocs GeniX Low Divergence CuKα radiation source setup with scatterless slits.[42] For this set-up, the sample-detector distance was 2.48 m with the wavelength tuned to 1.54 Å yielding a measurement q range of 0.006 to 0.15 $Å^{-1}$. Multiple frames of 30 minutes were collected and showed no radiation damage. 2D frames were radially averaged with the CONEX program,[43] and later summed for better statistics. Peaks in the final 1D radially averaged profiles were Gaussian- fitted using X+.[44]

2.3 Results and Discussion

2.3.1 Grafting Density and Effective Thickness of Self-Assembled DNA Bottlebrushes

The co-assembly of the C_4K_{12} diblocks with DNA to form self-assembled DNA bottlebrushes is mainly driven by electrostatic interactions, see Figure 2.2 for a schematic image of these DNA bottlebrushes. Hence we are able to control the grafting density and the induced stiffening due to the bottlebrush by varying the protein to DNA ratio and the salt concentration. For determining the grafting density of C_4K_{12} diblocks on the DNA backbone, we have used static light scattering (SLS) on short self-assembled

DNA bottlebrushes with a length of the DNA main-chain of 300 bp (≈ 100 nm), that should be essentially rod-like. From the ratio of scattering intensities of complexes and that of the bare DNA, we can infer the mass ratio of bound protein to DNA (Γ_{bound}), as described before.[39] Results for Γ_{bound} as a function of the total mass ratio of protein over DNA, $\Gamma = C_{C_4K_{12}}/C_{DNA}$ are shown in Figure 2.3 for a range of salt concentrations.

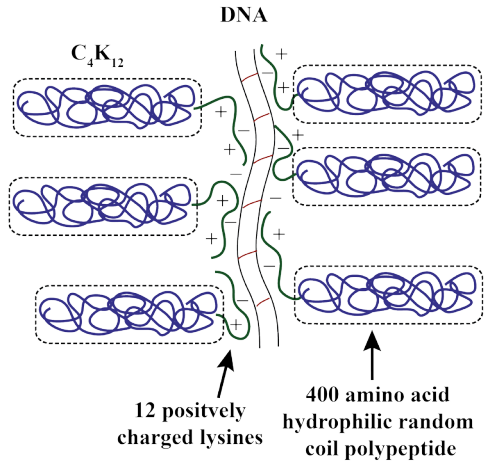

Figure 2.2: *DNA bottlebrushes consisting of DNA as the backbone molecule and C_4K_{12} protein polymers as the side chains. These side chains have a 400 amino acid stabilizing block and 12 positively charged lysines as a binding block to bind to the negatively charged DNA backbone.*

The initial steep slope indicates that initially most of the added protein attaches to the DNA backbone. Beyond some value of Γ, binding of protein polymers to DNA saturates. According to Figure 2.3, the amount of bound diblocks at saturation is a strong function of the ionic strength of the solution. Assuming that full coating corresponds to perfect neutralization of DNA phosphate charges by lysines on the K_{12} binding blocks of the proteins, the maximal value of Γ_{bound} is 10. This would correspond to a grafting density of 1 side chain per 2 nm (along the contour of the DNA). We find that at 160 mM NaCl, coverage is only 20% to 30%, corresponding to grafting densities of respectively, 1 side chain per 10.2 nm and 1 side chain per 6.8 nm. For 10 mM Tris-HCl, and no further added salt, coverage is about 75% such that the grafting density is about 1 side chain per 2.7 nm.

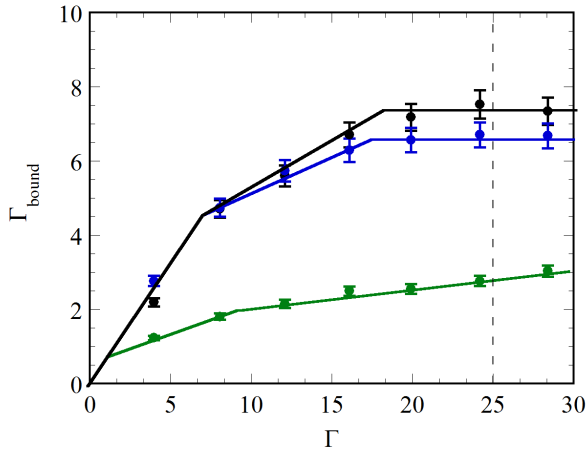

Figure 2.3: *Mass ratio of bound protein to DNA,* Γ_{bound}*, as a function of the mass ratio of total protein to DNA,* Γ*.* Γ_{bound} *was determined for ionic strengths of 10 mM (black), 60 mM (blue) and 160 mM (green) using light scattering. All measurements were performed in 10 mM Tris buffer, for ionic strengths of 60 and 160 mM additional NaCl was added.* $\Gamma_{\text{bound}} = 10$ *represents stoichiometric ratios between DNA and* C_4K_{12}*. The solid lines are a guide to the eye. The dashed line point to the composition of the lyotropic liquid crystalline samples cf. Figure 2.6.*

The thickness of the DNA bottlebrushes was determined by determining the translational diffusion constant of the short, rod-like DNA bottlebrushes using dynamic light scattering. For approximately relating the measured diffusion constant to the thickness of the brush, we use the following theoretical expression for the diffusion constant of a rod-like particle of length L, radius r and aspect ratio $p = L/r$, following DeRouchey *et al.*:[34]

$$D_t = \frac{A(p)\mathrm{k_B}T}{3\pi\eta L} \tag{2.4}$$

$$A(p) = \ln(p) + 0.312 + \frac{0.565}{p} - \frac{0.1}{p^2} \tag{2.5}$$

where D_t is the translational diffusion coefficient, $\mathrm{k_B}$ the Boltzmann constant, T the absolute temperature and η the solvent viscosity. Since the length L is known, from the translational diffusion constants, we can infer the aspect ratio p, and hence the hydrodynamic radius of the bottlebrushes. The thickness D (diameter) of the brushes is given as a function of the protein to DNA mass ratio Γ in Figure 2.4. We have not been able to

precisely determine the diameter of bare DNA using DLS, since the scattering intensity of the short bare DNA molecules was too low for a reliable determination. Therefore, in Figure 2.4, for the diameter of bare DNA, we use the known value of around 2.4 nm. As shown in Figure 2.4, for the case of a low ionic strength (10 mM Tris-HCl, *p*H 7.6), with increasing protein concentration, the hydrodynamic diameter of the brush rapidly increases, to saturate at values of around 30 nm. Saturation of both the brush diameter and the grafting density occurs at a protein to DNA mass ratios larger than $\Gamma \approx 15 - 20$. Since the translational diffusion constant depends only logarithmically on the aspect ratio (through Eqns. (2.4) and (2.5)), small errors in the diffusion constants lead to rather large uncertainties in the final values for the hydrodynamic diameters (see the values for the diffusion constants and hydrodynamic diameters in Table 2.1). Nevertheless, the data do show a clear trend of increasing diameters at low protein to DNA mass ratios and a saturation at hydrodynamic radii of about 30 nm at higher ratios.

Table 2.1: *Translational diffusion constants (D_t) from dynamic light scattering and the corresponding hydrodynamic diameter (D) of the DNA bottlebrushes as a function of the protein to DNA mass ratio* Γ.

Γ	D_t	D
(-)	($\times 10^{-12}$ m^2s^{-1})	(nm)
4.0	8.00 ± 0.5	20.0 ± 2.4
8.1	6.91 ± 0.9	26.2 ± 5.7
12.1	6.26 ± 0.3	31.1 ± 2.6
16.1	6.02 ± 0.9	33.3 ± 8.0
19.9	5.93 ± 1.1	34.1 ± 10.1
24.2	6.86 ± 2.4	32.5 ± 14.9
28.4	5.79 ± 1.5	35.4 ± 13.8

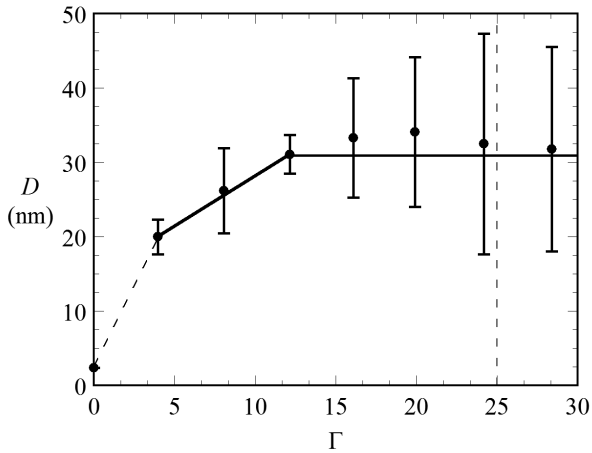

Figure 2.4: *Hydrodynamic diameters D of self-assembled DNA bottlebrushes as a function of the mass ratio of total protein to DNA,* Γ*, as deduced from translational diffusion constants of short, rodlike DNA bottlebrushes determined with dynamic light scattering. The point at* $\Gamma = 0$ *is the known value of the hydrodynamic diameter of bare DNA of 2.4 nm. Solution conditions: 10 mM Tris-HCl buffer of pH 7.6. The solid line is a guide to the eye and the vertical dashed line point to the composition of the lyotropic liquid crystalline samples cf. Figure 2.6.*

2.3.2 Lyotropic Liquid Crystalline Behaviour of Self-Assembled Bottlebrushes

In the remainder of the experiments it is less essential that DNA is entirely monodisperse. Hence for investigating the lyotropic liquid crystalline behaviour of bottlebrush DNA, we use 500-1000 bp fragments of sonicated calf thymus DNA (see Figure 2.1), that are more easily obtained in large amounts. An AFM image of the DNA coated with the C_4K_{12} diblock copolymer, a protein to DNA mass ratio of $\Gamma = 25$, is shown in Figure 2.5. Apart from the polydispersity in the contour lengths of the bottlebrushes, the images are very similar to those of DNA bottlebrushes obtained before with monodisperse DNA.[35] From the AFM images we have extracted the height and width (at half height) of the bottlebrushes at 30 random locations along the DNA contours, giving a height of 1.5 ± 0.1 nm, and a width of 25 ± 6 nm. While drying of the complexes undoubtedly affects their width, and tip-convolution may lead to further differences between the real diameter and that observed using AFM, we nevertheless note that it is gratifying that this value is of the same order of magnitude as that obtained using DLS.

Next, a series of concentrated samples was prepared with varying DNA concentration, but at a fixed protein to DNA mass ratio of $\Gamma = 25$, and imaged using crossed polarizers. Low ionic strength solution conditions were chosen (only 10 mM Tris-HCl buffer, *p*H 7.6), in order to reach a maximum coverage. The value of $\Gamma = 25$ was chosen to be in the vicinity of a saturated brush, but not much above. Images of the samples between crossed polarizers are shown in Figure 2.6. From the figure it is clear that at DNA concentrations above around 8 mg/ml, the samples show very clear birefringence, indicating a liquid crystalline arrangement of the DNA bottlebrushes.

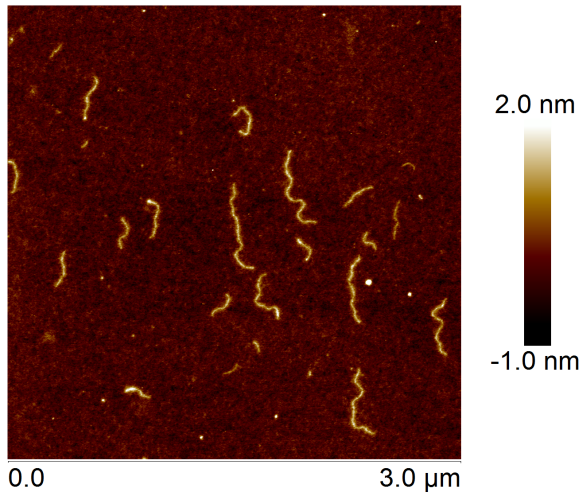

Figure 2.5: *AFM image of DNA bottlebrushes made from sonicated Calf Thymus DNA coated with C_4K_{12}. The bottlebrushes were incubated in a 10 mM Tris-HCl buffer pH 7.6 for 24 hours before deposition onto a silica wafer.*

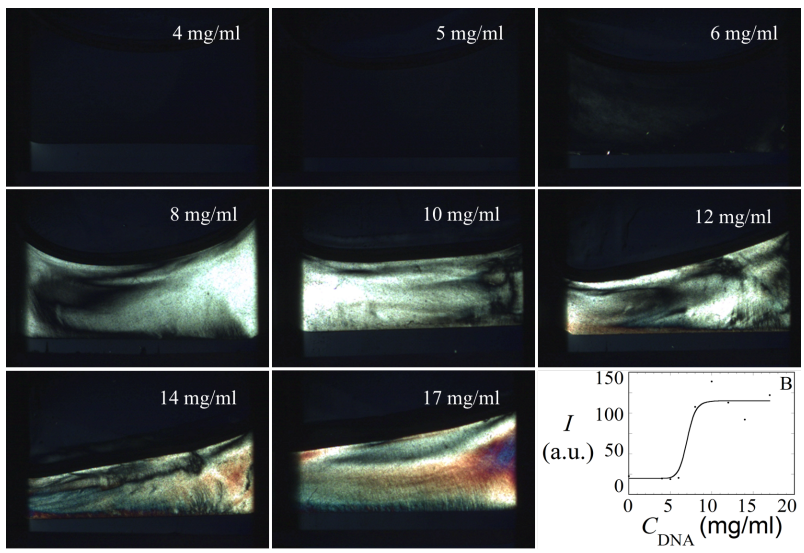

Figure 2.6: *Birefringence as a function of the concentration of DNA bottlebrushes. The concentration of DNA is indicated in the images, the mass ratio of protein to DNA is constant, $\Gamma = 25$. (B) Intensity of the birefringence as a function of C_{DNA}. Samples are contained in glass cuvettes of 1 mm thickness.*

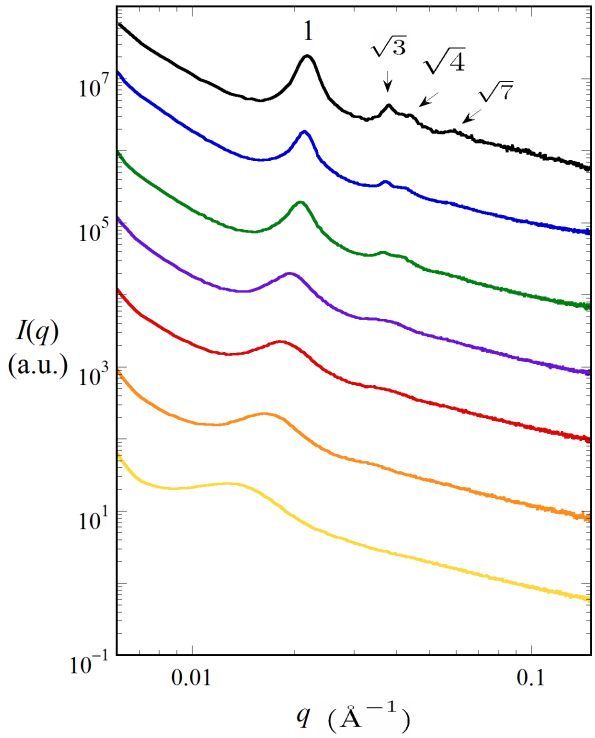

Figure 2.7: *X-ray scattering intensity I of DNA bottlebrushes as a function of the magnitude q of the wavevector. DNA concentrations: 20 mg/ml (black), 15 mg/ml (blue), 13 mg/ml (green), 11 mg/ml (purple), 9 mg/ml (red), 7 mg/ml (orange) and 4 mg/ml (yellow). The mass ratio of C_4K_{12} to DNA is $\Gamma = 25$.*

X-ray experiments were conducted to obtain more detailed information on the type of liquid crystalline arrangement of the DNA bottlebrushes. Scattering curves for the series of concentrated DNA bottlebrushes are shown in Figure 2.7. At the lowest concentrations, a single, rather broad correlation peak is found. With increasing DNA concentrations, the peak position (q_n) shifts to higher q-values. At the highest concentrations (13 mg/ml and higher), multiple sharper peaks appear. These correspond to hexagonal ordering with relative peak positions of 1, $\sqrt{3}$, $\sqrt{4}$, $\sqrt{7}$. A 2D-scattering pattern of the 20 mg/ml DNA bottlebrush sample (Figure 2.8) shows that in fact, the sizes of the hexagonal domains in these concentrated samples are at least comparable to the size of the beam, which was 0.8×0.8 mm^2.

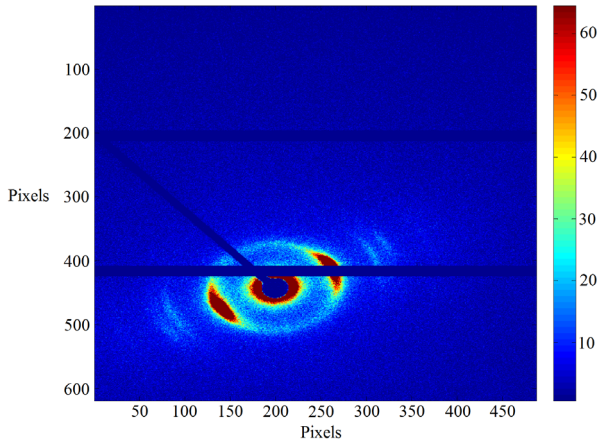

Figure 2.8: *Scattering intensity as a function of the x-y position on the 2D detector for a sample with a DNA concentration of 20 mg/ml at a protein to DNA mass ratio of* $\Gamma = 25$.

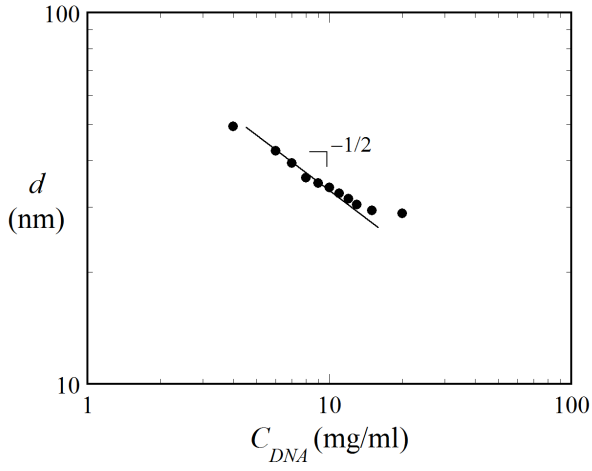

Figure 2.9: *The characteristic distance d between DNA bottlebrushes as a function of the DNA concentration* C_{DNA}*, as determined from the X-ray scattering. The line with slope* $-1/2$ *is a guide to the eye.*

Distances d between the DNA bottlebrushes were determined from the position of the first Bragg peak (q_n) using

$$d(\text{nm}) = \frac{2\pi}{q} \tag{2.6}$$

and are shown as a function of the DNA concentration (at a fixed mass ratio of protein to DNA) in Figure 2.9. Over most of the concentration range, we find the scaling of the distance d with DNA concentration of $d \sim C_{DNA}^{-1/2}$ that is expected for parallel alignment of the DNA bottlebrushes. At the highest concentrations, from 13 - 20 mg/ml DNA, distances start deviating from this behaviour. In this same concentration range, the intensity of the $\sqrt{3}$, $\sqrt{4}$ and $\sqrt{7}$ Bragg peaks become more pronounced. While we did not find any indications for macroscopic phase separation of coexisting nematic and hexagonal phases, such a coexistence[45] could explain the deviations from the $C_{DNA}^{-1/2}$ scaling of the distances d at higher concentrations.

2.3.3 Numerical Estimates

The concentration at which semiflexible polymers start forming lyotropic nematic phases is a strong function of the aspect ratio γ of the segments of the polymer, $\gamma = l_p/D$, where l_p is the persistence length and D the diameter. In the limit of very large aspect ratio's, $\gamma \gg 1$, the volume fractions ϕ_i and ϕ_n of the coexisting isotropic and nematic phases are:[46,47]

$$\phi_i = \mu_i \frac{D}{l_p} \tag{2.7}$$

$$\phi_n = \mu_n \frac{D}{l_p} \tag{2.8}$$

where μ_i and μ_n are numerical constants. Strictly speaking this theory applies only quantitatively when the aspect ratio $\gamma \geq 300$ and $L \gg l_p$. For example, for schizophyllan with $\gamma \approx 70$, the transition concentration agrees with the Semenov and Khokhlov theory only to within 15%.[48] For bare DNA, which has $\gamma \approx 20$, the second-virial approximation is no longer valid. Nevertheless, also for semiflexible polymers with lower aspect ratio's, for which the Khokhlov-Semenov theory is no longer valid, the critical concentration at which lyotropic liquid crystalline phases start forming, is expected to be a very strong function of the aspect ratio. For DNA bottlebrushes, we need to separate main-chain and side-chain contributions to both the effective thickness and the effective persistence length, and hence to the effective aspect ratio:

$$D_{eff} = D_{DNA} + D_{brush} \tag{2.9}$$

$$l_{p,eff} = l_{p,DNA} + l_{p,brush} \tag{2.10}$$

Note that the complexation of proteins onto the DNA effectively reduces the charge density on DNA and therefore we do not expect an electrostatic contribution to the effective persistence length. The effective aspect ratio γ_{eff}:

$$\gamma_{eff} = \frac{l_{p,DNA} + l_{p,brush}}{D_{DNA} + D_{brush}} \tag{2.11}$$

We have found experimentally that by applying the C_4K_{12} bottlebrush coating to DNA, we have shifted the critical DNA concentration at which lyotropic liquid crystalline phases start forming from around 120 mg/ml down to about 8 mg/ml.[49] A parallel experiment from bare sonicated DNA showed that DNA fragments (~500-1000 bp) become liquid crystalline around 60 mg/ml in a 10 mM Tris-HCl buffer. But does that mean that the bottlebrush coating has in fact increased the effective aspect ratio and hence, has promoted liquid crystallinity? First, we estimate the effective aspect ratio of the bottlebrushes based on our experimental data. From the work of Hernandez *et al.*,[35] we have $l_{p,eff} \approx 250$ nm at $\Gamma = 20$, whereas we have found $D_{eff} \approx 30$ nm, at $\Gamma = 25$. Hence, the DNA bottlebrushes have an effective aspect ratio $\gamma_{eff} \approx 8$, which is much lower than the aspect ratio of $\gamma \approx 20$ for bare DNA. Hence, the bottlebrush coating has significantly reduced the effective aspect ratio, but apparently not so much that lyotropic liquid crystals no longer form.

Next, let us compare this to theoretical predictions. There is little disagreement about scaling predictions for the thickness of cylindrical bottlebrushes. Previously, we have combined analytical scaling theory and numerical self-consistent field theory to address the effective stiffness and thickness of bottlebrush polymers.[26] For a bottlebrush with a spacing h between side chains of N monomers with segment lengths a we found

$$D_{brush} = \mu_D \frac{N^{3/4} a^{5/4}}{h^{1/4}} \tag{2.12}$$

with a numerical coefficient $\mu_D = 0.6$. A number of mutually conflicting scaling predictions have been proposed for the main-chain stiffening of bottlebrushes. By comparing scaling predictions with numerical self-consistent field equations we have previously shown that it is crucial to know the numerical value of the prefactor of the scaling expression. This numerical value in fact turns out to be a very small number. Our previous result is:

$$l_{p,brush} = \mu_l \frac{N^2 a^3}{h^2} \tag{2.13}$$

with a numerical constant of only $\mu_1 \approx 0.02$..[26] When applied to our case with $N = 400$, $a = 0.5$ nm, and $h = 2.0$ nm, we find $l_{\mathrm{p},brush} \approx 100$ nm. Accounting for the contribution to the persistence length of the DNA itself we get an effective persistence length of $l_{\mathrm{p},eff} \approx 150$ nm which is somewhat smaller than the $l_{\mathrm{p},eff} \approx 250$ nm estimated from the nanopore and AFM experiments.[38]

We use Eqs. 2.11, 2.12 and 2.13 to estimate how the effective aspect ratio of bottlebrush polymers changes as our DNA main-chains get progressively coated with more and more side chains. We also use the same equations to estimate how the effective aspect ratio changes at a fixed grafting density, when increasing the length of the side chains. Results are shown in Figure 2.10. In the calculations, we use $l_{\mathrm{p},DNA} = 50$ nm and $D_{\mathrm{DNA}} = 2.4$ nm, and $a = 0.5$ nm. For the case of a fixed side chain length we use $N = 400$, and for the case of a fixed grafting density we use $h = 2.0$ nm, both corresponding to the case of a fully coated DNA bottlebrush. Clearly, for small N, the effective thickness of the bottlebrush increases faster than the effective persistence length such that the aspect ratio decreases. Only at $N > 300$, the effective aspect ratio starts increasing again, but for $N = 400$, the predicted value of the aspect ratio is still only $\gamma \approx 8$, close to our experimental estimate. Likewise, at a fixed side chain length of $N = 400$, increasing the grafting density $1/h$ first leads to a decrease of the effective aspect ratio, followed by an increase at very high grafting densities, $1/h > 0.2$ nm^{-1}.

In summary, the numerical estimates clearly illustrate that for most practical conditions, bottlebrush coatings of semiflexible main-chains will lead to a decrease of the effective aspect ratio. Only for very extreme conditions (extremely long side chains at very high grafting densities), one may expect that the bottlebrush enhances the effective aspect ratio (as compared to that of the main-chain). The argument also holds for flexible main-chains, and explains why there are only few bottlebrush systems that exhibit lyotropic liquid crystalline behaviour.

Finally, the occurrence of lyotropic liquid crystalline behaviour is not only determined by the effective aspect ratio of the bottlebrushes, but also by their concentration, or more accurately, by their total mutually excluded volume. For our case, we observe that the effective aspect ratio is decreased by a factor of approximately 2...3. This means that for the bottlebrushes, liquid crystallinity may be expected to set in at higher volume fractions, where the relevant volume fraction is that corresponding to the hydrated volume of the bottlebrushes. For DNA the volume fraction where liquid crystallinity sets in is typically $\phi \approx 10\%$.[49] For our bottlebrush DNA with a protein to DNA mass ratio of $\Gamma = 25$, it sets in at around 8 mg/ml of DNA.

At this concentration, the typical distance between the DNA centers, as estimated from Figure 2.9, is $d \approx 40$nm. Assuming a parallel arrangement of the DNA bottlebrushes, and a diameter of the DNA bottlebrushes of $D \approx 30$nm, leads to an estimated effective volume fraction of bottlebrushes of $\phi_{eff} \approx 50\%$ when they start forming liquid crytalline phases, which is indeed much higher than for the bare DNA.

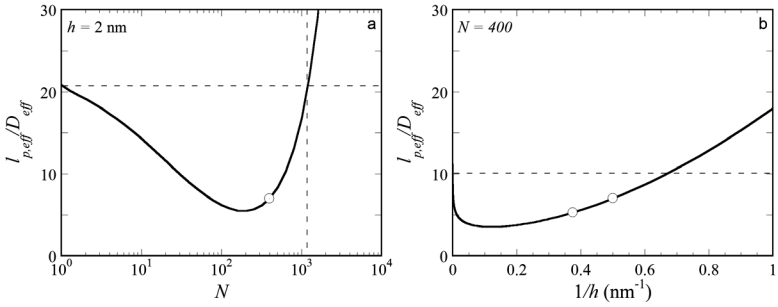

Figure 2.10: ***(a)*** *The predicted effective aspect ratio of DNA bottlebrushes plotted as a function of the number of side chains N, for DNA with $l_{DNA} = 50$ nm and at a grafting distance $h = 2$ nm. The vertical and horizontal dashed lines are used to identify where the original aspect ratio (bare DNA) is recovered by the DNA bottlebrush. The mark indicates a side chain length of $N = 400$.* ***(b)*** *The predicted effective aspect ratio of DNA bottlebrushes plotted as a function of the grafting density $1/h$ for DNA with $l_{DNA} = 50$ nm and $N = 400$ nm. The marks on the curve represent a grafting distance of 2.7 nm and 2 nm, from left to right.*

2.4 Conclusions

In summary, we have shown that grafting long linear side chains by electrostatic interactions on semiflexible DNA, leads to a reduction of the effective aspect ratio. Importantly, our results confirm a conjecture from numerical SCF modeling of polymer bottlebrushes, namely that at low grafting densities the aspect ratio decreases with coverage, while the expected increase occurs only at high grafting densities and large side chains. In this paper we have shown that our self-assembled DNA bottlebrushes still form lyotropic liquid crystalline phases, such that in our case the effective aspect ratio apparently did not decreases so much that lyotropic liquid crystalline behaviour was completely abolished. In nature,

molecular bottlebrushes, such as neurofilaments, also form lyotropic phases. Such neurofilaments combine a semi-flexible core with polypeptide projection domains. Our DNA bottlebrushes has similar characteristics and therefore may be a unique model system to understand more about these neurofilaments in ordered phases.

References

(1) Janmey, P. A.; Leterrier, J.-F.; Herrmann, H. *Curr. Opin. Colloid Interface Sci.* **2003**, *8*, 40–47.

(2) Beck, R.; Deek, J.; Jones, J. B.; Safinya, C. R. *Nat. Mater.* **2009**, *9*, 40–46.

(3) Hesse, H. C.; Beck, R.; Ding, C.; Jones, J. B.; Deek, J.; MacDonald, N. C.; Li, Y.; Safinya, C. R. *Langmuir* **2008**, *24*, 8397–8401.

(4) Beck, R.; Deek, J.; Safinya, C. R. *Biochem. Soc. Trans.* **2012**, *40*, 1027–1031.

(5) Beck, R.; Deek, J.; Choi, M. C.; Ikawa, T.; Watanabe, O.; Frey, E.; Pincus, P.; Safinya, C. R. *Langmuir* **2010**, *26*, 18595–18599.

(6) Kumar, S.; Yin, X.; Trapp, B. D.; Hoh, J. H.; Paulaitis, M. E. *Biophys. J.* **2002**, *82*, 2360–2372.

(7) Jones, J. B.; Safinya, C. R. *Biophys. J.* **2008**, *95*, 823–835.

(8) Fuchs, E.; Cleveland, D. W. *Science* **1998**, *279*, 514–519.

(9) Figlewicz, D. A.; Krizus, A.; Martinoli, M. G.; Meininger, V.; Dib, M.; Rouleau, G. A.; Julien, J. P. *Hum. Mol. Genet.* **1994**, *3*, 1757–1761.

(10) Klein, J. *Science* **2009**, *323*, 47–48.

(11) Klein, J. *Polym. Adv. Technol.* **2012**, *23*, 729–735.

(12) Seror, J.; Merkher, Y.; Kampf, N.; Collinson, L.; Day, A. J.; Maroudas, A.; Klein, J. *Biomacromolecules* **2011**, *12*, 3432–3443.

(13) Seror, J.; Merkher, Y.; Kampf, N.; Collinson, L.; Day, A. J.; Maroudas, A.; Klein, J. *Biomacromolecules* **2012**, *13*, 3823–3832.

(14) Raviv, U.; Giasson, S.; Kampf, N.; Gohy, J.-F.; Jerome, R.; Klein, J. *Nature* **2003**, *425*, 163–165.

(15) Sanjuan, S.; Perrin, P.; Pantoustier, N.; Tran, Y. *Langmuir* **2007**, *23*, 5769–5778.

(16) Wintermantel, M.; Gerle, M.; Fischer, K.; Schmidt, M.; Wataoka, I.; Urakawa, H.; Kajiwara, K.; Tsukahara, Y. *Macromolecules* **1996**, *29*, 978–983.

(17) Zhang, B.; Gröhn, F.; Skov Pedersen, J.; Fischer, K.; Schmidt, M. *Macromolecules* **2006**, *39*, 8440–8450.

(18) Borner, H. G.; Beers, K.; Matyjaszewski, K.; Sheiko, S. S.; Möller, M. *Macromolecules* **2001**, *34*, 4375–4383.

(19) Lecommandoux, S.; Chécot, F.; Borsali, R.; Schappacher, M.; Deffieux, A. *Macromolecules* **2002**, *35*, 8878–8881.

(20) Shi, Y.; Zhu, W.; Chen, Y. *Macromolecules* **2013**, *46*, 2391–2398.

(21) Rzayev, J. *Macromolecules* **2009**, *42*, 2135–2141.

(22) Chen, P.; Li, C.; Liu, D.; Li, Z. *Macromolecules* **2012**, *45*, 9579–9584.

(23) Jha, S.; Dutta, S.; Bowden, N. B. *Macromolecules* **2004**, *37*, 4365–4374.

(24) Engler, A. C.; Lee, H.; Hammond, P. T. *Angew. Chem. Int. Ed.* **2009**, *48*, 9334–9338.

(25) Fredrickson, G. H. *Macromolecules* **1993**, *26*, 2825–2831.

(26) Feuz, L.; Leermakers, F. A. M.; Textor, M.; Borisov, O. V. *Macromolecules* **2005**, *38*, 8891–8901.

(27) Rathgeber, S.; Pakula, T.; Wilk, A.; Matyjaszewski, K.; Beers, K. L. *J. Chem. Phys.* **2005**, *122*, 124904-2–12.

(28) Saariaho, M.; Ikkala, O.; Szleifer, I.; Erukhimovichm, I.; ten Brinke, G. *J. Chem. Phys.* **1997**, *107*, 3267–3276.

(29) Rouault, Y.; Borisov, O. V. *Macromolecules* **1996**, *29*, 2605–2611.

(30) Wintermantel, M.; Fischer, K.; Gerle, M.; Ries, R.; Schmidt, M.; Kajiwara, K.; Urakawa, H.; Wataoka, I. *Angew. Chem. Int. Ed.* **1995**, *34*, 1472–1474.

(31) Ikkala, O.; Ruokolainen, J.; ten Brinke, G.; Torkkeli, M.; Serimaa, R. *Macromolecules* **1995**, *28*, 7088–7094.

(32) Ruokolainen, J.; Tanner, J.; ten Brinke, G.; Ikkala, O.; Torkkeli, M.; Serimaa, R. *Macromolecules* **1995**, *28*, 7779–7784.

(33) Ruff, Y.; Moyer, T.; Newcomb, C. J.; Demeler, B.; Stupp, S. I. *J. Am. Chem. Soc.* **2013**, *135*, 6211–6219.

(34) DeRouchey, J.; Walker, G. F.; Wagner, E.; Rädner, J. O. *J. Phys. Chem. B* **2006**, *110*, 4548–4554.

(35) Hernandez-Garcia, A.; Werten, M. W. T.; Cohen Stuart, M. M. A.; de Wolf, F. A.; de Vries, R. *Small* **2012**, *8*, 3491–3501.

(36) Levy-Sakin, M.; Ebenstein, Y. *Curr. Opin. Biotechnol.* **2013**, *24*, 690–698.

(37) Dorfman, K. D.; King, S. B.; Olson, D. W.; Thomas, J. D. P.; Tree, D. R. *Chem. Rev.* **2013**, *113*, 2584–2667.

(38) Zhang, C.; Hernandez-Garcia, A.; Jiang, K.; Gong, Z.; Guttula, D.; Ng, S. Y.; Malar, P. P.; van Kan, J. A.; Dai, L.; Doyle, P. S.; de Vries, R.; van der Maarel, J. R. C. *Nucleic Acids Res.* **2013**, 1–8.

(39) Golinska, M. D.; de Wolf, F. A.; Cohen Stuart, M. M. A.; Hernandez-Garcia, A.; de Vries, R. *Soft Matter* **2013**, *9*, 6406–6411.

(40) Huang, N.; Vörös, J.; de Paul, S. M.; Textor, M.; Spencer, N. D. *Langmuir* **2002**, *18*, 220–230.

(41) Altgelt, K.; Hodge, A. J.; Schmitt, F. O. *Proc. Natl. Acad. Sci. U. S. A.* **1961**, *47*, 1914–1924.

(42) Li, Y.; Beck, R.; Huang, T.; Choi, M. C.; Divinagracia, M. *J. Appl. Cryst.* **2008**, *41*, 1134–1139.

(43) Gommes, C. J.; Goderis, B. *J. Appl. Cryst.* **2010**, *43*, 352–355.

(44) Ben-Nun, T.; Ginsburg, A.; Szekely, P.; Raviv, U. *J. Appl. Cryst.* **2010**, *43*, 1522–1531.

(45) Van der Schoot, P. *J. Chem. Phys.* **1996**, *104*, 1130–1139.

(46) Khokhlov, A. R.; Semenov, A. N. *Physica A* **1981**, *108*, 546–556.

(47) Odijk, T. *Polym. Commun.* **1985**, *26*, 197–198.

(48) Odijk, T. *Macromolecules* **1986**, *19*, 2313–2329.

(49) Livolant, F.; Leforestier, A. *Prog. Polym. Sci.* **1996**, *21*, 1115–1164.

3 Loss of Bottlebrush Stiffness due to Free Polymers

Abstract

A recently introduced DNA-bottlebrush system, which is formed by the co-assembly of a genetically engineered cationic polymer-like protein together with DNA, is subjected to osmotic stress conditions. We measure the inter-DNA distances by X-ray scattering. Our co-assembled DNA-bottlebrush system is one of a few bottlebrushes known to date that shows liquid crystalline behaviour. Interestingly, the alignment of the DNA bottlebrushes did not always improve upon increasing the pressure. Molecularly detailed self-consistent field calculations targeted to complement the experiments, focused on the induced persistence length due to the side chains in the bottlebrush architecture, as well as on the pressure built-up upon reducing the distance between the bottlebrushes. Notably, the calculations were also used to consider the response of DNA-bottlebrush to freely dispersed protein-polymers. It was found that both the thickness of the bottlebrush side chains as well as the backbone persistence length drop with increasing protein-polymer bulk concentrations above the overlap concentration. The latter is more significant and therefore the bottlebrush aspect ratio, l_p/D, decreases with protein-polymer concentration. We argue that both freely dispersed polymers as well as a reduction of inter-DNA distances undo the induced stiffening. Therefore, at high concentrations the bottlebrush rigidity relaxes back to that of the original backbone. This loss of rigidity is yet another argument why molecular bottlebrushes rarely order in anisotropic phases.

In preparation: Storm, I. M.; Kornreich, M.; Beck, R.; Voets, I. K.; de Vries, R.; Cohen Stuart M. A.; Leermakers, F. A. M. Loss of Bottlebrush Stiffness due to Free Polymers

3.1 Introduction

The term "bottlebrush" denotes macromolecular architectures that consist of a backbone with many densely attached and therefore stretched side-chains compared to the Gaussian dimensions.[1] Bottlebrush systems have been investigated intensively by experimentation,[2–4] theory[5–8] and simulations.[9–15] A well known application for polymer brushes can be found in lubrication of materials.[16–20] The aggrecan molecule is a famous biological lubricant. Aggrecan is part of the articular cartilage that ensures the lubrication of joints in the human body.[21–24] This molecule in fact has a bottlebrush on a bottlebrush structure which means that the side-chains have a bottlebrush structure themselves. Aggrecan has highly charged polysaccharide side chains and therefore has a tremendous capability to hold water even under large pressures. This ability to attract water results in a swollen structure that reduces the friction of the joints and thereby prevents wearing down of these joints.

Another biological bottlebrush system is the anisotropic neurofilament gel-like network which provides mechanical stability and strength to high aspect ratio neuronal cells. Neurofilaments have a compact rigid cylindrical core with polypeptide side-chains, which have an unstructured polymer-like domain that stretch away from the core due to electrostatic- and steric lateral interactions. The liquid crystalline network that neurofilaments form arguably have a role to resist external pressures.[25–29]

Recently we introduced a model bottlebrush system which is extremely well defined in molecular terms. Moreover, it is definitely less complicated than the natural counterparts, yet having comparable physical properties. In addition, this system is able to show liquid crystalline behaviour.[30] We use the semi-flexible double stranded DNA (dsDNA) chain as the core of the bottlebrush. For the side chains we use a recombinant protein polymer. These macromolecules are unique because they are strictly monodisperse and chirally pure. The name that is used, C_4K_{12}, reflects its functionality.[31] The binding block consist of 12 positively charged lysines (K_{12}) that bind electrostatically to the negatively charged DNA backbone. The C_4-block is a 400 aa hydrophilic randomly structured collagen-like block, a concatination of four sequences of 100 aa. This collagen-like block has no significant secondary or tertiary structure and forms the corona of the co-assembly.[32] As the grafting density of the corona is sufficiently high, the thickness of the corona is more than twice the radius of gyration of the free protein, the C_4-chain blocks are strongly stretched.[30] That is why we can refer to these constructs as co-assembled molecular DNA-bottlebrushes.

From a theoretical perspective we expect that co-assembled bottlebrushes can, to first order, be considered as molecular bottlebrushes with covalently grafted side chains. Fredrickson was the first to analyze the effect of side chains on the physical properties of the bottlebrush and hypothesized that the side chains would help flexible backbones (main-chains) to form liquid crystalline phases.[33] Subsequent self-consistent field modelling revealed that the induced persistence length increases quadratically with the coverage of side chains along the main-chain, i.e. $l_p \propto (N/h)^2$ where N is the number of segments of the side chains and h the distance between the side chains along the backbone, see Figure 3.1(a).[7] Theoretical approaches[7,34] agree that the thickness of a bottlebrush scales as $D \propto N^{3/4}h^{-1/4}$ and therefore one would expect the segment aspect ratio l_p/D to increase with increasing N and decreasing h. Although this behaviour is undisputed for large N, the very small value for the numerical prefactor for the mentioned persistence length l_p dependence, leads to the insight that in experimental cases the aspect ratio l_p/D remains small. Accordingly, it explains why most bottlebrushes are flexible and so few are known to form liquid crystals. In the current paper we will argue that there is yet another reason why bottlebrushes show a low tendency towards liquid crystallinity.

Bottlebrush molecules are critical components of systems which are required to withstand high external pressures.[35–38] To investigate how pressure influences the distances and alignment of our DNA-bottlebrushes we submitted the system to an external osmotic pressure. We used a poly(ethyleneglycol) (PEG) solution,[39,40] separated by a membrane to avoid the loss of C_4K_{12} chains. The inter-DNA spacing was measured by means of small angle X-ray scattering (SAXS) in the regime where the system is liquid crystalline. The alignment and also the loss in liquid crystalline alignment were investigated by complementary self consistent field (SCF) calculations. In line with our experiments, the SCF calculations indicate that the presence of free polymer does not necessarily promote liquid crystalline behaviour.

In our system the bottlebrushes are formed by a co-assembly of protein-polymers with dsDNA. In such a system the freely dispersed polymers cannot be ignored. We will present evidence that these freely dispersed polymers do affect the aspect ratio of the bottlebrush molecules. This observation is relevant for the biological context, as in biological systems bottlebrushes will never be in a single molecule state and invariably surrounded by freely dispersed macromolecules. The response of molecular bottlebrushes on such crowding effects has been partly

addressed in the literature. The effect of bottlebrush concentration was theoretically considered by Borisov,[41] and experimentally shown by Rathgeber and Bolisetty,[42,43] but the effect of free polymer has not been explicitly considered.

3.2 Materials and Methods

3.2.1 Production and Purification of C_4K_{12}

The protein used in this work, C_4K_{12}, was biosynthesized by genetically modified *Pichia Pastoris* cells, carrying a gene that encodes for the secreted expression of the diblock protein polymer C_4K_{12}.[31]

After the fermentation was completed the protein solution was separated from the yeast cells by centrifugation (16000 *g*, 30 min, 4 °C) and filtration (0.2 μm Acropak 200 capsules with Supor membrane from Pall Corporation). To purify the produced C_4K_{12} protein we first increased *p*H to 8 using NaOH and centrifuged (16000 *g*, 30 min, 4 °C) the protein solution to remove the majority of medium salts. After centrifugation C_4K_{12} proteins were separated from secreted *Pichia Pastoris* proteins by selective precipitation with ammonium sulphate (45% saturation). This precipitation step was performed for 30 minutes at 4°C. The C_4K_{12} pellet was redissolved in 0.2 times the original volume ($\sim$ 1 l) of 50 mM formic acid and extensively dialysed against 50 mM formic acid. During the last dialysis step the proteins were dialysed against a 10 mM formic acid solution. Consecutively, the C_4K_{12} solution was freeze dried.

3.2.2 DNA Preparation

For the preparation of the DNA bottlebrushes we used DNA type II fibers (Sigma). The DNA was dissolved in a 10 mM Tris-HCl buffer of *p*H 7.6 to a concentration of 2 mg/ml. The DNA solution was sonicated with a Bandelin Sonopuls GM 70 (power 2/3 and 100% cycle) to decrease the length of DNA. The solution was sonicated for 10 minutes to obtain DNA fragments of approximately 500-1000 base pairs (bp).[30]

3.2.3 Sample Preparation

The concentrated DNA-C_4K_{12} co-assemblies were prepared by mixing the DNA and C_4K_{12} in the desired ratio in a dilute solution. After overnight incubation the samples were concentrated using centrifuge filters (Amicon Ultra-0.5 ml 3K membrane). The samples were washed with a 10 mM

Tris-HCl buffer of *p*H 7.6 with 0.05% NaN_3 to remove excess salt. The DNA-C_4K_{12} complexes were placed in small 3.500 MWCO Slide-A-Lyzer MINI dialysis units. These dialysis units were placed in 50 ml falcon tubes with a solution consisting of a specific PEG concentration. This PEG solution was made by first making a 40 wt% PEG solution in a 10 mM Tris-HCl buffer of *p*H 7.6 with 0.05% NaN_3. The 40 wt% PEG solution was then diluted with Tris buffer to the appropriate PEG concentration. The incubation period was one week. Conversion from wt% PEG to pressure was done according to:

$$\Pi = 10^{a+b\times(wt\%)^c} \tag{3.1}$$

where $a = 1.57$, $b = 2.75$ and $c = 0.21$.[39]

3.2.4 SAXS

Our concentrated samples were placed in Hilgenberg quartz capillaries with an outer diameter of 1 mm and a wall thickness of 0.01 mm. The concentrated samples for the osmotic stress experiments were measured on a SAXS-LAB instrument with a Xenocs GeniX Low Divergence Cu Kα X-ray source in combination with a Pilatus 300 K detector (Dectris, Baden, Switzerland). A wavelength of 1.54 Å was used together with sample-detector distances of 110, 710 and 1510 mm respectively. With these configurations we have a q-range available of 0.006-2.41 $Å^{-1}$. A typical data acquisition time was 1800 s. The 2D data was then radially averaged using the SAXSGUI software to produce 1D plots of intensity as a function of q.

The samples that consisted of a low concentration of DNA and protein polymers were used to determine the brush thickness of the DNA-bottlebrushes. For the samples we used 250 μg/ml λ-DNA in the presence of a three times excess amount of C_4K_{12} protein polymer of 7.5 mg/ml, which is denoted as $\Gamma = 30$. For the sample consisting only of free protein we used a concentration of 30 mg/ml. These low concentration samples were measured at the I911-4 beamline at MAXlab II, Lund, in Sweden. The q-range we used corresponded to 0.008-0.550 $Å^{-1}$ with an incident wavelength of 1.2 Å. The samples were measured in a 'high throughput solution scattering set-up' to properly subtract the buffer from the sample at exactly the same location in the capillary. The detector used was a PILATUS 1M detector from Dectris. The acquisition time for each sample was 20 minutes. The data processing was done by using SASview 3.0.0 software.

To fit our scattering data we used two types of models. To describe the experimental data collected for the free C_4K_{12} protein polymers in solution we used a model for polymers with excluded volume,[44,45] for the DNA-bottlebrushes we used a model for randomly oriented homogeneous cylinders.[46,47]

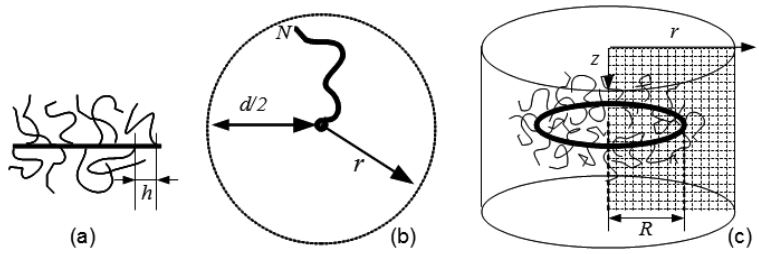

Figure 3.1: *A schematic bottlebrush molecule used in the SCF calculations where h is depicted as the distances between side chains (a). A top-view of a schematic representation of the cell model: where the backbone of the bottlebrush is in the middle of the figure going into the plane of the figure. The circular dotted line represents a mirror boundary condition, N the length of the side chains, d/2 is the distance between the brush and its image and r represents radial coordination (b). The third figure shows a two gradient cylindrical coordination system with a homogeneously curved bottlebrush. R is the radius of curvature (curvature is J = 1/R), z the direction along the longest axis of the cylinder and r the radial coordinate (c).*

3.2.5 SCF-Calculations

Numerical self-consistent field calculations with the discretisation scheme of Scheutjens and Fleer (SF-SCF)[48] have been performed using the sfbox program. In this approach the volume is represented by a lattice with characteristic size $b = 5 \times 10^{-10}$ m. All linear lengths are given in units b. Macromolecules are modelled as freely jointed chains (FJC) with segment size equal to the lattice site. In the FJC model two consecutive bonds along the chain have uncorrelated directions, while nearest neighbour segments occupy nearest neighbour lattice sites. In contrast to Gaussian chains, FJC thus have a finite extensibility. Below we will use a one-gradient cylindrical coordinate system (cell model) to evaluate the pressure-distance relation for compressed bottlebrushes (cf. Figure 3.1(b)). In this case we have cylindrically curved layers of lattice sites $\mathbf{r} = r = 1,\ 2,\ \cdots\ d/2$, where d is the distance between two DNA chains. The number of lattice sites at r is given

by $L(r) = 2r - 1$. A two-gradient cylindrical coordinate system is used to evaluate the induced persistence length (cf. Figure 3.1(c)). In this case we have coordinates $\mathbf{r} = (z, r)$, where the radial coordinate is similar to the one-gradient case and the z-coordinate is used to number lattice layers in the direction along the cylinder axis $z = 1, , 2 \cdots, M$.

Typical for the SCF theory a local mean-field approximation is introduced, which means that at a given coordinate $\mathbf{r}$ the segment densities are averaged, so that the relevant concentration can be expressed as a volume fraction $\varphi(\mathbf{r})$. Using this mean-field approximation it is possible to enumerate the number of contacts between segments in the system and each contact is weighted by the Flory-Huggins interaction parameters, which are non-zero for all unlike contacts. The SCF theory is based on optimization of a free energy functional, which leads to a SCF "machinery" working as follows. The effect of surrounding molecules on the conformation of a particular component is expressed in terms of a potential field $u(\mathbf{r})$ which is computed from the volume fractions $\varphi_X(\mathbf{r})$ of the segments. The volume fraction, in turn, can be found after statistical evaluation of the conformations.

Osmotic Stress Calculations

Osmotic stress calculations are performed in a one-gradient cylindrical coordinate system. A graphical representation is given in Figure 3.1(b). The DNA chain is assumed to sit with its center-of-mass at $r = 0$. The bottlebrush is composed of N segments of which the first segment is constrained to be at the DNA main-chain location. For each calculation the number of chains per unit length $(1/h)$ of the DNA is an input quantity.

For a given SCF solution we have the free energy of the system available. The free energy can be expressed in terms of the volume fraction and segment potential profiles $F = F(\{\varphi, u\})$.[48] In the cell model we can compute the free energy for a given value of the cell size $d/2$. At the system boundary we have reflecting boundary conditions which implies that the 6 'images' (assuming hexagonal ordering) of the central DNA chain are located at a distance d from the central chain. After the SCF equations are solved the free energy is recorded as $F(d/2)$. Subsequent variations of the value of d give a free energy interaction

$$\Delta F(d/2) = F(d/2) - F(\infty) \tag{3.2}$$

which has units of $k_B T$ per unit length b of the DNA chain. A pressure has the units $k_B T/b^3$, and we use the cross-sectional area $A(d) = \pi (d/2)^2$

to convert the free energy of interaction to a pressure as a function of the distance.

$$\Pi(d) = \frac{\Delta F(d/2)}{A(d)} \tag{3.3}$$

with units $k_{\mathrm{B}}T/b^3$. Using a lattice size $b = 5 \times 10^{-10}$ m, gives for $\Pi(d) = 1$ a pressure 32×10^6 Pa.

Induced Persistence Length

Referring to Figure 3.1(c) for an illustration, we position a bottlebrush chain with its backbone location $\mathbf{r} = (M/2, R)$ such that the radius of curvature is R and the curvature of the backbone is $J = 1/R$. Onto the backbone we pin linear chains with length N by their first segment. The contour length of the torus-like backbone is $L = \pi(2R - 1)$ and thus we fix the number of chains to the backbone to be $n = L/h$. The mean-field approximation allows for non-integer number of grafted chains. In the calculations we allow for freely floating PEG polymers in solution. As the volume fraction of these chains is an input quantity, we compute the characteristic free energy of the system as

$$\Omega(J) = F(J) - n_{C_4}\mu_{C_4} \tag{3.4}$$

where μ_{C_4} is the chemical potential of the protein-polymers (unique function of the volume fraction in the bulk), and n_{C_4} is the number of C_4 (free-floating) chains in the system. As J is a small quantity with respect to the uncurved bottlebrush, we can expand in a taylor series the free energy per unit length $\omega = \Omega/L$:

$$\omega(J) = \omega(0) + \frac{1}{2}k_c J^2 \tag{3.5}$$

Here $k_c = \frac{\partial^2 \omega}{\partial J^2}$ is the bending rigidity which has the units $k_B T l$. The odd terms in J can be omitted for symmetry reasons and higher order terms are omitted as we will consider only the limit of small values of J. Dividing the bending rigidity by the thermal energy may be identified as the induced persistence length

$$l_{\mathrm{p}} = \frac{k_c}{k_B T} \tag{3.6}$$

It is easily checked that bending a chain with length $2l_{\mathrm{p}}$ with a curvature given by $J = 1/l_{\mathrm{p}}$ will deflect the chain by about 60 degrees from its original direction.

In practice we evaluate $\omega(J)$ for a series of J values and then plot $(\omega(J) - \omega(0)) \times 2/J^2$ as a function of J. The idea is that a horizontal line will result, which lies at k_c. Important for this procedure is an accurate value of $\omega(0)$.

As lattice artifacts introduce numerical noise in the calculations, we fine tune the value of $\omega(0)$ such that the predictions of k_c are evenly distributed around an average value, which is then taken as the final results.

Bottlebrush Cross-Sectional Diameter

In this section we examine the cross-sectional radius of the bottlebrush. We compute this in the cell model with freely dispersed C_4 chains in solution. The radial volume fraction profile for the grafted chains is directly available after the SCF equations have been solved. We use the first moment of the distribution of the end-segments of the grafted chains to estimate the extension (height) of the bottlebrush:

$$D = \frac{1}{h} \sum_r r n(r) \tag{3.7}$$

Where $n(r) = \pi(2r-1)\varphi_e(r)$ is the number of end-points located at a distance r (in lattice units) from the central DNA chain. The factor $1/h$ equals the number of (side) chains per unit length along the DNA main-chain.

3.2.6 Modelling Parameters

As mentioned before, all linear lengths are presented in lattice units b, for which we take $b = 5 \times 10^{-10}$m. In the experiments we have C_4K_{12} chains of which the 12 lysines represents the binding domain. We do not cover here the physisorption mechanism and represent the bottlebrush by covalently linked chains onto a rigid phantom backbone. Freely dispersed polymers are therefore also taken to have 400 segments. In theoretical studies one typically chooses athermal solvent conditions. However, as we are aiming the calculations to represent the experimental case, we consider a 'marginal' solvent having a more realistic (still ad hoc) value $\chi = 0.4$, typical for many water-soluble polymers. The distance between chains in the bottlebrush is estimated from previously measured binding isotherms to be around 2 nm which implies $h \approx 4$.[30] We have varied h around this estimated value and used $h = 2$, 4, and 8.

3.3 Results and Discussion

In this section we will first discuss X-ray scattering experiments on dilute samples from which we extract the bottlebrush structure in the presence

of freely dispersed protein-polymers. In the analysis of the osmotic stress experiments we focus on the position and the width of the first structure peak. These results are the targets of the SCF calculations which are presented in the second half of this section.

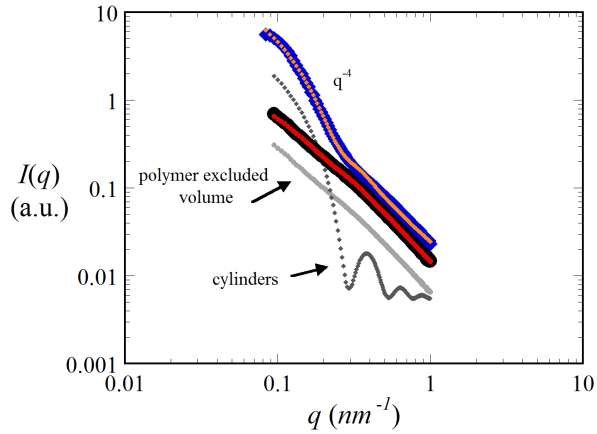

Figure 3.2: *Small angle X-ray scattering $I(q)$ curves of (i) the DNA-C_4K_{12} complexes (250 µg/ml of DNA) (blue) in the presence of excess protein polymers ($\Gamma = 30$) and (ii) C_4K_{12} protein solution (10 mg/ml) (black) with corresponding fittings as discussed in the text. The gray curves represent the relative contributions to the fit of the total scattering curve. For clarity reasons, the relative contributions were scaled down.*

3.3.1 Thickness of Brush Layer

In principle one can extract the structural information of the molecular bottlebrushes from small angle X-ray scattering. These experiments are challenging because the data have to be taken at concentrations low enough to ignore the structure factor, implying long acquisition times. Fortunately, the structure factor information can be pushed to lower values of q such that it is possible to extract the cross-sectional information from the X-ray scattering from the $0.1 < q < 2$ nm^{-1} range, cf. in Figure 3.2. In this example we have besides the DNA-bottlebrush also freely dispersed protein polymers. That is why the fitting is still non-trivial.

Let us focus first on the scattering of freely dispersed protein polymers C_4K_{12} also shown in Figure 3.2 (in black). In this case the free protein-polymer has a concentration of 10 mg/ml and is dissolved in a 10 mM Tris-HCl buffer of *p*H 7.6. These molecules behave polymer like and that

is why we used a "polymer excluded volume" model. The corresponding fit (red) gives a radius of gyration of 8.3 nm for the protein polymer C_4K_{12} which is reasonable for a polymer consisting of 400 segments.

The DNA-bottlebrushes in the presence of free protein produce the blue scattering profile in Figure 3.2. The data was fitted by a model combining two scattering entities: (i) a cylinder and (ii) a polymer with excluded volume. The fitting parameters for the polymer excluded volume model were taken from the reference sample of free C_4K_{12} protein polymer. The information for the brush diameter can be obtained from the q-range: $0.1 < q < 0.3$ nm^{-1} were the rod-like structure dominates the scattering of the free protein. As a brush radius we find 13 nm, which is about twice the radius of gyration of the free protein. This means that the side-chains were forced to stretch when attached to the DNA backbone molecule. This is in line with previously reported binding isotherms[30] from which it was estimated that under the present conditions there is about one C_4K_{12} chain per 2.7 nm DNA contour length, which implies short grafting distances. Much closer than the R_g value of 8.3 nm for the free protein.

3.3.2 Osmotic Stress Experiments

The driving force for bottlebrush formation is the attraction of opposite charges. More specifically, the positive charges of the lysines tend to form ion pairs with the negative phosphate charges on the DNA. When this happens, the C_4 block becomes concentrated in the corona of the complex. Considering this mechanism it is clear that with increasing protein coverage the net negative charge on the complex decreases. Hence the driving force for adsorption decreases. For this reason it is not expected that full coverage is found at $\Gamma = 10$ g/g, which is the (charge)stoichiometric ratio. In addition, we have chosen to use a three-fold excess in protein-polymers, that is $\Gamma = 30$ g/g. At this ratio, at least two out of three of the protein polymers are free in solution. Considering the fact that there is generally little bulk volume, we infer that the protein-polymer solution, under these conditions, is in the semi-dilute regime.

In previous experiments[30] we concentrated DNA-protein-polymer complexes by centrifugation and then changed concentration by dilution. In such experiments it is unknown at what osmotic pressures the resulting complexes reside. Therefore we performed osmotic stress experiments. The liquid crystallinity of our samples facilitated the measurement of the inter-DNA distances by X-ray scattering. We performed the osmotic stress experiments by bringing the DNA protein-polymer solution in contact with

a PEG solution. We first tried to do this without using a membrane. It was found that the PEG solution phase separated from the DNA-bottlebrush solution but that individual protein polymers slowly diffused into the PEG phase. Over time the protein-polymers detached from the DNA, which was concluded from a drift in the inter-DNA spacing. For this reason a membrane was used which prevented the protein-polymers from leaving the system and also prevented the PEG solution from entering the system. The equilibration time of the osmotic stress experiments is faster than one day as proven by the time evolution of the position of the first Bragg-peak shown in Figure A7.1 of the Appendix. To be on the safe side we, therefore, equilibrated our samples for one week prior to SAXS measurements.

The inter-DNA distances d are found from the positions of the first Bragg-peaks of the X-ray scattering curves. To find precise peak positions, we fitted $I(q) \times q$ by a parabola: $I = I(q_0) + b_q(q - q_0)^2$ in a q-range near the first Bragg peak. From this fit we found the position of the maximum q_0, and the corresponding distance d follows from

$$d(\text{nm}) = \frac{2\pi}{q_0} \tag{3.8}$$

We also determine the dimensionless width as

$$w = b_q q_0^2 \tag{3.9}$$

The resulting distances d are presented in Figure 3.3(a) as a function of the osmotic pressure of the PEG solution (the corresponding scattering data I(q) for both $\Gamma = 10$ and $\Gamma = 30$ can be found in the Appendix, cf. Figure A7.2 and A7.3 respectively). In Figure 3.3(b) we give the corresponding dimensionless width of the first Bragg peak.

Figure 3.3(a) shows that, for given values of the osmotic pressure, the sample with the excess amounts of protein polymer ($\Gamma = 30$) has about 5 nm larger distances between the DNA backbone of two adjacent DNA-bottlebrushes than that at stoichiometric composition ($\Gamma = 10$). Recall that the typical size of the brush has a diameter of 26 nm. Hence when the inter-DNA distance is less than 26 nm the brushes are confined by the applied osmotic stress. Inspection of Figure 3.3(a) shows that in the range of applied pressures all distances are significant less than the unperturbed diameter, and we conclude that the brushes are compressed, to a maximum extent of about a factor of two.

To a reasonable approximation the distance between the bottlebrushes is a logarithmic function of the osmotic pressure. Below we will show that an

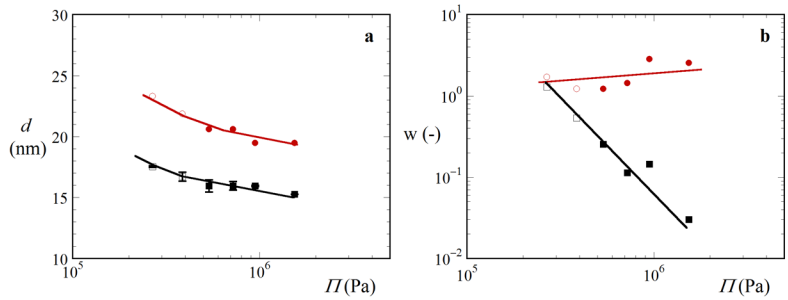

Figure 3.3: *a) The distances, d (nm), estimated from the position of the first Bragg peak between DNA-bottlebrushes as a function of the osmotic pressure* Π *(Pa) in lin-log coordinates. b) The corresponding dimensionless width w as a function of the pressure* Π *(Pa) in log-log coordinates. The red data points represent samples with a protein to DNA charge ratio of* $\Gamma = 30$ *and the black data points have a ratio of* $\Gamma = 10$*. Closed symbols belong to anisotropic samples and open symbols correspond to isotropic samples.*

even better linear dependence of $d(\log \Pi)$ is predicted by SCF calculations in a cell model. Experimentally, upon reducing the distance between the bottlebrushes one will always concentrate the proteins because they can not escape from the system. In the modelling, this concentration effect is not accounted for. Hence we argue that the slight non-linearity of the $d(\log \Pi)$ curve must be attributed to the concentrating-effect of the freely dispersed proteins, which comes on top of the compression of the bottlebrushes.

In passing we mention that already at very low applied pressures ($< 4 \times 10^5$ Pa) the anisotropy of the solution was lost as judged from illumination through a crossed-polarizer set-up. The points for which this was the case are given by the open symbols, whereas all the anisotropic solutions are represented by closed symbols in Figure 3.3. Note that no jump in distances is observed at the pressure where the anisotropy of the solution is lost, indicating that the density differences between the isotropic and anisotropic phases is minute.

One might expect that with increasing applied osmotic pressure the bottlebrushes are pushed against each other and therefore would become more perfectly ordered. One thus would expect the first Bragg peak to sharpen up upon an increase of the osmotic pressure. Upon comparing the scattering curves of $\Gamma = 10$ with $\Gamma = 30$ (Figure A7.2 and A7.3 in the Appendix) it can be seen that the Bragg peaks of $\Gamma = 10$ seem to become

sharper and more pronounced, but the peaks of the $\Gamma = 30$ samples do not. So the expected increase in order upon the increase of the osmotic pressure is seen for $\Gamma = 10$ but not for $\Gamma = 30$ samples.

Furthermore, we measured the width of the first Bragg peaks and present the results in Figure 3.3(b). Inspection of this figure proves that the width decreases (as a power-law) for the stoichiometric case $\Gamma = 10$, whereas it is almost constant or becomes even wider with pressure for the protein overdosed system, $\Gamma = 30$. At this stage we may speculate about why the order for the $\Gamma = 30$ samples does not increase. Possibly, the excess of protein-polymer takes up so much space that the alignment is disrupted. At this point we have no plausible explanation and we return to this point in our modelling system.

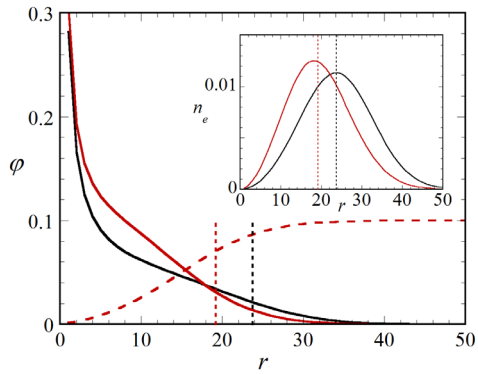

Figure 3.4: *Radial volume fraction profile $\varphi(r)$ for the default case $h = 4$ and side chains $N = 400$ for marginal solvent conditions $\chi = 0.4$ in the absence of free polymer (black curve) and in the presence of free polymers (red curve). The free polymers are $N = 400$ segments long with a bulk volume fraction of $\varphi^b = 0.1$ (dashed profile). In the inset we give the number distribution $n(r)$ of the free ends of the grafted chains, both in the presence (red) and in the absence (black) of free polymer. The vertical dotted lines represent the mean position of the end-points which is a measure for the thickness of the brush D (in lattice units).*

3.3.3 Self Consistent Field Calculations

We use SCF theory (applying the discretisation scheme of Scheutjens and Fleer) to model molecular bottlebrush structure and thermodynamics (mechanics) with the aim to find possible explanations for the rather surprising results of the osmotic stress experiments. We decided not to consider the electrostatic binding adsorption mechanism and opted for a bottlebrush model for which the grafting density is an input quantity ($h = 4$ is the default and $h = 2$, 8 are used for comparison reasons). We have seen that, experimentally, there is an effect of freely dispersed polymer and that is why we keep the bulk concentration of polymer as an extra control parameter in the calculations. A bulk volume fraction of $\varphi^b \approx 0.01$ signals the start of the overlap (semi dilute) regime. We stress that in experiments the polymer concentration and the grafting density are coupled parameters. Not so in our model for which we can treat these parameters as independent.

Let us first focus on the SCF prediction of the cross-sectional distribution of the side chains. In Figure 3.4 we present the radial volume fraction distribution of the grafted side chains. Wijmans *et al.* have shown that in the first few layers a power-law decay is found which gives way to a quasi-parabolic profile in the outer region of the profile.[49] Completely in line with this the radial concentration profile drops quickly with increasing distance from the main-chain (increasing r). When free polymer is added to the system we notice a significant compression. Clearly, as soon as the concentration of polymer exceeds the local density in the brush, it becomes favourable for the brush chains to reduce the tension along the chain and become more dense. Below we will quantify this effect. In the inset of Figure 3.4 we present the distribution of the free ends. This distribution is bell-shaped: the ends can distribute throughout the brush albeit that they tend to avoid the region extremely close to the backbone. The average position of the ends is taken as a measure of the brush size and is indicated by the vertical dotted lines.

The brush dimension D is computed for three values of h (2, 4, and 8) as a function of the bulk volume fraction of freely dispersed polymers and presented in lin-log coordinates in Figure 3.5. Obviously the brush height increases with increasing grafting density (decreasing h) closely following the theoretical power-law prediction $D \propto h^{-1/4}$ (not shown). With respect to the dependence on the polymer concentration in the bulk, there are clearly two regimes. As long as the polymer concentration in the bulk remains dilute the brush height is independent of the polymer concentration. For higher concentrations the height drops steeply (approximately logarithmic)

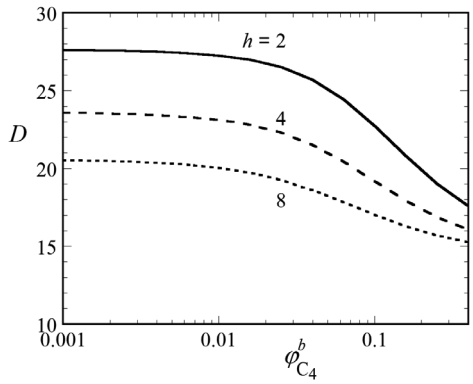

Figure 3.5: *The brush height (D) in lattice units b as a function of the volume fraction φ^b of freely dispersed C_4 (400 segments long) chains for three values of the grafting distance $h = 2, 4, 8$.*

with the bulk volume fraction. Below we will show that the brush thickness decreases when the DNA chains are pushed towards each other by an applied osmotic stress.

The compression of the brush by free polymers may also be seen as a compression due to an applied osmotic stress. In this case the stress is due to the concentration of the polymers. In the semi-dilute regime the mean-field pressure of a polymer solution is expected to scale quadratically with the polymer concentration. Hence the almost linear drop with $\log(\varphi^b)$ implies a corresponding drop with applied $\log(\Pi)$. One may argue that there is a difference between compressing the brush with an opposing brush or with freely dispersed polymers. However these differences are minor especially as the dominant factor is driven by the polymers avoidance from interpenetration.

Before presenting the results of the cell-model we will first briefly present our results of the induced persistence length of the bottlebrush as a function of the bulk volume fraction of freely dispersed polymers ($\varphi^b_{C_4}$). To the best of our knowledge there are no predictions in the literature for this dependence. In Figure 3.6 we show the results in double logarithmic coordinates for three values of the grafting density. Analytical theory predicts that the induced persistence length increases quadratically with $1/h$ and the calculations are in good agreement with this.[7,34] As in

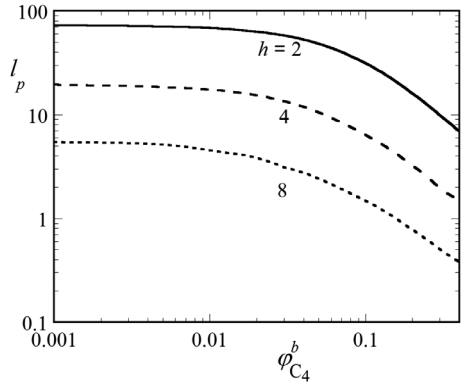

Figure 3.6: *Induced persistence length (l_p) of the bottlebrush as a function of bulk volume fractions φ^b of the freely dispersed C_4 polymers for three values of the grafting density (i.e. distance between grafts $h = 2, 4, 8$) in double logarithmic coordinates.*

Figure 3.5, which depicts D vs. $\varphi^b_{C_4}$, we again see two regimes. For concentrations below overlap the bending rigidity of the bottlebrushes is independent of $\varphi^b_{C_4}$. However, above this concentration there is a power-law dependence with a slope not far from −1. Hence the induced persistence length drops inverse proportionally to the bulk volume fraction of freely dispersed polymers as soon as the bulk concentration of polymers is in the semi-dilute regime. Apparently, as soon as the brush chains are no longer strongly stretched, the bottlebrush loses part of its induced rigidity.

As explained above, within a cell model we can confine a central bottlebrush by a homogeneously distributed set of neighbouring bottlebrushes. The primary result is an increase of the free energy of the system with decreasing spacing d between the chains. Here we do not present such 'interaction' curves. Instead we focus on the distance between the bottlebrushes as a function of the (computed) osmotic pressure. The result is given in Figure 3.7 for three values of the grafting density and in the absence of freely dispersed polymers. These predictions should be compared to the experimental results given in Figure 3.3. Quite obviously the distance is a decreasing function of the osmotic pressure. On the lin-log scale we find, in accordance with the experimental data, roughly a straight line and the slope is consistent with experiments albeit that the slopes appear to be almost independent of the grafting density. Clearly, with

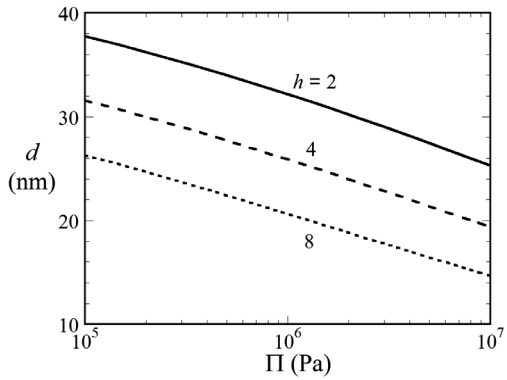

Figure 3.7: *SCF predictions for the distances (d) (in lattice units) between bottlebrushes as a function of osmotic pressure* Π *(Pa) computed within a "cell model" for three values of the distance between the grafted chains* $h = 2, 4, 8$ *in the absence of free polymer.*

increasing grafting density (reduction of h) for given pressure the distances are larger when the grafting density is higher (h smaller); the explanation for this is analogous to that given for D versus φ^b.

3.4 Discussion

In this paper we have presented osmotic stress experiments of DNA-bottlebrushes formed by the attraction of positively charged C_4K_{12} protein polymers to negatively charged DNA and compared the results to self-consistent field predictions. We found a close to quantitative agreement for the compression curves $d(\Pi)$.

In the absence of free polymers, SCF results showed linear behaviour of $d(\log \Pi)$ upon compression. However, in complementary calculations wherein we fixed the amount of free polymer at a given initial distance between the bottlebrushes and then reduced the distance between the bottlebrushes, we did see a similar non-linear behaviour as in our experimental results. We do not present these results in more detail here, because the results depend strongly on the initial distance at which the interaction curves were taken. Even though experimentally a similar problem may exist we decided not to further elaborate on this.

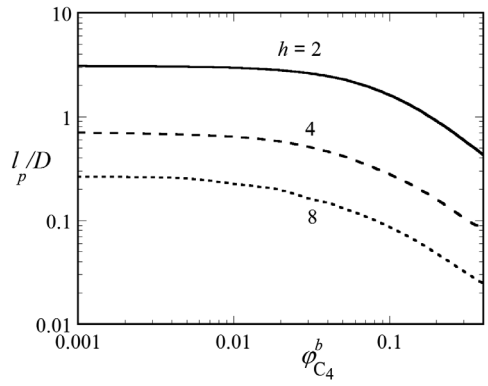

Figure 3.8: *SCF predictions for the aspect ratio (l_p/D) as a function of the volume fractions φ^b of C_4 for three values of the grafting density (distance between grafts $h = 2, 4, 8$). These results are found by combination of results of Figure 3.6 and 3.5.*

The second issue that presented itself in analysing the osmotic stress experiments was the fact that the alignment of the DNA bottlebrushes with increased osmotic stress did only occur in the system for which the free polymer concentration was low. In the case where the protein-polymer concentration was relatively high, it was found that the brush height did increase as expected. The alignment, however, of the DNA bottlebrushes failed to go up as proven by the insensitivity of the peak width of the first Bragg-peak in the X-ray scattering curves with increased osmotic pressure. Our SCF results showed that increased concentration of free polymer, especially above the overlap concentration, caused a drop of the brush height. This would enhance alignment. However, the modelling results also proved that the induced persistence length also dropped with increasing free polymer concentration. In Figure 3.8 we present the corresponding predictions for the aspect ratio l_p/D as a function of the free polymer concentration for three values of the grafting density. As expected the aspect ratio is independent of the polymer concentration in the dilute regime. However, the aspect ratio drops sharply with polymer concentration in the semi-dilute regime. This drop is expected because the induced persistence length is much more affected than the brush height when the polymer concentration is increased. Clearly, the free polymer concentration induces a flexibilisation of the bottlebrush in the semi-dilute

regime. This flexibilisation has a negative influence on the alignment of the DNA bottlebrushes.

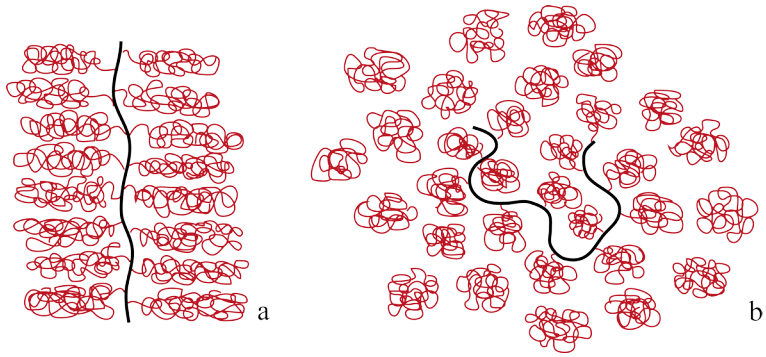

Figure 3.9: *Schematic representation of a bottlebrush molecule in the dilute regime (a) and a bottlebrush molecule in a concentrated polymer solution (b). In the presence of excess amounts of free polymer the backbone molecule loses its stiffness and effectively becomes a flexible polymer again.*

We argued above that there is a close analogy between compressing a polymer brush by increasing the free polymer concentration and by reducing the distance between two bottlebrushes. In the latter case the height of the brush is pushed back with the help of a similar brush whereas in the former case this is done by isotropic chains. The central chain feels the compressing brush similarly as freely dispersed chains in an external pressure. In the case of the opposing brushes it is the pressure imposed by the PEG solution. In the case of freely dispersed polymer it is the osmotic pressure in the bulk solution which is an increasing function of the polymer concentration. Hence, our conclusions regarding the effect of free polymer on the flexibilisation of the molecular bottlebrush can be generalised to the flexibilisation upon increasing the bottlebrush concentration.

The use of side chains in a molecular bottlebrush architecture was thought to be a generic way to turn a flexible backbone into a semi-flexible macromolecule which would upon increasing concentration go to a liquid-crystalline ordering.[33] Yet, it rarely happens; our case of co-assembled DNA bottlebrushes is one of the few examples of molecular bottlebrushes that does show such anisotropic ordering. We now understand that by increasing the polymer concentration, the compression of the bottlebrushes leads to a reduction of the stretching of the side chains. This in turn reduces the induced persistence length. This reduction by freely dispersed polymer is believed to be analogues to the reduction upon

increasing bottlebrush concentration which is already discussed in literature.[41–43] As a result of this, the induced persistence length decreases sharply with increase of free polymer concentration or with increase of the bottlebrush concentration (Figure 3.9). In other words, at high concentrations of the bottlebrushes it is the bare persistence length of the backbone that counts; in our experimental case the bare chain is DNA, which is semi-flexible with a significant persistence length of 50 nm. Hence this system can maintain its ordering upon compression. However, a bottlebrush made of a flexible backbone may not show similar behaviour and will randomise its directions upon concentrating the solution. We therefore arrive at the conclusion that orientational order of molecular bottlebrushes may only be expected for the case of semi-flexible backbone chains.

3.5 Conclusion

We investigated the effect of free polymers and externally induced osmotic pressure using X-ray and SCF calculations on liquid crystalline co-assembled DNA-bottlebrushes. The co-assembly was formed by attraction of a positively charged protein polymer to a negatively charged semi-flexible DNA backbone. We compared experimental to self-consistent field calculations using a molecularly realistic model. We find quantitative agreements between theory and experiment. The mean separation between the bottlebrushes decreases logarithmically with imposed pressure. We find that with increasing pressure the alignment of the DNA bottlebrushes only occurred when there was a low concentration of freely dispersed protein polymers in solution. We argue that freely dispersed polymers have a negative effect on the aspect ratio of the bottlebrush polymers. When the free polymer concentration is in the semi-dilute regime, it compresses the bottlebrush side chains. This implies a reduction of the stretching of the side chains which in turn sharply reduces the induced persistence length: the flexibility of the bottlebrush reduces to that of the backbone. Our results may explain why in practice it is necessary to start with a semi-flexible backbone chain in order to come up with molecular bottlebrushes that feature liquid crystalline ordering. This conclusion is relevant for practical applications of bottlebrushes and their implication for the understanding of biological relevant bottlebrush systems.

Appendix

Equilibration of Samples

We performed an osmotic stress experiment to investigate how long it takes for the DNA-C_4K_{12} complexes to equilibrate against a PEG solution. We plotted the distances between the DNA backbone as a function of the number of days the sample has been equilibrated (Figure A7.1). Using SAXS We found that intermolecular spacing remain constant, for different PEG concentration, for ~ 1 month period. In Figure A7.1 we checked the equilibration time for two different PEG concentrations, namely 15 and 25wt% of PEG. Importantly, after 1 day the DNA-C_4K_{12} appeared to reach equilibrium.

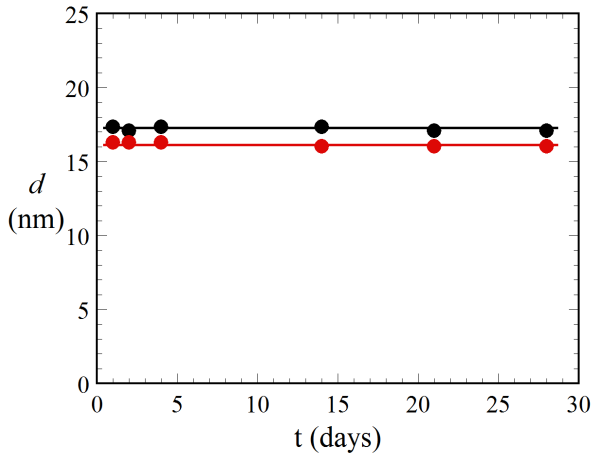

Figure A7.1: *The distance between the DNA-bottlebrushes as a function of the number of days the samples were equilibrated in a PEG solution. The black data point represent samples equilibrated against 15 wt% and the red data points were equilibrated against 25 wt% of 20 kDa PEG solution. Each sample equilibrated to a 25 wt% PEG solution became birefringent and all the samples equilibrated to a 15 wt% PEG solution were not birefringent.*

Scattering Data of Concentrated DNA-C_4K_{12} Complexes

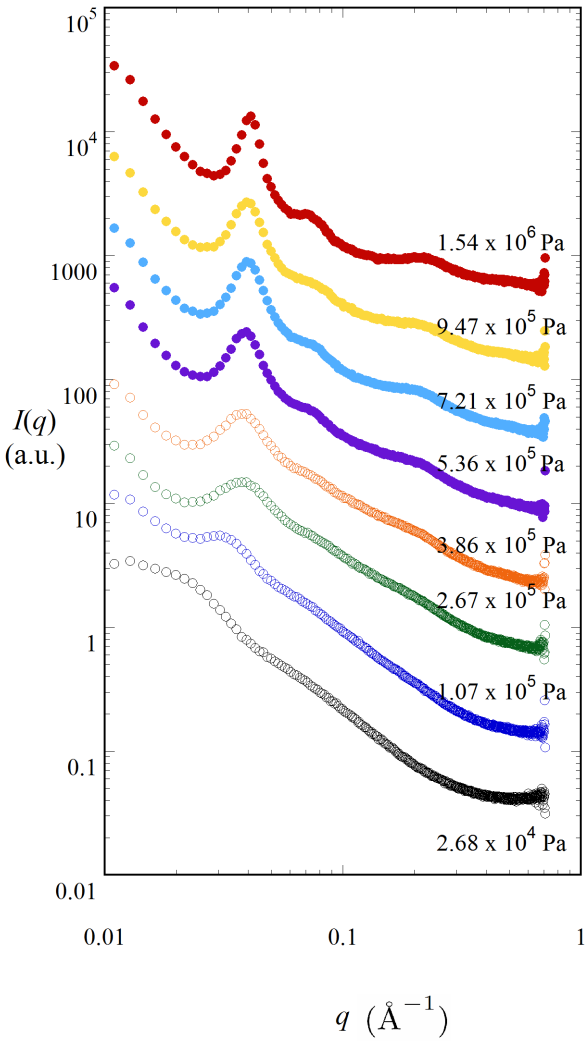

Figure A7.2: *SAXS intensity as a function of q for DNA-bottlebrushes with a protein to DNA ratio of* $\Gamma = 10$. *The samples were equilibrated against PEG solutions of: 30 (red), 25 (yellow), 22.5 (light blue), 20 (purple), 17.5 (orange), 15 (green), 10 (dark blue), 5 wt%(black). Open symbols represent isotropic samples and closed symbols are birefringent samples. The curves have been shifted horizontally for clarity.*

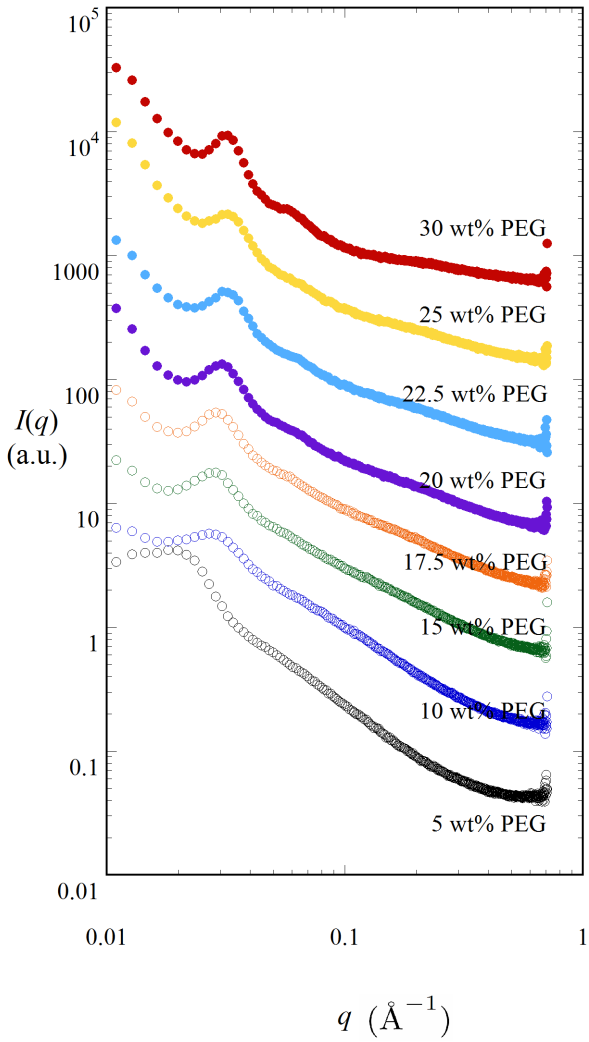

Figure A7.3: *SAXS intensity as a function of q for DNA-bottlebrushes with a protein to DNA ratio of* $\Gamma = 30$. *The samples were equilibrated against PEG solutions of: 30 (red), 25 (yellow), 22.5 (light blue), 20 (purple), 17.5 (orange), 15 (green), 10 (dark blue), 5 wt%(black). Open symbols represent isotropic samples and closed symbols are birefringent samples. The curves have been shifted horizontally for clarity.*

References

(1) Milner, S. T. *Science* **1991**, *251*, 905–914.

(2) Wintermantel, M.; Fischer, K.; Gerle, M.; Ries, R.; Schmidt, M.; Kajiwara, K.; Urakawa, H.; Wataoka, I. *Angew. Chem. Int. Ed.* **1995**, *34*, 1472–1474.

(3) Wintermantel, M.; Gerle, M.; Fischer, K.; Schmidt, M.; Wataoka, I.; Urakawa, H.; Kajiwara, K.; Tsukahara, Y. *Macromolecules* **1996**, *29*, 978–983.

(4) Ikkala, O.; Ruokolainen, J.; ten Brinke, G.; Torkkeli, M.; Serimaa, R. *Macromolecules* **1995**, *28*, 7088–7094.

(5) Birshtein, T. M.; Borisov, O. V.; Zhulina, Y. B.; Khokhlov, A. R.; Yurasova, T. A. *Polym. Sci. U.S.S.R.* **1987**, *29*, 1293–1300.

(6) Subbotin, A.; Saariaho, M.; Stepanyan, R.; Ikkala, O.; ten Brinke, G. *Macromolecules* **2000**, *33*, 6168–6173.

(7) Feuz, L.; Leermakers, F. A. M.; Textor, M.; Borisov, O. V. *Macromolecules* **2005**, *38*, 8891–8901.

(8) Subbotin, A.; Saariaho, M.; Ikkala, O.; ten Brinke, G. *Macromolecules* **2000**, *33*, 3447–3452.

(9) Saariaho, M.; Szleifer, I.; Ikkala, O.; ten Brinke, G. *Macromol. Theory Simul.* **1998**, *7*, 211–216.

(10) Saariaho, M.; Ikkala, O.; Szleifer, I.; Erukhimovichm, I.; ten Brinke, G. *J. Chem. Phys.* **1997**, *107*, 3267–3276.

(11) Darinskii, A. A.; Neelov, I. M.; Zarembo, A.; Balabaev, N. K.; Sundholm, F.; Binder, K. *Macromol. Symp.* **2003**, *191*, 191–200.

(12) Theodorakis, P. E.; Hsu, H.-P.; Paul, W.; Binder, K. *J. Chem. Phys.* **2011**, *135*,

(13) Hsu, H.-P.; Paul, W.; Binder, K. *Macromol. Theory Simul.* **2011**, *20*, 510–525.

(14) Hsu, H.-P.; Paul, W.; Binder, K. *Macromolecules* **2014**, *47*, 427–437.

(15) Grest, G. S.; Murat, M. *Macromolecules* **1993**, *26*, 3108–3117.

(16) Klein, J.; Perahia, D.; Warburg, S. *Nature* **1991**, *352*, 143–145.

(17) Raviv, U.; Giasson, S.; Kampf, N.; Gohy, J.-F.; Jerome, R.; Klein, J. *Nature* **2003**, *425*, 163–165.

(18) Klein, J.; Kumacheva, E.; Mahalu, D.; Perahia, D.; Fetters, L. J. *Nature* **1994**, *370*, 634–636.

(19) Grest, G. S. In *Polymers in Confined Environments*, Granick, S., Binder, K., de Gennes, P.-G., Giannelis, E., Grest, G., Hervet, H., Krishnamoorti, R., Leger, L., Manias, E., Raphael, E., Wang, S.-Q., Eds.; Advances in Polymer Science, Vol. 138; Springer Berlin Heidelberg: 1999, pp 149–183.

(20) Raviv, U.; Klein, J. *Science* **2002**, *297*, 1540–1543.

(21) Seror, J.; Merkher, Y.; Kampf, N.; Collinson, L.; Day, A. J.; Maroudas, A.; Klein, J. *Biomacromolecules* **2011**, *12*, 3432–3443.

(22) Seror, J.; Merkher, Y.; Kampf, N.; Collinson, L.; Day, A. J.; Maroudas, A.; Klein, J. *Biomacromolecules* **2012**, *13*, 3823–3832.

(23) Kiani, C.; Chen, L.; Wu, Y. J.; Yee, A. J.; Yang, B. B. *Cell Res.* **2002**, *12*, 19–32.

(24) Klein, J. *Polym. Adv. Technol.* **2012**, *23*, 729–735.

(25) Beck, R.; Deek, J.; Safinya, C. R. *Biochem. Soc. Trans.* **2012**, *40*, 1027–1031.

(26) Beck, R.; Deek, J.; Jones, J. B.; Safinya, C. R. *Nat. Mater.* **2009**, *9*, 40–46.

(27) Janmey, P. A.; Leterrier, J.-F.; Herrmann, H. *Curr. Opin. Colloid Interface Sci.* **2003**, *8*, 40–47.

(28) Kumar, S.; Yin, X.; Trapp, B. D.; Hoh, J. H.; Paulaitis, M. E. *Biophys. J.* **2002**, *82*, 2360–2372.

(29) Laser-Azogui, A.; Kornreich, M.; Malka-Gibor, E.; Beck, R. *Current Opinion in Cell Biology* **2015**, *32*, 92–101.

(30) Storm, I. M.; Kornreich, M.; Hernandez-Garcia, A.; Voets, I. K.; Beck, R.; Cohen Stuart, M. A.; Leermakers, F. A. M.; de Vries, R. *J. Phys. Chem. B.* **2015**, *119*, 4084–4092.

(31) Hernandez-Garcia, A.; Werten, M. W. T.; Cohen Stuart, M. M. A.; de Wolf, F. A.; de Vries, R. *Small* **2012**, *8*, 3491–3501.

(32) Werten, M. W. T.; Wisselink, W. H.; Jansen-van den Bosch, T. J.; de Bruin, E. C.; de Wolf, F. A. *Protein Eng.* **2001**, *14*, 447–454.

(33) Fredrickson, G. H. *Macromolecules* **1993**, *26*, 2825–2831.

(34) Rouault, Y.; Borisov, O. V. *Macromolecules* **1996**, *29*, 2605–2611.

(35) Milner, S. T.; Witten, T. A.; Cates, M. E. *Macromolecules* **1988**, *21*, 2610–2619.

(36) Balko, S. M.; Kreer, T.; Costanzo, P. J.; Patten, T. E.; Johner, A.; Kuhl, T. L.; Marques, C. M. *PLoS ONE* **Mar. 2013**, *8*, e58392.

(37) Kreer, T.; Balko, S. M. *ACS Macro Lett.* **2013**, *2*, 944–947.

(38) Milchev, A.; Binder, K. *Soft Matter* **2014**, *10*, 3783–3797.

(39) Parsegian, V. A.; Rand, R. P.; Fuller, N. L.; Rau, D. C. *Meth. Enzymol.* **1986**, *127*, 400–416.

(40) Parsegian, V. A.; Rand, R. P.; Rau, D. C. *Meth. Enzymol.* **1995**, *259*, 43–94.

(41) Borisov, O.; Birshtein, T.; Zhulina, Y. *Polymer Science U.S.S.R.* **1987**, *29*, 1552–1559.

(42) Bolisetty, S.; Rosenfeldt, S.; Rochette, C. N.; Harnau, L.; Lindner, P.; Xu, Y.; Müller, A. H. E.; Ballauff, M. *Colloid and Polymer Science* **2008**, *287*, 129–138.

(43) Rathgeber, S.; Pakula, T.; Wilk, A.; Matyjaszewski, K.; Lee, H.-i.; Beers, K. L. *Polymer* **2006**, *47*, 7318–7327.

(44) Benoit, H., *Comptes Rendus*; 245, 1957, pp 2244–2247.

(45) Hammouda, B. *Adv. Polym. Sci.* **1993**, *106*, 87–133.

(46) Guinier, A.; Fournet, G., *Small-Angle Scattering of X-Rays*; John Wiley and Sons, New York: 1955.

(47) Pedersen, J. S. *Advances in Colloid and Interface Science* **1997**, *70*, 171–210.

(48) Fleer, G. J.; Cohen Stuart, M. A.; Scheutjens, J. M. H. M.; Cosgrove, T.; Vincent, B., *Polymers at interfaces*; Chapman and Hall, London: 1993.

(49) Wijmans, C. M.; Leermakers, F. A. M.; Fleer, G. J. *Langmuir* **1994**, *10*, 4514–4516.

4 Electrostatic Stiffening and Induced Persistence Length for Co-Assembled Molecular Bottlebrushes

Abstract

In this paper we report on a self-consistent field analysis of tunable contributions to the persistence length of semi-flexible chains including co-assembled DNA-bottlebrushes. When the chain is charged, i.e. for polyelectrolytes, there is in addition to an intrinsic rigidity an electrostatic stiffening effect, because the electric double layer resists bending. For molecular bottlebrushes there is the sterically induced persistence length, due to the lateral excluded-volume interactions of (chemically) grafted side chains. We explore cases beyond the classical phantom main-chain approximation, and elaborate molecularly more realistic models where the backbone has a finite volume, necessary for co-assembled bottlebrushes. We find that the way in which the linear charge density or the grafting density is regulated is important. Typically, the stiffening effect is reduced when there is freedom for these quantities to adapt to the curvature stresses. Electrostatically driven co-assembled bottlebrushes, however, are relatively stiff because the chains have a low tendency to escape from the compressed regions because the electrostatic binding force is largest in the convex part. For co-assembled bottlebrushes the induced persistence length is a non-monotonic function of the polymer concentration: for low polymer concentrations the stiffening grows quadratically with coverage; for semi-dilute polymer concentrations the brush chains retract and regain their Gaussian size. When doing so they loose their induced persistence length contribution. Our results correlate well with observed physical characteristics of electrostatically driven co-assembled DNA-bio-engineered protein-polymer bottlebrushes.

In preparation: Storm, I. M.; Cohen Stuart M. A.; Leermakers, F. A. M. Electrostatic Stiffening and Induced Persistence Length for Co-Assembled Molecular Bottlebrushes

4.1 Introduction

The persistence length l_p of double stranded DNA (dsDNA), that is the length below which DNA can be seen as a rod and above which it is a coil,[1] has a value of 50 nm. dsDNA has two charges per base pare, which amounts to a high linear charge density of $v = -6$ charges per nm contour length. Obviously, the double helix gives the DNA its intrinsic stiffness but due to its charge there is an ionic strength dependent contribution as well. The intrinsic rigidity, measured at high ionic strengths, may be as low as 30 nm.[2] The charge on the DNA sets up a diffuse layer of co- and counterions. Such electric double layer resists bending and hence contributes to the bending rigidity by an amount known as electrostatic stiffening. The electrostatic stiffening of semi-flexible polyelectrolytes has been analyzed theoretically by Fixman, Skolnick and Odijk[3,4] and according to these authors grows quadratically with the linear charge density and decreases linearly with ionic strength φ_s (i.e. growth is quadratic with the Debye length). Hence the apparent persistence length of 50 nm should be understood as being composed of a bare and an electrostatic stiffening effect.

Recently, we have reported on the complexation of a bio-engineered protein polymer C_4K_{12} with DNA.[5] This C_4K_{12} is an extremely well defined protein polymer that consists of 12 positively charged lysines (K_{12}) and a 400 aa, randomly coiled collagen-like block (C_4) which forms a water soluble coil that lacks a clear secondary or tertiary structure (and is basically neutral). Opposite charges attract,[6] and therefore the lysine block binds to the DNA chain by electrostatic interactions.[5,7] The C_4-block points away from the DNA and builds up an extended corona around the DNA. This kind of a topology is referred to as a bottlebrush. Our case, more precisely, is a co-assembled protein-DNA bottlebrush.

It was found that co-assembled DNA-bottlebrushes can have a sufficiently high aspect ratio l_p/D (D is the cross-sectional dimension of the chain) that allows them to reach an ordered state, i.e. they form liquid crystalline phases at high enough DNA-bottlebrush concentrations.[5] That attaching side chains to a backbone can lead to stiffening and potentially to liquid crystalline behaviour, was first elaborated by Fredrickson.[8] He argued that it should be possible to stiffen the flexible main-chain sufficiently to make lyotropic phases. The backbone of our assembled objects, DNA, is itself already semi-flexible, and hence able to form liquid crystalline phases.[9] From this perspective it may not be too much of a surprise that we were able to also observe liquid crystallinity for the co-assembled bottlebrushes. However, from the many failed experiments in

our laboratory to form co-assembled DNA-bottlebrushes with lyotropic properties we know that our recent result[5] is far from trivial.

Much experimental and theoretical work on bottlebrushes is motivated by the potential lyotropic properties. However there are only few reports in the literature. Wintermantel et al.,[10] Tsukahara et al.[11] and Nakamura et al[12] showed that bottlebrushes with relative short polystyrene grafts on a flexible methyl methacrylate main-chain make ordered phases at high concentrations. The lack of comparable examples, brings up many questions about the origin of the lyotropicity in this system. Neurofilaments are a prominent example in nature[13–16] which features liquid crystallinity. In this case there is a rigid core from which a triplet of polyampholytic polypeptide chains emerge. As neurofilaments have a very stiff core, the contributions of the grafted chains are possibly only a perturbation (at least at fysiological conditions). In order to know, e.g., how our co-assembled DNA bottlebrush relates to the neurofilament case, it is timely to consider the tunable contributions to the persistence length of (charged) molecular bottlebrushes. To this end we calculate persistence length, cross section and aspect ratio, theoretically. Our calculations are targeted to unravel and understand stiffening issues for our co-assembled DNA-bottlebrushes. We haste to mention that our results are applicable and relevant for semi-flexible polyelectrolytes and bottlebrushes in general.

Upon co-assembly of the C_4K_{12} chains and DNA, bottlebrushes are formed and the linear charge density along the DNA backbone is reduced. As the charge density of naked DNA is above the Manning condensation limit,[17] the reduction of linear charge density is not very important for low C_4K_{12} coverages (an effect not covered by the Fixman-Odijk law[3,4]), but near stoichiometric binding the decline of the charge density is significant and the electrostatic stiffening effect is largely suppressed. However, the bottlebrush itself also resists bending, and this contribution is known as the induced persistence length.[18,19] At low coverages, when the grafts are far apart there is little stiffening effect, however, as soon as the side chains overlap laterally and stretch away from the DNA, the rigidity increases. According to the scaling analysis for brushes, the induced persistence length increases quadratically with the grafting density of the side chains ($1/h$, with h the distance between side chains) and also increases quadratically with the length N of the side chains.[18,20] To quantify the contribution of the induced persistence length to the stiffening, it is necessary to also know the proportionality constant. Numerical self-consistent field (SCF) results of Feuz *et al.*[18] proved that the numerical prefactor is unusually small, i.e. of order 10^{-3}. Recently, it has been suggested that this low prefactor

can be attributed to the possibility of side chains to translocate from the compressed convex to the expanded concave side of the curved backbone.[20]

When, for bottlebrushes, translocation effects are important to quantify the chain stiffening, it also becomes relevant to account for the finite volume of the backbone. To see this, we can imagine a short side chain permanently grafted to a point on the curved backbone; let that chain be compressed during the backbone deformation. As the chain is short, it cannot reach the uncompressed regions. Very long chains on the other hand will be able to 'travel around' the backbone and then the excluded volume of the backbone is less important. The effect of the finite size of the backbone is expected to be relevant in our DNA-bottlebrush system because the chains that physisorb onto the DNA-backbone are not extraordinary large: the unperturbed coil size of our C_4K_{12} molecules is only about twice the cross-sectional diameter of the DNA chain.[5] Therefore, we will explicitly introduce a finite volume of the backbone in our SCF model calculations.

Andreev and Victorov have analyzed the electrostatic stiffening in a model that goes beyond the phantom main-chain approximation.[21] They considered the case that the backbone has a finite diameter, e.g. relevant for stiffness of worm-like micelles[22] composed of charged surfactants. They fixed the charge on the wormlike micelle such that half the charge is in the compressed convex side and the other half in the expanded concave side of the curved cylinder. They reported large deviations from the Fixman-Odijk predictions especially when the ionic strength is relatively high. Only in the limit of very low ionic strength they recovered the $1/\varphi_s$ dependence for the chain rigidity.[21] We expect that models that allow for an annealed charge distribution have a lower persistence length than systems for which the charge is quenched. The same applies to the brush. When, upon bending, the chains can rearrange, we expect a low induced persistence length compared to the quenched situation. Below we will introduce models wherein the grafting or charge distribution is regulated in various ways. For co-assembly there is the equilibration of brush-forming chains with the bulk. In such a case the concentration of freely dispersed polymers becomes another tuning parameter for the apparent bending rigidity of co-assembled molecular bottlebrushes.

It is largely unknown how the above effects (that contribute to the stiffening of the charge driven co-assembled DNA-bottlebrush) compete with each other. For example, which effect dominates in which regime and how the various contributions relate to one another quantitatively. We do not know of computer simulations that have addressed all these issues in a single model. Such comparison is possible using SCF theory for models

which disregard the flexibility of the backbone. It should be noted that our results are therefore relevant for the understanding of large length scale bending. This is more appropriate for semi-flexible backbone systems (i.e. for the DNA case) than for very flexible backbones. The purpose of this paper is to use the SCF theory to elaborate on tunable contributions to the persistence length. We will first present how this follows from the analysis of the free energy of the system. We will then elaborate on the SCF theory,[23] mention the main characteristics and prerequisites, and present the molecular models that are used. The results are split up in three subsections. The first one deals with the electrostatic stiffening and how the classical results are modified when more detailed molecular models are introduced. In the second part we discuss the induced persistence length and focus once again on the influence of the finite size of the backbone on the induced rigidity. In the third part we will discuss the self-assembled bottlebrushes and analyze the difference between two models for adsorption and pay attention to the effects in the plateau of the isotherm, where the polymer concentration increase to semi-dilute values. In the discussion we will consider the results in the context of our co-assembled DNA-bottlebrush experiments.

4.2 The Self-Consistent Field Theory for Tunable Parts of the Persistence Length of Semi-Flexible Chains.

Below we will elaborate on the self-consistent field (SCF) theory which is used to evaluate the induced persistence length and the electrostatic stiffening. We employ models where excluded-volume effects of the main-chain are introduced in various ways (cf. Figure 4.1). In particular, our target is to predict the stiffness of co-assembled bottlebrushes that form by electrostatic interaction of an ionic copolymer with an oppositely charged backbone, mimicking our experimental DNA-bottlebrush system. Before we focus on the details of the calculations, we need to clearly identify the key characteristics from which these persistence length issues emerge. Therefore we will first briefly visit the thermodynamic background of electrostatic stiffening and induced persistence length calculations.

4.2.1 The Bending Modulus and Persistence Length of Wormlike Chains.

One of the key characteristics of a polymer chain is its persistence length.[1,24] By definition, the persistence length is the length along the

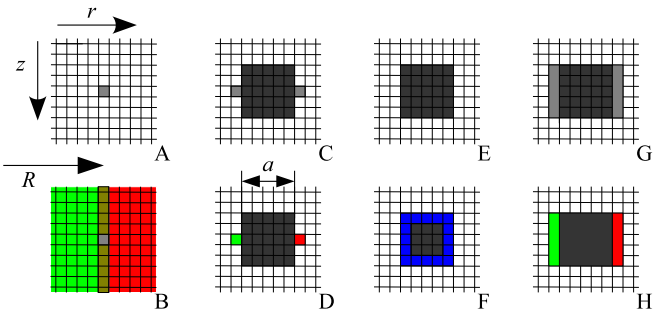

Figure 4.1: *Illustration of models for the 'backbone chain'. The two-gradient coordinate system* (z,r) *as well as the radius of curvature* R *are indicted only in panel A. A,B Phantom chains, C-H backbone chain with finite size (here* $a = 5$ *sites), and segment type S: (A) no constraints; grafts (not shown) emanate from gray site. (B) spatial constraints: half of the chains grafted at gray site have to stay in the red region and other half of the chains are fixed to the green half-space (regions overlap at* $r = R$*). (C) Chain with fixed size (black): annealed grafting in gray sites. (D) Chain with fixed size: quenched grafting; equal number of chains grafted on green and red site. (E) Chain with fixed size; homogeneous adsorption energy* $\chi_S < 0$ *for K-stickers. (F) Main chain with fixed size and fixed charge density (blue sites have fixed valency). (G) Chain with fixed size: Annealed charges in gray zones (total charge is fixed). (H) Chain with fixed size: quenched charge distribution. Equal amount of charge in red and green regions. More details are in the text. See also Table 4.1 for extra info and how the models are being used.*

backbone below which the direction of the chain is preserved and above which the directions becomes random due to thermal fluctuations. One way to estimate the persistence length in model calculations is to compute the free energy per unit (contour) length that is needed to take a chain and curve it homogeneously with radius of curvature R, and hence impose a curvature $J = 1/R$. When the curvature is a small parameter we can use a Taylor series expansion, similarly as Helfrich has done for bilayers:[25]

$$f(J) = f(0) + \frac{\partial f}{\partial J} J + \frac{1}{2} \frac{\partial^2 f}{\partial J^2} J^2 + \cdots \tag{4.1}$$

In this equation the sign of J should not matter and therefore the odd terms must be zero. Therefore we can write

$$f(J) = f(0) + \frac{1}{2} k_c J^2 + \cdots \mathcal{O}(J^4) \tag{4.2}$$

where we introduced the rigidity $k_c \equiv \frac{\partial^2 f}{\partial J^2}$ which has the units $k_B T \times l$ (i.e. energy times length). The rigidity is a direct measure for the persistence

Table 4.1: *The link between the schematic models given in Figure 4.1 and the labels used to refer to the models in figs 4.2, 4.3 and 4.5, 4.6. In this table there is also a brief description of the models used. Volume of the black regions in Figure 4.1 are inaccessible for the molecules in the solution.*

Fig	label	Fig. 4.1	model description used in SF-SCF calculations
2	Ph	A	"Phantom" chain: The backbone occupies all gray sites of the coordinate at $(z_M/2, R)$. In the refs[3,4] the main-chain is volumeless.
2	S	F	Even charge distribution around backbone.
2	Q	H	Quenched charge: equal charge density on (green) convex- and (red) concave sides.
2	A	G	Charge on backbone sits on gray sites. The charge is 'Annealed'.)
3	Ph	A	"Phantom" chain: Brush grafted at $(z_M/2, R)$. Backbone is volumeless.
3	Q	D	Quenched grafting. Equal number of chains on (green) convex- and (red) concave sides.
3	A	C	Chains grafted on gray sites: annealed grafting i.e. chains can flip from convex to concave side.
3	H	B	Half the chains are grafted on backbone at the (green) convex- and other half from (red) concave side. Chains can not escape the half-space indicated by the colored regions which overlap by 1 site.
5	solid	F	Even charge distribution around backbone.
5	dashed	E	Homogeneous χ_S around backbone.
6	-	F	Even charge distribution around backbone.

length:

$$l_p = \frac{k_c}{k_{\mathrm{B}}T} \tag{4.3}$$

because if we curve a piece of the chain with length $2l_p$ with a homogeneous curvature of $J = 1/l_p$ the free energy changes by $\big(f(1/l_p) - f(0)\big)2l_p = k_{\mathrm{B}}T$ which is the thermal energy. After bending such a chain part the tangent of the chain has changed directions by $360/\pi \approx 60°$.

We note that l_{p}, as introduced above, is relevant for sufficiently stiff semi-flexible main-chains, or in other words, it is the stiffness in the weak curvature limit. We know from multiple computer simulation studies that a flexible main-chain can be rather flexible on the monomer scale and

only show its thermodynamic stiffness on larger length scales. In other words, bottlebrushes feature a length scale dependent stiffening.[26–29] Co-assembled DNA-bottlebrushes have an intrinsically semi-flexible backbone and therefore we expect that for this system the large length scale stiffening is the most relevant limit.

In passing we should also mention that the Fixman Odijk predictions[3,4] and in particular the quadratic scaling of the persistence length with the Debye length has been subject to both experimental, theoretical and simulation studies (see e.g. ref.[30] for an overview). As the early predictions are made in the Debye Hückel limit, it is clear that these do not capture ion condensation effects. Any complication such as the finite thickness of the chain as well as discrete versus smeared charges along the chain introduces a small length scale which must be overcome by the Debye length before the Fixman Odijk predictions are expected to hold. Also intrinsically flexible chains pose a problem. For example, Barrat and Joanny[31] argued that the intrinsic persistence length l_0 of the chain must exceed the value $l_0 > 1/(L_B v^2)$, with L_B the Bjerrum length (approximately 0.7 nm for water) and v the linear charge density, before the Fixman Odijk trend can be expected. It is unknown how charge regulation should enter this picture.

As explained above, our focus here is in the mean field free energy per unit length $f(J)$ which contains the contributions due to the electric double layers (very much in the spirit of Odijk and Fixman) and polymer side chains, the so-called tunable contributions. The intrinsic contribution l_0 is deliberately not accounted for. We will assume that the backbone is sufficiently rigid so that small length scale fluctuations of the backbone are of minor importance. In other words, we focus on the large length scale stiffening only. We expect that a superposition rule will apply, that is that the total persistence length is given by the sum of intrinsic one and the tunable contributions.

4.2.2 SCF-Machinery and the Molecular Models

From the above it is clear that we need to evaluate a free energy of the system focusing on electrostatic and polymer brush contributions (the tunable contributions). We will evaluate this free energy using the self-consistent field framework of Scheutjens and Fleer (SF-SCF).[23] These authors suggested to use a lattice to discretise space and use the freely jointed chain model wherein chain molecules are composed of segments that fit the lattice site. Hence such SF-SCF calculations use only one length scale (here and below we will choose a length close to the Bjerrum length,[32]

$b = 5 \times 10^{-10}$m) to reduce all linear lengths to dimensionless ones, e.g. the chain length is reduced to the number of segments N (each with size b). We will reduce all energy units by the thermal energy $k_B T = 4 \times 10^{-21}$ J so that the bending modulus k_c is directly interpreted as l_p.

From the above it is clear that the target of the calculations is a free energy per unit length $f(J)$ as a function of the imposed curvature of a polymer chain $J = 1/R$. Unless specified otherwise the cross-section of the backbone, illustrated in fig 4.1C-H, is a square of 5×5 lattice sites of segment type S, roughly matching the size of a DNA chain. Segments on the surface of this cross-section may have a fixed charge, quantified by the valency v (fig 4.1F). In the phantom chain models (fig 4.1A-B) the volume of the backbone is ignored in the case of the bottlebrush or strongly reduced so that the cross-section is just one segment S with valency v (for models with a line charge).

It will be clear that the exact type of free energy that needs to be used in the Taylor series expansion of Eqn 4.1 should depend on details of the calculations. When we fix the chemical potential of the molecular species involved, e.g. free polymer or ions, we need to focus on the grand potential $\Omega = F - \sum_i \mu_i n_i$ where F is the Helmholtz energy, μ is the chemical potential and n is the number of molecules and i is an index which runs over all molecular species. For chemically grafted molecular bottlebrushes, however, we need to fix the number of chains per unit length and then the characteristic function is a Helmholtz energy. When we have both permanently grafted chains and freely dispersed ions (for example), it is clear that we have a semi-grand canonical, or partial open canonical ensemble and we will refer to the free energy as free energy partial open.[33] In general the relevant free energy per unit length f is given by

$$f = \frac{F'}{L} = \frac{1}{L}\left(F - \sum_j{}' \mu_j n_j\right) = \frac{1}{L}\left(\Omega + \sum_k{}'' \mu_k n_k\right) \tag{4.4}$$

where F' is the characteristic free energy of the system, and L is the length of the backbone. From Eqn 4.4 it is clear that we can compute the characteristic function in two ways; either starting from the Helmholtz energy and subtracting the chemical contribution terms for all molecules that are mobile and for which the chemical potential is imposed (indicated by the prime on the sum sign), or starting from the grand potential Ω and adding the chemical contribution of all molecular species for which the number of molecules is fixed, e.g. for the grafted chains (indicated by the double prime on the sum sign). It turns out that these thermodynamic

quantities are accurately available when the relevant self-consistent field equations have been solved.[23]

Besides thermodynamic information our interest might be on the distribution of molecular species around the backbone chain. In the case of the charged backbone it is the distribution of the ions expressed in dimensionless concentration distributions (also called volume fractions $\varphi_i(\mathbf{r})$, where the value of i may refer to a molecular species). In the field of colloid science the distribution is referred to as the diffuse part of the electric double layer.[34] In the analytical theory the results are obtained in the framework of the Debye-Hückel approximation.[3,4,21,34] We will solve the Poisson Boltzmann equations (on the level of lattice-approximations). Here and below we have a 1:1 electrolyte named Na ($i = 1$, valency +1) and Cl ($i = 2$, valency −1) for simplicity reasons. Besides the fact that the ions have a fixed monomer volume b^3, we will assume these ions to be ideal, having athermal interactions with a monomeric solvent W ($i = 0$) and all other molecular components (no specific adsorption energies). In the case of the chemically grafted bottlebrush we consider chains ($i = 4$) with segment ranking numbers $s = 1,\ 2\ \cdots,\ N$, for which the first segment is constrained to be on a specified coordinate $\mathbf{r} = \mathbf{r}^*$ (phantom model), or a set of coordinates $\mathbf{r}^* \in \{\mathbf{r}_1^*,\ \mathbf{r}_2^*,\ \cdots\}$ (cross-section as specified in Figure 4.1). The distance between the side chains is given by h (in lattice units, a value of $h = 2$ corresponds to 1 nm distance between side chains). We will assume that the solvent quality is good, that is, all Flory-Huggins interaction parameters of the segments with the solvent are set to the athermal value $\chi = 0$.[23,33,35] Alternatively, the polymer chains may be freely dispersed in solution and adsorb onto the backbone.

We follow the experimental system closely, which implies that the adsorbing polymers have exactly 12 adsorbing segments (K_{12}) connected to 400 non-adsorbing ones, the so-called C_4 block, specified as C_4K_{12}. Again the solvent quality is strictly kept athermal: $\chi_{WK} = \chi_{WC} = 0$ and also we ignore possible non-zero mixing contributions, i.e. we use $\chi_{KC} = 0$ (and similarly for the interactions with the ions). We consider two models: (i) the fixed adsorption energy case, and (ii) electrostatic binding. Let S denote the unit which specifies the backbone (cf. fig:1). In the context of (i) we realize that adsorption is an exchange process; a solvent molecule is exchanged by a K segment. Hence the effective adsorption energy is given by $\chi_s = \chi_{SK} - \chi_{SW}$. As we set $\chi_{SW} = 0$ the adsorption strength is fully specified by χ_{SK}. Typically, the value of this parameter is negative for adsorption and one needs to divide by 6 to obtain the adsorption energy in units of $k_B T$ (the value of 6 is related to the fact that a cubic lattice is used).

In the context of (ii) we consider electrostatic binding energy. Now the backbone surface has a negative charge density, specified by the valency of the S group $v < 0$. This value is fixed, where it is understood that fractional charges are allowed: e.g. a value of $v = -1/2$ means that every other surface group carries a negative charge. The valency of the K segment is $v_K = +1$. We stress that in the case of electrostatically driven adsorption no specific adsorption energy is included. The bulk concentration of polymer is a free (input) parameter.

Summarizing the above, we typically consider segment type X distributions $\varphi_X(\mathbf{r})$ where $X = W, Na, Cl, C, K, S$ (only the distribution of S is fixed during the calculations). In the SCF approach we have for each segment type X a conjugate, so-called segment potential $u_X(\mathbf{r})$ distribution. The mean field free energy is a functional of both types of fields $F = F(\varphi, u)$. The electric double layer is typically solved for ions being point charges. In the lattice approach we will go beyond this level of approximation and allow ions also to occupy lattice sites. In such a case the optimisation of the free energy requires a compressibility relation. Typically, we will assume that the system is (even locally) incompressible, that is, for each coordinate $\mathbf{r}$ we require that the sum of the volume fractions equals unity, i.e.,

$$\sum_X \varphi_X(\mathbf{r}) = 1 \tag{4.5}$$

and the free energy functional as used in the SF-SCF approach read

$$F = -\ln Q(\{u\}) - u \cdot \varphi + F^{\text{int}}(\{\varphi\}) + \alpha \left(\sum_X \varphi_X - 1 \right) \tag{4.6}$$

where we omitted spatial coordinates for simplicity, and employ the notation $u \cdot \varphi = \sum_{\mathbf{r}} \sum_X u_X(\mathbf{r}) \varphi_X(\mathbf{r})$. Q is the partition function of the system which in the mean-field approximation[33] can be decomposed as $Q = \Pi_i q_i^{n_i}/n!$ with single chain (molecular) mean-field partition functions $q = q(\{u\})$, which can be computed when all segment potentials $u_X(\mathbf{r})$ are known. The free energy of interaction F^{int} should contain all interactions that are experienced by the molecules. In the current calculations just two contributions are accounted for: the first is (i) the adsorption energy for the segments of type K for the surface (in the case of the adsorption of C_4K_{12}). Only when the distance between a segment K and a surface site S (from the backbone) is exactly unity (lattice unit b) the adsorption energy is active and the energy of the system changes proportional to the Flory-Huggins parameter χ_{SK}. In fact, as we take the reference for adsorption $\chi_{SW} = 0$, we

can interpret $\chi_{SK}/6$ as the adsorption energy in units $k_B T$ when a segment K sits next to the surface S and by doing so displaced a solvent W. The factor $1/6$ comes from using a cubic lattice. (ii) When there are charges in the system we have the usual electrostatic contribution $\frac{1}{2}\epsilon \sum_{\mathbf{r}} E^2(\mathbf{r})$, with $E = -\nabla\psi$ the electric field strength for which it is necessary to evaluate the electrostatic potential ψ. Probably the best electrostatic potentials for the system are found when these are computed using the Poisson equation:[36]

$$\nabla^2\psi = -\frac{\sigma}{\epsilon} \tag{4.7}$$

the exact form depends on the geometry (specified below). This form of the Poisson equation is appropriate because we will not allow for gradients in dielectric permittivity ϵ. The charge density distribution is easily obtained from the distribution of the ionic species in the system:

$$\sigma(\mathrm{r}) = e\sum_X \varphi_X(\mathrm{r})v_X \tag{4.8}$$

with e the elementary charge. The final term in the mean field free energy functional, Eqn 4.6, is a Lagrange multiplier for each coordinate $\alpha(\mathbf{r})$ which is coupled to the incompressibility relation.

The first goal is to find the optimal segment potential and segment density distributions so that the mean-field free energy is at an extremum. It turns out that the free energy must be maximized with respect to the segment potentials and the Lagrange field and minimized with respect to the volume fractions. Hence a saddle point is needed. This optimization must be done numerically.[37] In practice we search iteratively to find a situation for which the first derivatives of the free energy are zero:

$$\frac{\partial F}{\partial \varphi_X(\mathbf{r})} = -u_X(\mathbf{r}) + \frac{\partial F^{\mathrm{int}}}{\partial \varphi_X(\mathbf{r})} + \alpha(\mathbf{r}) = 0 \tag{4.9}$$

$$\frac{\partial F}{\partial u_X(\mathbf{r})} = -\frac{\partial \ln Q}{\partial u_X(\mathbf{r})} - \varphi_X(\mathbf{r}) = 0 \tag{4.10}$$

$$\frac{\partial F}{\partial \alpha(\mathbf{r})} = \sum_X \varphi_X - 1 = 0 \tag{4.11}$$

From Eqn 4.10 we obtain the rule how to compute the best volume fractions φ_X. From Eqn 4.9 we obtain how to compute the best potentials u_X and when we obey to Eqn 4.11 we know that the Lagrange field is optimal. We can easily rewrite Eqn 4.9 and arrive at an expression for the segment potential. Physically $u_X(\mathbf{r})$ is the work needed to bring a segment X from the

bulk to the position **r**. This quantity is normalized by the thermal energy so that the segment potential is dimensionless. The result is a lattice variant of the Boltzmann weight as used in the Poisson Boltzmann theory, augmented with a specific adsorption energy contribution and a term which accounts for the finite size of the segments:

$$u_X(\mathbf{r}) = \alpha(\mathbf{r}) + \frac{v_X e\psi(\mathbf{r})}{k_B T} + \chi_{SX}\langle\varphi_S(\mathbf{r})\rangle \tag{4.12}$$

The angular brackets in this equation will be discussed below in more detail. Here it suffices to mention that the last term of Eqn 4.12 is only non-zero when the coordinate **r** neighbours a surface site S (for which all positions are specified) and then has the value $\lambda_1\chi_{SX} = \chi_{SX}/6$. Again, the third term only is present when we consider the physisorption of C_4K_{12} chains with a fixed adsorption energy. The second term only exist when there are charges in the system. The first term in the segment potential is there in all cases and is the only term when a brush on uncharged segments is considered. Both the electrostatic potential ψ as well as α approach zero in the bulk. The classical Poisson-Boltzmann approach follows from Eqn 4.12 by ignoring the volume of the ions: only the second term survives in this case.

The evaluation of the volume fraction distribution, which obeys the rule Eqn 4.10, depends on the chain model that is used. Ideally one would like to use a self-avoiding chain as this model is most accurate with respect to the excluded-volume interactions. Such a model can only be implemented for very short chains. Here we have used the freely jointed chain (FJC) model[24] for which there exists an efficient propagator formalism to evaluate the single-chain partition function and corresponding volume fraction distributions (see below). In the FJC model we ignore bond orientation correlations even between two neighbouring bonds. The only requirement that is implemented is that two neighbouring segments along the chain occupy neighbouring lattice sites. Such FJC model thus allows for chain backfolding events. We recall that this is fully in the spirit of the mean-field approximation as exemplified by the focus on the evaluation of single-chain partition functions, which (obviously) ignores inter-chain crossings. The incompressibility relation of Egn 4.5 is there to correct for these unrealistic situations. Indeed this constraint makes sure that each lattice site, on average, is occupied only once by a segment of a polymer, a solvent or ion molecule and that at the position occupied by the backbone no other segments can be placed. Hence, inter- as well as intra-molecular excluded-volume effects are handled on the same (approximate) footing.

We now briefly outline how to find, starting from the segment potentials

the distribution of the molecules. For obvious reasons we need a notation to specify which segment of the chain is of which type. For this we introduce $\delta_{i,s}^{A}$, which takes the value unity when segment s of molecule i is of type A and is zero otherwise. All δ values are known from the input. First, we generalize the segment potential to be dependent on the segment ranking number by

$$u_i(\mathrm{r}, s) = \sum_A \delta_{i,s}^{A} u_A(\mathrm{r}) \tag{4.13}$$

Next, we compute the segment Boltzmann weight $G_i(\mathrm{r}, s) = \exp -u_i(\mathrm{r}, s)$ and refer to it as the free segment distribution function. As the potentials are zero in the bulk reference phase, the Boltzmann weights are unity in the bulk. We note that the distributions of the monomeric species $m \in \{Na,\ Cl,\ W\}$ already follow from such free segment distribution functions:

$$\varphi_m(\mathrm{r}) = C_m G_m(\mathrm{r}, 1) \tag{4.14}$$

because these molecules are just one segment long. In grand canonical calculations the value of the bulk volume fraction φ_m^b is known and then $C_m = \varphi_m^b$. Note that in the classical Poisson-Boltzmann theory the very same Boltzmann equation is used to find the distribution of the ions.[34] We note that also in the bulk the system has to obey to the compressibility relation as well and we have

$$\sum_X \varphi_X^b = 1 \tag{4.15}$$

and typically the volume fraction of the solvent in the bulk is computed from $\varphi_W^b = 1 - \sum_{j \neq W} \varphi_j^b$. When there are charged segments or ions in the system, it must be true that the bulk is electroneutral:

$$\sum_X \varphi_X^b v_X = 0 \tag{4.16}$$

This means that the volume fraction in the bulk of one of the ion species can not be given by the input, but is computed from the electroneutrality constraint (Eqn 4.16). Typically the bulk concentration of the other ion is used to set the ionic strength.

The next step is to consider so-called end-point distribution functions of the type $G_i(\mathbf{r}'', s''|\mathbf{r}', s')$,[38] which specify the combined statistical weight of all possible conformations of chain fragments that start with segment s' at coordinate $\mathbf{r}'$ and finish at segment s'' at coordinate $\mathbf{r}''$. Clearly, when $s' = s''$, it is necessary that $\mathbf{r}', \mathbf{r}''$ is a free segment and $G_i(\mathbf{r}'', s'|\mathbf{r}', s') = G_i(\mathrm{r}', s')$. We can integrate over 'starting' positions: $G_i(\mathbf{r}'', s''|s') = \sum_{\mathbf{r}'} G_i(\mathbf{r}'', s''|\mathbf{r}', s')$. In

the propagators two of such (integrated) end-point distribution functions are used, namely one for which the starting segment is $s' = 1$, $G_i(\mathbf{r}'', s''|1)$ and the other one for which the starting segment is $s' = N$, $G_i(\mathbf{r}'', s''|N)$. At this point we realize that the double primes are no longer necessary and we drop these from our notation. The end-point distributions are generated by the propagators, which are discrete implementations of the Edwards diffusion equation,[39] by extending the chain fragment with one segment.

$$G_i(\mathbf{r}, s|1) = G_i(\mathrm{r}, s) \sum_{\mathrm{r}'}^{*} \lambda_{\mathrm{r},\mathrm{r}'} G_i(\mathbf{r}', s-1|1) = G_i(\mathrm{r}, s)\langle G_i(\mathbf{r}', s-1|1)\rangle \quad (4.17)$$

$$G_i(\mathbf{r}, s|N) = G_i(\mathrm{r}, s) \sum_{\mathrm{r}'}^{*} \lambda_{\mathrm{r},\mathrm{r}'} G_i(\mathbf{r}', s+1|N) = G_i(\mathrm{r}, s)\langle G_i(\mathbf{r}', s+1|1)\rangle \quad (4.18)$$

which defines the angular brackets. Here $\lambda_{\mathrm{r},\mathrm{r}'}$ are *a priori* step probabilities which are taken according to the geometry of the system and are consistent with the FJC model. As in the FJC the two neighbouring segments must be on neighbouring lattice sites, we realize that the sum is only necessary over coordinates r′ that neighbour coordinate **r**. This is indicated by the asterisk above the sum sign. The transition probabilities add up to unity as $\sum_{\mathrm{r}'}^{*} \lambda_{\mathrm{r},\mathrm{r}'} = 1$. When a three-gradient Cartesian coordinate system is used, i.e. $\mathbf{r} = (x, y, z)$, we can use a cubic lattice and then set all λ-values to $1/6$. By readjusting the initialization of the propagators, we can implement the grafting condition for the polymers. Below we will, for such case, focus on the situation that the first segment is not free to go to all possible positions. Typically the first segment is placed only on a subset of coordinates. Let these pinning coordinates given by the set $\{\mathbf{r}_\mathrm{p}\}$ (again specified by the input). Then the starting of the forward propagator reads

$$G_i(\mathbf{r}, s|1) = G_i(\mathbf{r}, 1)\delta_{\mathbf{r},\mathbf{r}_\mathrm{p}} \quad (4.19)$$

wherein $\delta_{\mathbf{r},\mathbf{r}_\mathrm{p}} = 1$ when $\mathbf{r} \in \{\mathbf{r}_\mathrm{p}\}$ and zero otherwise.

We can now evaluate all distributions and thermodynamic quantities, because from the above it will be clear that we can start the propagators by setting $G_i(\mathbf{r}, 1|1) = G_i(\mathbf{r}, 1)$ and $G_i(\mathbf{r}, N|N) = G_i(\mathbf{r}, N)$. After $N-1$ steps we arrive at the other end of the chain and from these end-point distributions we compute the chain partition function. Both for freely floating chains as well as for pinned (grafted) chains we can use

$$q_i = \sum_{\mathbf{r}} G_i(\mathbf{r}, N|1) \quad (4.20)$$

Very efficiently, the volume fraction distributions of the chain segment are found by combining Eqns 4.17 and 4.18 using the so-called composition

law:

$$\varphi_i(\mathrm{r},s) = C_i \frac{G_i(\mathbf{r},s|1)G_i(\mathbf{r},s|N)}{G_i(\mathrm{r},s)} \tag{4.21}$$

In this equation the division by $G_i(\mathrm{r},s)$ is necessary to correct for the double counting of the segment weight. The normalization constant C_i can be expressed in terms of the number of molecules in the system n_i in the case of canonical calculations or in terms of the bulk volume fraction in grand canonical calculations:

$$C_i = \frac{n_i}{q_i} = \frac{\varphi_i^b}{N_i} \tag{4.22}$$

Summarizing, from the above it follows that it is possible to compute the volume fractions as soon as the segment potentials are available (Eqns 4.14 and 4.21) and when the segment volume fractions are available we can compute the segment potentials (cf. Eqn 4.12). As already mentioned, a fixed point of these equations is found routinely in an iterative manner, wherein the potentials are systematically tuned until the volume fractions are found which both follow from the potentials and determine the same potentials, while they obey to the incompressibility relations (Eqns 4.5 and 4.15). Routinely we obtain 7 significant digits in order 100 iteration steps.[37] This fixed point is referred to as the self-consistent field solution. For such SCF solution we can compute the free energy using Eqn 4.6. Other relevant thermodynamic quantities can be computed straightforwardly as the chemical potentials of the mobile components follow from the Flory-Huggins theory[35]

$$\mu_i \equiv \frac{\mu_i}{k_\mathrm{B}T} = \ln\varphi_i^b + \ln N_j + 1 - N_i \sum_j \frac{\varphi_j^b}{N_j} \tag{4.23}$$

wherein the interaction terms were omitted because in all calculations discussed below the FH χ-parameters were taken to have the athermal value. When, in the bulk, there are only monomeric species the dimensionless FH chemical potential reduces to $\mu_i = \ln\varphi_i^b$.

4.3 The Geometry

The spatial coordinates $\mathbf{r}$ have not yet been specified. The above notation suggests a Cartesian coordinate system $\mathbf{r} = (x,y,z)$, but calculations for such a system are CPU intensive and very time consuming. Making use of symmetry allows us to reduce the number of gradient directions and to implement a mean-field approximation in the other direction(s).[23] The

focus here is on a main-chain which is homogeneously curved in one direction. This can be captured in a cylindrical coordinate system with gradients in a radial direction (indicated by the radial layer number r) and a direction along the axis of the cylinder (indicated by a z-coordinate).[18] More specifically (cf. Figure 4.1 where a small part of the coordinate system is presented) we implement $\mathbf{r} = (z, r)$, wherein r is a radial coordinate $r = 1,\ 2,\ \cdots,\ r_M$, and z is a direction along the long axis of the cylinder $z = 1,\ 2,\ \cdots,\ z_M$. At all system boundaries we have implemented reflecting (mirror-like) boundary conditions, which means that for all end-point distributions and also for the volume fractions and electrostatic potential profiles it is implemented that the gradients at the system boundaries are zero. For example, for the electrostatic potential $\psi(z_M + 1, r) = \psi(z_M, r)$ for all r values and $\psi(z, r_M + 1) = \psi(z, r_M)$ for all z values. Typical values for r_M and z_M is 400.

Such a two-gradient cylindrical coordinate system requires a few modifications of the above equations. The important point is that the number of lattices sites at position $\mathbf{r} = (z, r)$ grows as $L(r) = A(r) - A(r-1) = \pi(2r-1)$, as we use for $A(r) = \pi r^2$. The angular brackets defined in Eqns 4.17 and 4.18, will be modified to account for this geometry. Introducing step probabilities $\lambda_{z,r;z,r-1} = \frac{1}{6}S(r-1)/L(r)$, $\lambda_{z,r;z,r+1} = \frac{1}{6}S(r)/L(r)$ and $\lambda_{z,r;z-1,r} = \lambda_{z,z+1} = 1/6$, so that the step probability which does not change coordinates will have the value $\lambda_{z,r;z,r} = 2/6$ as the circumference $S(r) = 2\pi r$ we can implement the site average of a quantity X at (z, r) by

$$\langle X(z,r)\rangle = \frac{2}{6}X(z,r) + \sum_{i=-1,1}(\lambda(z,r;z+i,r)X(z+i,r) + \lambda(z,r;z,r+i)X(z,r+i)) \tag{4.24}$$

The partition function is now computed by $q_i = \sum_z \sum_r L(r) G_i(z, r, N|1)$ and the number of grafted chains per unit length along the backbone can be computed from the radial volume fraction profile of the polymer (recall that the polymer has the index $i = 4$):

$$n_4 = \frac{1}{N_4}\sum_z \sum_r L(r)\varphi_4(z,r) \tag{4.25}$$

where it is understood that $h = 1/n$ (in lattice units).

The length of the torus is found from the central position of the DNA chain in this cylindrical coordinate system. As indicated in Figure 4.1, the center is at (z', R) and then the length of the backbone chain (curved in a ring or torus) is given by $L = \pi(2R-1)$ and the curvature is given by $J = 1/R$.

Lattice-Noise

We have used Eqn 4.2 to evaluate k_c and thus l_p. We note that

$$l_p = \frac{k_c}{k_B T} = (f(J) - f(0)) \frac{2}{J^2} \tag{4.26}$$

So when the reference value for the appropriate free energy per unit length of the chain in the straight configuration $f(0)$ is available, we can evaluate $l_p = 2(f(J) - f(0))R^2$. The use of a lattice is not completely without consequences. It turns out that both $f(J)$ as well as $f(0)$ can have small lattice contributions so that the l_p value is slightly dependent on the radius R used in the calculations.[40] That is why the radius of the torus is varied over a significant range and l_p is computed by averaging over these results. It turned out that for this procedure it is not necessary to compute $f(0)$ explicitly. We typically adjust $f(0)$ so that l_p estimates are not a function of the explicit range of torus radii used. It was checked that the fitted value of $f(0)$ is indeed consistent with the free energy per unit length of the chain in the straight configuration.

4.4 Results and Discussion

Our results will be presented in the following order: (i) electrostatic stiffening of negatively charged backbone chains, which will be compared to the phantom chain predictions of Fixman and Odijk[3,4] and for backbone chains with volume to Andreev;[21] (ii) the induced persistence length of chemically fixed bottlebrushes and these results will be compared to results of Feuz;[18] (iii) co-assembled bottlebrushes for which the predictions are relevant for our co-assembled DNA-bottlebrushes.

4.4.1 Electrostatic Stiffening

In Figure 4.2 we present our numerical SCF results for electrostatic stiffening. In Figure 4.2a the electrostatic persistence length is given as a function of the ionic strength in double logarithmic coordinates for a linear charge density of $v = -1.5$ charges per lattice site (which amount to 3 charges per nm relevant for ds DNA). In Figure 4.2b the electrostatic persistence length is given as a function of the charge density v along the chain for a salt volume fraction of $\varphi_s = 10^{-3}$ which is close to the experimentally relevant concentration of 10 mM salt,[5] again in double logarithmic coordinates. The labels on these figures refer to the different

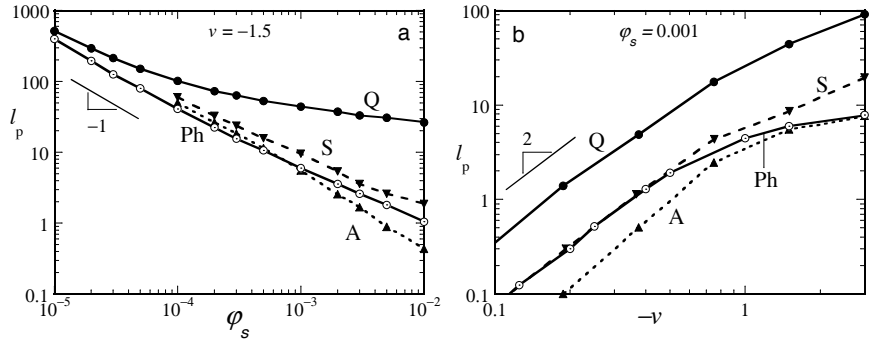

Figure 4.2: *a) The electrostatic stiffening l_p in units of lattice sites as a function of the salt concentration of a polymer chain with linear charge density $\nu = -1.5$ charges per lattice site in log-log coordinates. b) The electrostatic stiffening l_p in units of lattice sites as a function of the linear charge density for a given volume fraction of salt $\varphi_s = 0.001$ in log-log coordinates. Q) is quenched charge density, A) annealed charge density. Ph) the main-chain has minimum volume of one lattice site (phantom main-chain). S) is the fixed surface charge density around the DNA chain. 1:1 electrolyte. All interaction parameters are taken athermal. The indicated slopes give the prediction of Fixman and Odijk.[3,4] See Figure 4.1 and Table 4.1 for details of the models used.*

models that are used which are pictorially illustrated in Figure 4.1 and more specifically addressed in Table 4.1. The lines with slope −1 and 2 for the figs 4.2a and 4.2b, respectively, are the theoretical Fixman-Odijk predictions.

Our SF-SCF attempt to mimic the Fixman-Odijk predictions is labeled by *Ph*. As mentioned in Table 4.1 this case comes closest to the phantom chain: in SF-SCF the backbone occupies just one ring of lattice sites. Concerning the ionic strength dependence, for low salt concentrations our phantom (Ph) chain is exactly behaving according to the Odijk and Fixman predictions. For high salt we see that our phantom chain is slightly deviating from the −1 slope in Figure 4.2a. We attribute this deviation to the fact that in SF-SCF there is a finite size of the backbone which brings in a small length scale that is seen as soon as the Debye length becomes sufficiently small (that is at high salt concentrations). With respect to the dependence on the charge density (Figure 4.2b) we observe the expected scaling value of 2 at low charge density. The leveling off at high charge density is due to the onset of ion condensation. This is to be expected since we solve the full Poisson-Boltzmann equation which correctly accounts for ion condensation while this effect is ignored when the Debye Hückel approximation is used.

The model that quantitatively deviates most from the Fixman-Odijk limit is labeled by *Q*. Referring to Figure 4.1 and Table 4.1, this case stands for quenched charge, such that half the charge is on the convex and the other half on the concave side of the curved backbone (with finite volume) irrespective of the curvature *J*. The inability for the backbone charge to regulate its location upon bending obviously gives the highest value of the electrostatic stiffening. The dependence shown in Figure 4.2a is in very good agreement with the results of Andreev et al.[21] for the electrostatic stiffening of worm-like micelles. The full width of the backbone is seen, and hence the deviations from the Fixman-Odijk predictions show up already at very large values of the Debye length (low salt concentrations) and they are much larger than for our *Ph* results. Interestingly, fixing the charge upon bending (*Q*) gives for a reasonable ionic strength of 10 mM a ten-fold increased persistence length over the full range of charge densities, as can be seen from Figure 4.2b.

The other two models, labelled *A* and *S* implement different ways to regulate the charge upon bending. In the annealed (*A*) case we fix the overall charge on inner and outer faces of the backbone core (gray regions in Figure 4.1G), but upon bending the charge can locally adjust. In the fixed surface charge density (*S*), there is a 'hidden' regulation, as a curved backbone has more 'surface area' in the concave part than in the convex parts, hence the charge is distributed accordingly. In both cases there is a finite size backbone, but little of that is found back in the ionic strength dependences. The annealed case follows the Fixman-Odijk prediction in the full range of ionic strengths used. The fixed surface charge (*S*) case gives a result which is only marginally larger than for the phantom chain (*Ph*). With respect to the dependence on the linear charge density (Figure 4.2b), the annealed predictions tend to be a bit lower than the phantom chain results, especially at low charge densities, whereas the fixed surface charge results are a bit higher than the phantom chain results, especially at high charge densities. We can rationalize these results by realizing that a low charge density benefits more from charge regulation than a high charge density (for curve *A*), while the case with fixed surface charge density can possibly postpone the ion condensation effect by distributing the charge over a larger surface area.

The main message coming from Figure 4.2(a) is that assigning a finite volume to the backbone chain does not necessarily affect the electrostatic stiffening behaviour of the polymer. The Fixman-Odijk prediction is remarkably robust with respect to the volume of the backbone as soon as some charge regulation is possible. The quenched case is somewhat

artificial and the strong deviations are therefore not that important. When we consider the model of DNA (S), we see that the finite size of the double helix with a fixed charge density behaves close to the Fixman Odijk predictions, even though the linear charge density along the chain is slightly beyond the Manning condensation limit. The deviations due to this are hardly noticed from the ionic strength dependence, and make only a marginal correction to the charge density dependence. When we study the co-assembly mechanism, below, we will implement the homogeneous charge density (S) model.

A numerical estimate for the electrostatic stiffening of DNA at approximately 10 mM salt is only about 10 (lattice units), which translates to 5 nm. This value is small compared to an estimate of the intrinsic persistence length of 30 nm. At 1 mM salt, however, the electrostatic contribution has increased to approximately 40 lattice units, or equivalently to 20 nm, and the overall persistence length is then predicted to be 50 nm, rather close to the value often cited in the literature. Experiments below 1mM salt might produce an effective persistence length for DNA which is even larger (e.g. 80 - 100 nm), provided that the double stranded nature is conserved at such low ionic strengths.

4.4.2 Induced Persistence Length

Numerical SCF results for the induced persistence length of chemically grafted bottlebrushes are collected in Figure 4.3. Here the induced persistence length is given as a function of the chain length of the grafts in double logarithmic coordinates for a distance between grafts of 1 nm, that is for $h = 2$. In the corresponding Figure 4.3b the induced persistence length as a function of the grafting distance h (in lattice units) in double logarithmic coordinates is given for $N = 400$. The different models are illustrated in Figure 4.1 and elaborated on in Table 4.1. Both the phantom chain model Ph and the H model ignore the backbone volume: the first segment of the grafted chains is put at $(z_M/2, R)$. The other models take a finite volume of the backbone into account. To our knowledge such models have not been used in the literature yet.

The numerical result for the phantom chain approximation, that is a bottlebrush for which the backbone volume is completely ignored, labeled by Ph, is very well known and documented.[18] The fitting at sufficiently large N and small h reveals an approximate scaling of $l_p = 0.002(N/h)^{1.9}$. The deviation from the power-law coefficient of 2 is larger when the short chain data are included and less when only the longer chain lengths are

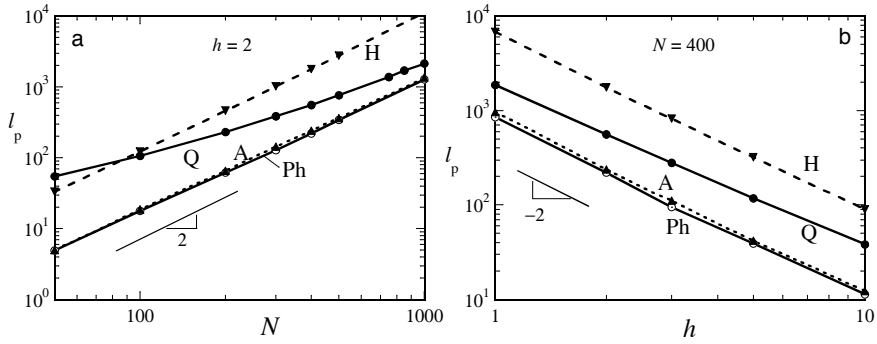

Figure 4.3: *a) The induced persistence length l_p in units of lattice sites as a function of the degree of polymerization of the side chains for a given distance between the grafts $h = 2$ lattice sites in log-log coordinates. b) The induced persistence length l_p in units of lattice sites as a function of the distance between the side chains for a given length of the side chains $N = 400$ in double logarithmic coordinates. Q) is quenched mobility of side chains, A) annealed mobility. Ph) volume of the main-chain is ignored: first segment of the side chains is fixed to $(M_z/2, R)$ (phantom chain). H) is the model in which chains can not translocate with any of the segments from the convex to the concave side. See Figure 4.1 and Table 4.1 for details of the models used. The theoretically expected slopes 2 in panel a and −2 in panel b, are indicated.*

used in the fitting. It is remarkable that the numerical coefficient deviates strongly from the expected value of unity. It must be noted that the scaling relations do not account for the translocation of segments, whereas in the numerical SCF results these translocations are allowed and accounted for.

The results labeled by H are computed using a model introduced by Mikhailov et al.[20] to explain why the numerical coefficient for the phantom chain model is dramatically low. In this model half the chains exit from the phantom backbone on the convex and the other half on the concave side of the backbone. In addition, the remainder of the chain segments have to stay at the respective half space, that is, the convex chains must have all their segments in the space with radial coordinates $r \leq R$, whereas the other chains must remain in the region $r \geq R$. This rather artificial model does not destroy the scaling. In fact, it gives results much closer to the analytical scaling predictions. Fitting of the H-curve of these results give $l_p = 0.012(N/h)^{1.99}$. Still, the coefficient is much less than unity, but already 6 times higher than for the phantom chain case. Moreover, the power law coefficient is closer to the expected value of 2. In effect, the difference between persistence lengths of the predictions Ph and H is a

factor of 10 over the whole range of N and h values used.

The H model is a rather artificial one. Introducing a finite size of the backbone is a more realistic alternative to put constraints on the ability to translocate segments upon bending from convex to concave parts. In the model Q we present a backbone with fixed volume, and now half the chains are grafted on the convex part and the other half are grafted on the concave side of the backbone. The grafting is quenched, which means that the chains can not move their grafting coordinate from the convex to the concave sides, but unlike in the H model, chain conformations are allowed to cross the $r = R$ coordinate. From Figure 4.3a we see that $l_p(N)$ deviates strongly from the power law dependence. The reason for this is clear. The finite size of the backbone introduces a new length scale and as long as the thickness of the corona is not large compared to this size we effectively have eliminated the possibility to cross the $r = R$ coordinate. For very short chains the l_p approaches the results of H. Indeed the stiffness can even exceed the H-value for very short chains. This effect must be attributed to the volume of the backbone which is excluded for the Q case and not present in the H-model. The longer the chains, the less they notice the backbone and therefore the induced persistence length l_p goes to the phantom chain value for large values of N. In Figure 4.3b results for $N = 400$ are given for which the importance of the backbone is still reasonably large. Also the scaling with respect to h is destroyed by the volume of the backbone. The larger the size of the corona is, the less important is, the volume of the backbone and therefore we see that the $l_p(h)$ approaches the phantom chain limit when h is small, and the deviations are largest for large values of h.

The final model A is where the grafting is annealed. Other features are the same as for the quenched case. Upon bending, the chains can choose to appear on the concave or convex side of the backbone with fixed volume. As can be seen from the results presented in Figure 4.3, the persistence length is extremely close to the phantom chain values. This is not too surprising because the finite volume of the backbone is sufficiently small so that a shift of the grafting point is only a small perturbation, especially when the chains can avoid the compressed region when necessary. We can also see the backbone as a small increase of the side chain length by a few (about 3) segments. This is a minor perturbation compared to the original system.

The topic of induced persistence length associated with the grafted chains on a backbone is less developed than the electrostatic stiffening. The finite volume of the backbone is of little importance as soon as there is some annealed character of the grafting. In principle this is good news for the co-assembled bottlebrushes which will be discussed next. Below we are

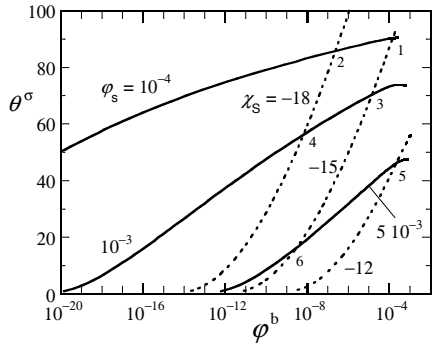

Figure 4.4: *The adsorbed amount of C_4K_{12} copolymers in number of segments per unit length of the DNA chain as a function of the volume fraction of copolymer in solution in lin-log coordinates. The solid lines are for the electrostatically driven adsorption (Figure 4.1F, $v = -3$). The ionic strengths $\varphi_s = 1\times10^{-4}$; 1×10^{-3}; 5×10^{-3} are indicated. The dashed lines are for the classical case with fixed adsorption energy (Figure 4.1E)). The adsorption energy $\chi_S = -18, -15, -12$ are indicated. Crossing point of the isotherms are numbered 1-6 and these point represent conditions for which the bending rigidity of the self-assembled bottlebrush are computed which are presented in Figure 4.5.*

interested in the formation of a bottlebrush by physisorption. In this case the chains are in equilibrium with chains in the bulk and this provides an annealing mechanism. Hence, we should expect that the phantom chain case is the relevant one to compare with.

4.4.3 Self-Assembled Bottlebrushes

Result in this section are selected to match the experimental situation we have for the DNA co-assembled bottlebrushes. Experimentally, we used C_4K_{12} protein polymers which we model here by $K_{12}A_{400}$ where A is an athermal uncharged segment and K is a segment which adsorbs onto the core, either with an adsorption energy χ_S, or by electrostatic attraction: then each segment K has a valency of +1. In the electrostatic binding case we consider DNA with $v = -3$, which translates to 6 negative charges per nm DNA contour length. This means that binding upto charge stoichiometry amounts to 0.5 chain per nm, or 0.25 chains per lattice unit. Below, we report adsorbed amounts computed in the two-gradient cylindrical coordinate system by

$$\theta^\sigma = \sum_z \sum_r L(r)\left(\varphi(z,r) - \varphi^b\right) \tag{4.27}$$

When we divide this by the chain length N we obtain the excess number of chains per unit length. Note that, by definition, the value θ^σ will go to zero in the limit of $\varphi^b \to 1$. Hence, adsorption isotherms in these units therefore typically have two regimes of behaviour. As long as the bulk volume fraction is below the overlap the adsorbed amount increases with bulk volume fraction, whereas above the overlap concentration the excess adsorption has the tendency to decrease. Charge stoichiometry occurs at $\theta^\sigma \approx 100$. Experimentally, data for the binding of C_4K_{12} onto DNA are available:[5] the maximum binding goes to approximately 70% coverage at 10 mM salt and it drops to $\approx$ 60% for 60 mM salt and to about 30% for 160 mM salt.

In Figure 4.4 we show the result of SCF calculations for the adsorbed amount, θ^σ, of C_4K_{12} protein polymer as a function of the volume fraction of C_4K_{12} in the bulk. The figure is in lin-log coordinates in the regime for which the bulk volume fraction remains below overlap. In this figure we see two sets of adsorption isotherms. The solid lines are for the electrostatic adsorption mechanism. The dashed curves are for the fixed adsorption energy case.

For all isotherms that lack cooperativity it is true that the slope $\partial\theta^\sigma/\partial\varphi^b$ decreases with increasing coverage. Interestingly, for the electrostatic adsorption mechanism even the slope $\partial\theta^\sigma/\partial\log\varphi^b$ decreases with coverage. This reduction in affinity is due to the adsorption mechanism. In the case of low coverage there are many free charges around the backbone and the electrostatic potential around the DNA is high and hence the driving force for adsorption is strong. For a high coverage there are not many 'free' charges left around the DNA backbone. The electrostatic potential becomes low and hence the driving force for adsorption reduces. The plateau of the isotherm is found at relatively low bulk volume fractions and the plateau is below charge stoichiometry. The lower the ionic strength, the closer the isotherms approach charge stoichiometry. The isotherms are truncated just before the bulk volume fraction of the polymer reaches the overlap concentration $\varphi^b \approx 0.0025$. The maximum coverage in terms of percentage of charge stoichiometry is 0.9 for $\varphi_s = 10^{-4}$ (1 mM), 0.7 for 10 mM salt and 0.5 for 50 mM salt. These numbers are in good agreement with the experimental data mentioned above.

The set of adsorption isotherms which corespond to a fixed adsorption energy are dramatically different in shape. As each chain has only a few adsorbing segments, the adsorption energy starts at a rather high bulk volume fraction. After the Henri regime (an initial linear increase of

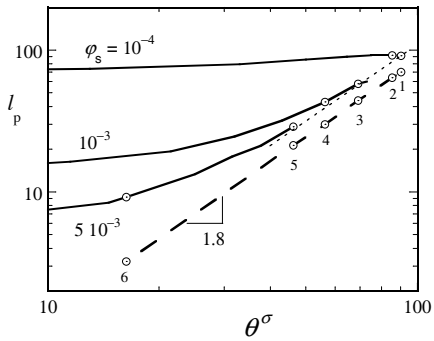

Figure 4.5: *The bending rigidity of the self-assembled bottlebrush in lattice units as a function of the amount of C_4K_{12} copolymers that are physisorbed per unit length (lattice units) onto the DNA chain in log-log coordinates. Solid lines are for the charged case. Three curves are given for ionic strengths $\varphi_s = 10^{-4}$, 10^{-3} and 5×10^{-3}, as indicated. The dashed line is for the fixed adsorption energy case. The symbols with numbers correspond to the crossings of the isotherms in Figure 4.4. The slope of the dashed line is 1.8. The dotted line (with same slope) is to guide the eye.*

$\theta^\sigma(\varphi^b)$) the isotherm becomes straight in lin-log coordinates, which implies logarithmic growth. The adsorbed amount grows with increasing adsorption energy at a given bulk volume fraction. It is found that θ^σ can exceed 100. At this coverage the adsorbing fragment K_{12} occupies all adsorbing sites when all the segments would be adsorbed in the so-called train conformation. However, at such high coverages the adsorbed layer also develops small loops and therefore θ^σ can exceed the monolayer coverage for the adsorbing block.

As the two sets of isotherms are dramatically different in shape, they cross each other. We have labeled in Figure 4.4 these crossing points for reference purposes: the numbers re-appear in Figure 4.5.

Figure 4.5 shows the persistence length of the DNA-bottlebrushes as a function of the amount of bound C_4K_{12} protein polymer, both for the electrostatic driving force as well as for the systems that have a fixed adsorption energy (dashed line), in double logarithmic coordinates. In the latter systems there is only a contribution of the adsorbed protein polymers. The persistence length data follow a power-law scaling with a slope of 1.8, which is very close to the corresponding results for chemically grafted brushes in the phantom chain limit. The value is a bit below the scaling prediction for brushes of 2. The deviation from 2 arguably is due to the fact that the chain length used, $N = 400$, for the stabilizing block is still rather

short. The symbols on the curve correspond to the crossing points of the isotherms in Figure 4.4. Note that these points are taken from isotherms that differ with respect to adsorption energy value. We conclude that for the persistence length only the coverage is important while both the bulk volume fraction of protein polymers and the adsorption energies (of course necessary to reach a particular coverage) are irrelevant for the stiffness.

The tunable contributions of the persistence length for the electrostatically driven bottlebrushes is more complex. In all cases the persistence length is above the value for fixed adsorption energy cases. The reason for this is clear. Apart from the brush there is a contribution due to the (residual) electric double layer. We present three curves for $l_p(\theta^\sigma)$, for different values of the ionic strength. Indeed at low polymer coverage ($\theta^\sigma << 50$) the tunable contribution to the persistence length is dominated by the electrostatic stiffening effect. The limiting values for vanishing coverages of the protein polymer of l_p decrease sharply with increasing ionic strength: its stiffening is well below 10 (lattice units) for $\varphi_s = 5 \times 10^{-3}$, about 15 for $\varphi_s = 10^{-3}$ and about 70 for $\varphi_s = 10^{-4}$. These limiting values do not exactly follow the Fixman Odijk prediction[3,4] because the charge density on the DNA is above the Manning condensation limit. At high coverages the induced persistence length dominates the tunable contributions. This is illustrated by the dotted line which is drawn with a slope of 1.8. All three curves approach the same brush-dominated trend asymptotically (dotted line).

From the above, we know that electrostatic stiffening roughly scales quadratically with linear charge density on the brush. We also know that there is a roughly quadratic scaling of the persistence length with grafting density (adsorbed amount). This means that we should expect an interpolation curve between the electrostatic stiffening limit and the brush limit without local minima or maxima. When the two limiting values are close, such as in the low ionic strength case ($\varphi_s = 10^{-4}$), there is a simple interpolation and the curve is close to horizontal. When the limiting values are further apart, we see that with decreasing adsorbed amount, the brush contribution first reduces according to the power-law scaling $l_p \propto (\theta^\sigma)^{1.8}$ from which it starts to level off as soon as the induced persistence length becomes of the same order as the electrostatic stiffening limit.

As mentioned already the symbols on the curves correspond to the crossings of the isotherms shown in Figure 4.4. Labels 1 and 2 correspond to the $\varphi_s = 10^{-4}$ system, 3 and 4 for $\varphi_s = 10^{-3}$ while 5 and 6 are for $\varphi_s = 5{\times}10^{-3}$. The persistence length for all points on the electrostatically driven brush formation are higher than their corresponding point on the curve for the

fixed adsorption energies. One may argue that the difference is simply the contribution of the electric double layer. However, close inspection shows that this cannot be the case. Based on the value of $l_p \approx 8$ (lattice units) for the electrostatic stiffening at $\varphi_s = 5 \times 10^{-3}$ and $\theta^\sigma = 10$, we expect for $\theta^\sigma \approx 40$ a 16× lower value (surface charge is reduced by a factor 4) of the electrostatic stiffening. Hence, for point 5, the contribution of the electrostatic stiffening must be below unity. Nevertheless, the difference in stiffening of the two points labeled 5 is still approximately 10 (lattice units)! The same applies to the difference of the persistence length for the two points labeled with 4: the observed difference for l_p is about 13 (lattice units), whereas the electrostatic stiffening is again expected to be less than unity. The low coverage limit at $\theta^\sigma = 10$ equals $l_p \approx 16$, and at $\theta^\sigma \approx 56$ the electrostatic contribution should have dropped by a factor of about 25, i.e. to 0.4. The same applies for the systems with label numbered 3. The observed difference in persistence length between the charged and the uncharged systems is too large to be simply related to the electrostatic persistence length contribution, even when we account for the Manning condensation effect.

We have discussed at length that systems that can regulate the grafting position have a very low persistence length, compared to the systems for which the mobility of the grafts is impaired. We therefore attribute the rather high persistence length for electrostatically driven adsorption to the fact that the chains accumulate preferentially at places where the electrostatic potential is highest. When the charged DNA chain is curved, the electrostatic potential is highest in the confined convex part of the chain and lowest at the expanded concave part. Hence, there may be a small preference for the C_4K_{12} protein polymer to be attached to the confined part of the curved DNA chain. Even when this effect is small, there may be a big effect on the persistence length. Indeed the differences in l_p of 10 to 15 (lattice units) are significant.

The results for the tunable contributions of the persistence length of Figure 4.5 are for the regime where the protein-polymer concentration is in the dilute regime. In Figure 4.6 we show how the persistence length changes with polymer concentration for the co-assembled DNA-bottlebrush system under intermediate ionic strength conditions, i.e. $\varphi_s = 10^{-3}$ (10 mM salt). Similarly as in Figure 4.5 the charge density on the DNA is $v = -3$. We select the regime for which the tunable contributions of the persistence length is dominated by the bottlebrush contribution. Inspection of Figure 4.6 reveals that below the overlap concentration the induced persistence length increases with polymer concentration, whereas above the overlap the

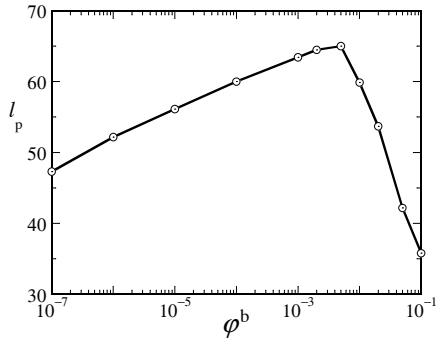

Figure 4.6: *The tunable contribution to the persistence length l_p in lattice units for co-assembled DNA-bottlebrushes as a function of the bulk volume fraction of C_4K_{12} for $\varphi_s = 0.001$ in lin-log coordinates. The charge $v = -3$ around the DNA chain is homogeneously distributed (cf. Figure 4.1F). The focus is on the behaviour near the overlap concentration.*

induced persistence length drops sharply. This result is comparable to our earlier prediction for chemically grafted bottlebrushes.[41] To explain this drop in induced persistence length, we must realize that in the bottlebrush corona the local polymer density is also in the overlap regime. As soon as the free polymer concentration becomes comparable to the polymer concentration in the corona, the free polymers impose an osmotic pressure such that the stretching of the corona chains diminishes: the typical shape of the corona chains relaxes back to Gaussian conformations. When the stretching of the chains diminishes, there is no information in the corona on the exact direction of the main-chain. Hence, there is less stiffening. Indeed, the result for the co-assembled DNA-bottlebrush stiffening is similar to the effect discussed earlier.[41]

4.5 Discussion

We have discussed various models for molecular bottlebrushes and focused on the tunable contributions to the persistence length. In particular, we introduced a number of models wherein the backbone volume was accounted for. We found that the backbone volume does not play a very important role, especially in cases wherein the charge along the backbone, or the grafting density of the side chains, have a degree of freedom to adjust to the imposed curvature stress. The so-called annealed cases gave persistence lengths similar to the ideal phantom chain models. Only when

rather irrealistic models were used in which the charge or the grafting density was quenched, we saw noticeable differences. We have seen that the electrostatic driving force for co-assembly leads to surprisingly large persistence lengths for the bottlebrushes. This result was traced to the reduced tendency of electrostatically bound chains to translocate from the compressed convex to the expanded concave sides of the curved DNA chain. The increased rigidity of the bottlebrush may translate to an increase in the persistence length of perhaps 10 nm, which is significant compared to the bare persistence length of DNA of about 30 nm, and tunable values which can be of the same order of magnitude.

Our main target was to understand the behaviour of our experimental system which is a bottlebrush formed by co-assembly of negatively charged double stranded DNA with a chemically well defined protein polymer, C_4K_{12}, which has 12 positively charged lysines connected to 400 aa long coil-like chain. Our co-assembled bottlebrush was found to show lyotropic behaviour, which is in fact a rare case for bottlebrush systems.[5] One might argue that naked DNA by itself forms liquid crystalline phases at sufficiently high concentration, and that it therefore is not too surprising that the corresponding bottlebrushes do the same. However, we have many failed attempts that use DNA as a backbone to make supramolecular bottlebrushes, but have different side chains than the C_4K_{12} protein polymer. Our numerical SCF analysis now gives us more insights why it is not so easy to find co-assembled bottlebrushes with lyotropic properties.

For liquid crystalline behaviour the l_p/D ratio must be significantly larger than unity. We have shown elsewhere that our bottlebrushes have a diameter in the order of 20 to 30 nm, which is about 10 times larger than the naked DNA. Clearly the co-assembled bottlebrushes did not increase the persistence length by the same factor of 10 compared to the naked DNA (including electrostatic stiffening). The above shows that at low ionic strength the induced persistence length of the brush simply replaces the electrostatic stiffening. At higher ionic strength the induced persistence length is larger than the electrostatic stiffening and thus l_p can be increased. Including the bare persistence length, we might have increased the overall persistence length from about 50 nm to perhaps 80 nm, but that's all. Apparently the l_p/D remained just large enough that lyotropic behaviour was kept.

We have seen in our experiments that overdosing the system with C_4K_{12} such that the free polymer concentration is above overlap, reduces the tendency to form lyotropic phases.[5] The results shown in Figure 4.6 explain this observation: to have lyotropic co-assembled bottlebrushes one

should avoid having a high polymer concentration in the bulk. We may now speculate why, in nature, bottlebrushes are used in lubrication applications. For lubrication one must endure compression forces such that the solution remains liquid and isotropic. Bottlebrushes can maintain flexibility and isotropy when embedded in a polymer solution.

The best conditions to form lyotropic co-assembled DNA-bottlebrushes as predicted by the numerical SCF modelling are: (i) polymer concentrations around the overlap concentration (ii) low ionic strength condition (when the ionic strength is very low the stiffening can be both due to the electrostatic double layer or to the brush), (iii) Long side chains with short anchor groups, (iv) polymers with a positive virial coefficient which endows stretching of the side chains.

We have seen that freely dispersed polymers above the overlap concentration have a negative effect on the bottlebrush stiffness. We expect the reduced stiffening of the bottlebrushes to also occur upon compressing bottlebrushes, e.g., by increasing the bottlebrush concentration. Hence solutions of bottlebrushes above the overlap concentration may have compressed coronas and hence a reduced rigidity. We expect that this is a general effect and does not only apply to co-assembled bottlebrushes. For example, classical chemically grafted bottlebrushes will experience similar compression induced flexibilisation, and may fail to produce anisotropic phases upon increasing the concentration. This might very well be the reason why it is so very difficult for bottlebrush systems to become liquid crystalline. Bottlebrush systems in nature often do not become liquid crystalline and this might very well be because their architecture is actually preventing this.[42]

4.6 Conclusion

We have used a numerical self-consistent field theory to analyze the electrostatic stiffening as well as the bottlebrush induced stiffening in molecularly realistic models for macromolecular bottlebrush systems. We found that the finite volume of the backbone is unimportant as long as the charge density or the brush grafting density is annealed, i.e. can adjust itself to relax the bending stresses. Our focus was to model co-assembled DNA-bottlebrushes which are formed by binding a well-defined protein polymer (C_4K_{12}) to dsDNA by electrostatic driving forces. We distinguish three terms to the overall persistence length: (i) the bare or intrinsic value, (ii) an induced persistence length caused by the bottlebrush side chains,

(iii) and an electrostatic contribution from the electric double layer around the DNA. In general, we found that when the side chains are bound to the DNA, the electrostatic stiffening is approximately replaced by the induced persistence length contribution. In other words, both terms are of the same order of magnitude. Interestingly, for electrostatically driven co-assembled DNA-bottlebrushes a remarkably high persistence length is found because the side chains have a low tendency to redistribute upon bending. This is because the chains bind best to the places where the electrostatic potential is highest, i.e. on the compressed convex side, rather than on the expanded concave side. This might be one of the reasons why our co-assembled DNA-bottlebrush system shows liquid crystalline behaviour. The calculations have furthermore shown that freely dispersed polymers above the overlap concentration can reduce the persistence length of bottlebrushes. We speculated that the crowding of bottlebrushes will induce a reduction of the stiffness as well, because both presence of free polymers and confinement cause a reduction of the stretching in the side chains. The loss of stretching leads to a flexibilisation of the chain as a whole. This flexibilisation mechanism may yet be another reason why there are so few reports on bottlebrushes in the literature that feature lyotropic behaviour.

References

(1) Semenov, A. N.; Khokhlov, A. R. *Usp. Fiz. Nauk (Soviet Physics - Uspekhi)* **1988**, *156*, 427.

(2) Brinkers, S.; Dietrich, H. R. C.; de Groote, F. H.; Young, I. T.; Rieger, B. *J. Chem. Phys.* **2009**, *130* 215105.

(3) Skolnick, J.; Fixman, M. *Macromolecules* **1977**, *10*, 944–948.

(4) Odijk, T. *J. Polym. Sci. Part B Polym. Phys.* **1977**, *15*, 477–483.

(5) Storm, I. M.; Kornreich, M.; Hernandez-Garcia, A.; Voets, I. K.; Beck, R.; Cohen Stuart, M. A.; Leermakers, F. A. M.; de Vries, R. *J. Phys. Chem. B.* **2015**, *119*, 4084–4092.

(6) Voets, I. K.; de Vries, R.; Fokkink, R.; Sprakel, J.; May, R. P.; de Keizer, A.; Cohen Stuart, M. A. *Eur. Phys. J. E* **2009**, *30*, 351–359.

(7) Hernandez-Garcia, A.; Werten, M. W. T.; Cohen Stuart, M. M. A.; de Wolf, F. A.; de Vries, R. *Small* **2012**, *8*, 3491–3501.

(8) Fredrickson, G. H. *Macromolecules* **1993**, *26*, 2825–2831.

(9) Livolant, F.; Leforestier, A. *Prog. Polym. Sci.* **1996**, *21*, 1115–1164.

(10) Wintermantel, M.; Fischer, K.; Gerle, M.; Ries, R.; Schmidt, M.; Kajiwara, K.; Urakawa, H.; Wataoka, I. *Angew. Chem. Int. Ed.* **1995**, *34*, 1472–1474.

(11) Tsukahara, Y.; Ohta, Y.; Senoo, K. *Polymer* **1995**, *36*, 3413–3416.

(12) Nakamura, Y.; Koori, M.; Li, Y.; Norisuye, T. *Polymer* **2008**, *49*, 4877–4881.

(13) Janmey, P. A.; Leterrier, J.-F.; Herrmann, H. *Curr. Opin. Colloid Interface Sci.* **2003**, *8*, 40–47.

(14) Jones, J. B.; Safinya, C. R. *Biophys. J.* **2008**, *95*, 823–835.

(15) Beck, R.; Deek, J.; Safinya, C. R. *Biochem. Soc. Trans.* **2012**, *40*, 1027–1031.

(16) Beck, R.; Deek, J.; Jones, J. B.; Safinya, C. R. *Nat. Mater.* **2009**, *9*, 40–46.

(17) Manning, G. S. *J. Chem. Phys.* **1969**, *51*, 924–933.

(18) Feuz, L.; Leermakers, F. A. M.; Textor, M.; Borisov, O. V. *Macromolecules* **2005**, *38*, 8891–8901.

(19) Birshtein, T. M.; Iakovlev, P. A.; Amoskov, V. M.; Leermakers, F. A. M.; Zhulina, E. B.; Borisov, O. V. *Macromolecules* **2008**, *41*, 478–488.

(20) Mikhailov, I. V.; Darinskii, A. A.; Zhulina, E. B.; Borisov, O. V.; Leermakers, F. A. M. *Soft Matter* **2015**, *11*, 9367–9378.

(21) Andreev, V. A.; Victorov, A. I. *J. Chem. Phys.* **2010**, *132* 054902.

(22) Lauw, Y.; Leermakers, F. A. M.; Cohen Stuart, M. A. *J. Phys. Chem. B* **2007**, *111*, 8158–8168.

(23) Fleer, G. J.; Cohen Stuart, M. A.; Scheutjens, J. M. H. M.; Cosgrove, T.; Vincent, B., *Polymers at interfaces*; Chapman and Hall, London: 1993.

(24) Grosberg, A. Y.; Khokhlov, A. R. *AIP press. Woodbury, NY* **1994**.

(25) Helfrich, W. *Zeitschrift fur Naturforschung. Teil C: Biochemie, Biophysik, Biologie, Virologie* **1973**, *28*, 693–703.

(26) Saariaho, M.; Ikkala, O.; Szleifer, I.; Erukhimovichm, I.; ten Brinke, G. *J. Chem. Phys.* **1997**, *107*, 3267–3276.

(27) Saariaho, M.; Szleifer, I.; Ikkala, O.; ten Brinke, G. *Macromol. Theory Simul.* **1998**, *7*, 211–216.

(28) Hsu, H.-P.; Paul, W.; Binder, K. *Macromol. Theory Simul.* **2011**, *20*, 510–525.

(29) Angelescu, D. G.; Linse, P. *Macromolecules* **2014**, *47*, 415–426.

(30) Fixman, M. *J. Phys. Chem. B* **2010**, *114*, 3185–3196.

(31) Barrat, J.-L.; Joanny, F. In *Advances in Chemical Physics*; John Wiley & Sons, Inc.: 2007, pp 1–66.

(32) Bjerrum, N. J. **1926**, *7*, 1–48.

(33) Hill, T. L., *An introduction to statistical thermodynamics*; Addison-Wesley, London: 1960.

(34) Lyklema, J., *Fundamentals of Interface and colloid science*; Academic Press: 1991; Vol. 1.

(35) Flory, P., *Principles of polymer chemistry*; Cornell University Press: 1953.

(36) Groot, R. D. *J. Chem. Phys.* **2003**, *118*, 11265–11277.

(37) Evers, O. A.; Scheutjens, J. M. H. M.; Fleer, G. J. *Macromolecules* **1990**, *23*, 5221–5232.

(38) Lifshitz, I. M.; Grosberg, A. Y.; Khokhlov, A. R. *Rev. Mod. Phys.* **1978**, *50*, 683–713.

(39) Edwards, S. F. *Proc. Phys. Soc.* **1965**, *85*, 613–624.

(40) Leermakers, F. A. M. *J. Chem. Phys.* **2013**, *138*, 154109.

(41) Storm, I. M. *In preparation* **2016**.

(42) Klein, J. *Polym. Adv. Technol.* **2012**, *23*, 729–735.

5 Inhibition of Hybridization of Complementary Single Stranded DNA by a Protein-Polymer Bottlebrush Coating

Abstract

We investigate the protein diblock copolymer C_8-Sso7d. Its Sso7d domain is a small basic protein from the hyperthermophilic archaeabacteria *Sulfolobus solfataricus* that binds DNA (both double and single stranded) sequences independently. The C_8 block is a long hydrophilic random coil. When the Sso7d domains binds to DNA, the C_8 chains stretch outward to form a bottlebrush structure. It has been found that the C_8-Sso7d protein polymer, to a large extent, prevents intrachain hybridization within single stranded DNA. Here we address the question whether the protein would also be able to prevent interchain hybridization of complementary ssDNA. If so, it could be a useful tool in displaying long ssDNA's in single-molecule sequencing approaches such as optical mapping. We first perform a thorough characterization of complexes of C_8-Sso7d with double stranded DNA, using light scattering, atomic force microscopy (AFM) and small angle X-ray scattering (SAXS). We find that the spacing between bound Sso7d domains is always much less than the size of their binding site. Consistent with a rather low grafting density, we find that the diameter of the brush is close to the size of the C_8 coils, and that the stiffening of the DNA due to the C_8 corona is much less than in the related diblock copolymer, C_4K_{12}, for which the grafting density is known to be higher. To investigate whether C_8-Sso7d can prevent interchain hybridization of complementary ssDNA, we start with 2kbp linear dsDNA. After alkaline denaturation, we add C_8-Sso7d and return to neutral *p*H. Complexes thus formed were investigated with AFM. Two distinct types of complexes are found, one appearing very flexible and sometimes branched, another one that is linear and (from AFM) has an estimated persistence length of around 50 nm. As expected, Mung

Bean nuclease rapidly degrades C_8-Sso7d coated M13 ssDNA, while complexes with dsDNA are not broken down. Complexes from the alkaline denaturation procedure were also broken down by Mung nuclease, but very slowly. In order to explain our findings we propose that complexes prepared with the alkaline denaturation procedure are indeed single-stranded, but that during the alkaline phase the Sso7d domains are unfolded, and that refolding during neutralization led to partial aggregation of the Sso7d domains on the DNA.

In preparation: Storm, I. M.; Cohen Stuart, M. A.; Leermakers, F. A. M.; de Vries, R. Inhibition of Hybridization of Complementary Single Stranded DNA by a Protein-Polymer Bottlebrush Coating

5.1 Introduction

Advances in the recombinant production of proteins have led to the development and production of protein-polymers:[1] de-novo designed polypeptides with a precisly defined, but repetitive aminoacid sequence such as the elastin-like polypeptides,[2–4] with the general sequence (VPGXG)n, where X is an arbitrary amino acid (but not proline). Most repetitive sequences that have been explored have been inspired by sequence motifs occurring in structural proteins such as collagen, silk and elastin protein-polymers[2–10] and can easily be combined in fusion constructs, with many different types of functional protein domains, to further broaden their scope of application, especially in biomedical engineering such as drug delivery[11] and tissue engineering.[12]

Another area where the unique advantages of protein-polymers can be exploited is for designing precisely structured polymer-DNA complexes. Such complexes have been studied especially in the context of non-viral gene delivery.[13] Most of the complexes used in non-viral gene delivery have very poorly defined morphologies, which is a problem since cells, tissues and organisms are known to be very sensitive to the precise dimensions and morphologies of nanoparticles.[14] It has even been difficult to design polymers that make complexes containing only a single DNA molecule. It appears however, that this can be achieved with cationic-neutral diblock copolymers with very short cationic blocks.[15–17]

Much better control over the morphology of polymer-DNA complexes can be obtained when using de-novo designed protein polymers produced via recombinant DNA technology. For example, we have shown that protein-polymers inspired by viral capsid proteins condense single DNA molecules into rod-shaped virus-like particles with a very precisely defined morphology, and good transfection efficiency.[18]

We have also worked with protein-polymer versions of cationic-neutral diblock copolymers. Neutral blocks were based on a 98 amino acid polypeptide motif rich in prolines, glycines and other uncharged hydrophilic residues.[5] In solution, this motif adopts random coil configurations for a wide range of solution conditions and hence is abbreviated as "C". As a cationic block, a simple oligolysine motif was used (K_{12}). Most experiments where done with a tetramer of the C block as the neutral block.[19]

Binding between double stranded DNA and the C_4K_{12} diblock protein-polymer is purely electrostatically driven, but due to the large asymmetry in the length of the two blocks, only complexes with single

DNA-molecules are formed. Each DNA molecule is covered with a layer of the C_4K_{12} diblocks, leading to the formation of self-assembled DNA bottlebrushes. From experiments of DNA-bottlebrushes confined in nanopores, we have found that the presence of the bottlebrush leads to a substantial increase of the persistence length, up to 250 nm, as compared to 50 nm for bare DNA.[20] The large persistence length of DNA bottlebrushes also implies that they start forming liquid crystals already at very low concentrations.[21]

Even though the C_4K_{12} protein polymer is able to manipulate the structure and properties of DNA in interesting ways, problems arise when it is being used in more complicated mixtures that apart from DNA also contain other negatively charged macromolecules. To avoid competitive adsorption in such cases, it would be better to have a diblock protein polymer with a DNA-binding block that is more specific to DNA. As a suitable candidate, we have identified the protein Sso7d from the hyperthermophilic archaeabacteria *Sulfolobus solfataricus*. The protein Sso7d and its homologues are well known for their sequence non-specific DNA binding, as well as their ability to withstand high temperatures.[22–25]

We have produced the protein-polymer fusion protein C_8-Sso7d, and investigated its interaction with various forms of DNA.[26] A remarkable difference was found between C_4K_{12} and C_8-Sso7d in the types of complexes that they formed with circular stranded ssDNA from bacteriophage M13mp18. Complexes of C_4K_{12} with the M13mp18 ssDNA were compact and branched, indicating substantial hybridization of stretches of complementary ssDNA, even after complexation with the protein polymer. On the other hand, when M13mp18 ssDNA was coated with the C_8-Sso7d protein-polymer the complexes were mostly circular, indicating that the protein-polymer largely prevented the hybridization of stretches of complementary ssDNA.

Here we wish to further elucidate this rather unique feature of the C_8-Sso7d diblock protein polymer, by investigating to what extent we can use C_8-Sso7d to prevent inter chain hybridization of complementary strands of ssDNA. The approach will be to alkaline denature pieces of linear dsDNA, coat them with C_8-Sso7d, and bring the *p*H back to neutral. Although not yet explored here, it is clear that being able to keep long complementary ss-DNA in a completely linear form, without any hybridization, could eventually be very useful for more easily accessing the sequence information presented by the exposed bases. In particular, we have already shown that stiffening of double stranded DNA by the C_4K_{12} protein diblock copolymer, allows for stretching long DNA's in rather wide nanochannels.[20] Stretching

DNA is a key step in the single-DNA sequencing technology called optical mapping, that allows for the rapid identification of the presence or absence of specific short sequences in very long, single DNA molecules.[27–30] So far, a convenient way of stretching long single stranded DNA is lacking, because of the problem of intra- and inter chain hybridization for long single stranded DNA's. Possibly, the C_8-Sso7d protein polymers could be used to stretch ssDNA in nanopores and allow for optical mapping.

First we perform a more quantitative characterization of the interaction of the C_8-Sso7d diblock protein polymer with dsDNA. We use static light scattering to estimate the amounts of protein bound to the DNA molecules in solution, and use small angle X-ray scattering (SAXS) to determine the thickness of the polymer coating that forms around the dsDNA molecules. The increase of the persistence length of dsDNA due to the protein polymer coating is quantified using atomic force microscopy (AFM) on dried protein-DNA complexes. Next we investigate what happens when dsDNA is denatured, coated with C_8-Sso7d and brought back to renaturation conditions. We use static light scattering (SLS) and AFM to characterize the complexes thus obtained. A comparison with the corresponding results for non-denatured dsDNA, plus digestion assays performed with ssDNA-degrading nucleases strongly suggest that also for completely complementary stretches of ssDNA, the C_8-Sso7d protein is able to prevent renaturation into dsDNA.

5.2 Materials and Methods

5.2.1 Fermentation and Purification of the Protein Polymer

The production and fermentation of this recombinant C_8-Sso7d diblock is described elsewhere.[26] In short, we used a *Pichia Pastoris* strain harboring a gene for the secreted expression of the diblock protein C_8-Sso7d. For the fermentation process we used a 2.5-L Bioflo3000 fermentor. Fed-batch fermentation was done for 2 days, from the moment of induction. During fermentation, the *p*H was kept at 3 by the controlled addition of ammonium hydroxide. The methanol content of the broth was maintained at 0.2% (w/v). When the fermentation was completed the protein containing supernatant was separated from the yeast cells by centrifugation at 16 000 × g for 30 minutes at 20 °C (SLA-rotor) and subsequent filtration using 0.2 μm AcroPak 200 capsules with a Supor membrane (Pall Corporation).

After acquiring the cell-free protein solution, medium salts were precipitated by NaOH addition until a *p*H of 8 was reached. The protein solution

was separated from the precipitated medium salt by centrifugation (16000 × g, 30 min, 4 °C, SLA-1500 rotor). The C_8-Sso7d protein was selectively precipitated from secreted Pichia Pastoris proteins by addition of ammonium sulphate (45% saturation) for 30 minutes at 4 °C and subsequent centrifugation (16000 × g, 30 min, 4 °C, SLA-1500 rotor). This precipitation step was repeated once. The precipitate was resuspended in 0.1 × the original cell-free broth volume of 50 mM formic acid and extensively dialysed against 50 mM formic acid. After refreshing the formic acid for 4 times the protein solution was dialysed once against 10 mM formic acid and subsequently frozen and freeze dried.

5.2.2 Light Scattering

Static light scattering (SLS) experiments were performed at an angle of 173° on a *Malvern Instrument zetasizer nanoseries*. We used 300bp dsDNA in a 10 mM Tris-HCl buffer of *p*H 7.6 for SLS experiments starting from a DNA concentration of 0.1 mg/ml. To acquire the plot in Figure 5.2, where Γ_{bound} is the mass ratio of bound protein over DNA, we performed a step-wise addition with a concentrated protein solution (4 mg/ml) in a similar buffer as the DNA solution. We determined this amount of bound protein, Γ_{bound}, by using the scattering intensity ratio of protein, $I_{protein}$, to bare DNA, I_{DNA}, according to Golinska *et al.*[31] and performed exactly the same as Storm *et al.*[21] except for the use of a different type of protein:

$$\frac{I_{\text{complex}}}{I_{\text{DNA}}} = (1 + \Gamma_{\text{bound}}\zeta)^2 \tag{5.1}$$

where ζ is the ratio of the respective refractive index increments of protein and DNA:

$$\zeta = \left(\frac{dn}{dC}\right)_{\text{prt}} \Big/ \left(\frac{dn}{dC}\right)_{\text{DNA}} \tag{5.2}$$

were we use $(dn/dc)_{\text{DNA}} = 0.165$ and $(dn/dc)_{\text{prt}} = 0.18$, that results in $\zeta = 1.091$.[32,33] Every addition of more protein results in an increase in total sample volume. To ensure the proper scattering ratio we corrected the scattering intensity for bare DNA with the dilution factor. When we assume negligible scattering intensity coming from the free protein in solution, the amount of bound protein to DNA, Γ_{bound}, equals:

$$\Gamma_{\text{bound}} = \frac{1}{\zeta}\left(\sqrt{\frac{I_{\text{complex}}}{I_{\text{DNA}}}} - 1\right) \tag{5.3}$$

5.2.3 Formation of Complexes with Alkaline Denatured DNA

For these experiments, 2 kbp monodisperse DNA was used (NoLimits 2000bp DNA fragments, Thermo Scientific). First, 20 μl of the DNA solution (0.5 μg/μl) was mixed with 180 μl of a 0.5 M NaOH solution. This mixture was heated for 10 minutes at 50°C. Subsequently, the required amount of C_8-Sso7d protein stock solution was added, and the complexes were incubated overnight under alkaline conditions. After incubation, centrifugal filtration at 13000 × g (*Amicon Ultra - 0.5mL 3K Membrane*) was used to extensively wash the samples with 10 mM Tris-HCl *p*H 7.6 and 0.05% NaN_3 to return to neutral *p*H.

5.2.4 AFM

Samples for AFM wafers were prepared by first incubating the DNA and C_8-Sso7d protein for approximately 24 hours. After incubation, 5 μl of the DNA-protein complexes (25 μg/ml of DNA) was deposited on a silicon wafer (after plasma cleaning treatment). After 10 minutes the sample was washed by adding 0.3 ml of MQ water onto the wafer, and drying the sample with N_2(g). Samples were analysed using a Digital Instrument Nanoscope V with a Silicon Tip on a Nitride Lever (Bruker) and a spring constant of 0.4 N/m. For the imaging process the ScanAsyst mode in air was used with a scanning speed of 0.977 Hz and a resolution of 512 samples/line (each scan line has 512 pixels).

5.2.5 AFM Data Treatment

AFM images were produced using Nanoscope Analysis 1.4 software. To estimate persistence lengths of the DNA-C_8-Sso7d complexes, we used the program 'Easyworm'.[34] At least 50 complexes were analysed for each persistence length (estimate) with a fitting parameter of 5. For the analysis we assumed the complexes were 2D-equilibrated and we used the end-to-end method to acquire the persistence length.

5.2.6 SAXS

Small angle X-ray scattering experiments were performed at MAXlab II, Lund, Sweden, on the I911-4 beamline. The detector distance was chosen such that the q-range corresponded to 0.008-0.550 $Å^{-1}$ with an incident wavelength of 1.2 Å and a PILATUS 1M detector from Dectris. Samples were measured using a 'high throughput solution scattering set-up' to properly

subtract the buffer from the sample at exactly the same location in the capillary.. Acquisition time was typically 20 minutes per sample.

For the samples we used 100 μg/ml ds λ-DNA coated with 0.25 ptn/nt of C_8-Sso7d protein polymer. The sample shown in Figure 5.4 has a protein to DNA ratio of 0.25 ptn/nt. For the sample consisting only of free protein we used a concentration of 30 mg/ml C_8-Sso7d.

Scattering data were analyzed using SASview 3.0.0 software. To fit our scattering data we used two types of models. To describe the experimental data collected for the free C_4K_{12} protein polymers in solution we used a model for polymers with excluded volume,[35,36] for the DNA-bottlebrushes we used a model for randomly oriented homogeneous cylinders.[37,38]

5.2.7 Mung Bean Nuclease Assay

Mung Bean nuclease, MBN, was obtained from New England Biolabs Inc. For the MBN assay, the DNA concentration used was always 50 μg/ml. To 20 μl of DNA, or DNA-protein complex, we added 20 units of MBN (20 × more nuclease than was recommended by the supplier). DNA with MBN were heated to 37°C for 1 hour up to 96 hours. After heating the DNA-MBN samples were heated to 60°C for 10 minutes to deactivate the enzyme. A 1% agarose gel was prepared using TAE electrophoresis buffer (40 mM Tris, 20 mM Acetic Acid, 1 mM EDTA). The DNA-ladder used was a 1kb plus DNA ladder (0.1 μg/μl) (Invitrogen). In all cases, wells were loaded with 5 μl of DNA solution or DNA-protein complex solution.

5.3 Results and Discussion

Schematic structures of the previously studied C_4K_{12} diblock[19,21] and the new C_8-Sso7d diblock bound to dsDNA are shown in Figure 5.1. The new C_8-Sso7d diblock differs in two ways from the previously studied C_4K_{12}. First, the hydrophilic random coil is twice as long (octamer of the 98 amino acid long "C" blocks, instead of a tetramer). Second, the 7 kDa binding block Sso7d binds specifically to nucleic acids (binding stronger to dsDNA than to ssDNA and RNA),[25,39] whereas the dodecalysine (K_{12}) binding block is completely aspecific, binding to any sufficiently negatively charged object. It has been shown that upon binding to dsDNA, Sso7d induced a kink in the DNA.[40] The protein-induced kinks make the DNA appear more flexible in single-DNA force-extension experiments.[41]

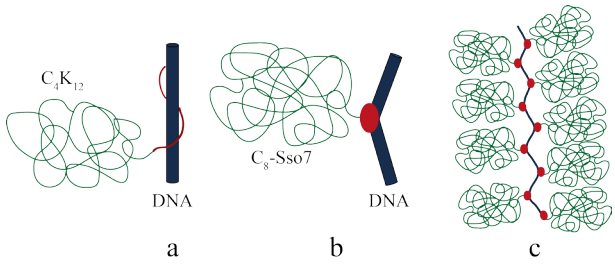

Figure 5.1: *Schematic representation of protein polymers bound to DNA. (a) C_4K_{12} protein polymer bound to DNA. (b) C_8-Sso7d bound to DNA. The Sso7d protein is known to induce a kink in the DNA structure. (c) A bottlebrush molecule constructed from DNA and C_8-Sso7d protein polymers.*

5.3.1 Interaction of C_8-Sso7d with dsDNA

Previously, the binding of C_8-Sso7d to dsDNA was analyzed using electrophoretic mobility shift assays,[26] here we use a more quantitative technique to determine the amount of protein that binds to the DNA, i.e. Static light scattering (SLS). From SLS, one can infer the molar mass of complexes in solution. Since the scattering of the free proteins is negligible as compared to that of the complexes, static light scattering leads to a straightforward estimate of the mass ratio Γ_{bound} of coated to non-coated DNA as a function of the solution concentration of DNA and protein (see Materials and Methods). From the mass ratio, we compute the degree of binding. In view of a later comparison with complexes with ssDNA, we plot the degree of binding as the molar ratio of the number of bound C_8-Sso7d proteins over the total number of nucleotides, $[C_8\text{-Sso7d}]_{bound}/[\text{nt}]$, as a function of the molar ratio of total protein over nucleotides, $[C_8\text{-Sso7d}]_{tot}/[\text{nt}]$. Results for dsDNA are show in Figure 5.2, for concentrations of 10 mM and 80 mM Tris-HCl solution.

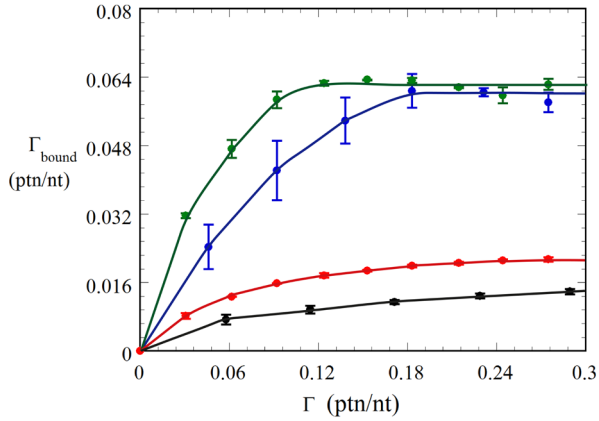

Figure 5.2: *Amount of bound C_8-Sso7d protein to DNA nucleotides, Γ_{bound} (ptn/nt), as a function of the total amount of protein to nucleotides, Γ (ptn/nt). The green and red curve represent double stranded DNA-C_8-Sso7d complexes in a 10 mM and 80 mM Tris-HCl solution of pH 7.6 respectively. The blue and black data corresponds to the amount of bound C_8-Sso7d protein polymer to M13mp18 single stranded DNA in a 10 mM and 80 mM Tris-HCl solution of pH 7.6 respectively.*

At an ionic strength of 10 mM (green) we see that initially, at low protein concentrations, the amount of bound protein (Γ_{bound}) increases fast before it reaches a plateau at roughly 0.064 ptn/nt. For the 80 mM (red) ionic strength we see a more gradual increase of bound protein polymer that already saturates around 0.016 ptn/nt. The size of the Sso7d binding site on dsDNA is known to be about 4 base pairs (or 0.25 ptn/nt).[25,39,42] Our data shows very clearly that this maximum coverage is never reached: coverage saturates at about 0.07 ptn/nt, about one third of the maximum coverage reported for Sso7d. Probably, very high coverage would require stretching of the C_8 blocks, that are too unfavorable, energetically. As for many DNA binding proteins, part of the binding affinity of Sso7d for DNA derives from electrostatic interactions, hence its binding is sensitive to ionic strength.[42] For the C_8-Sso7d diblocks we expect that the salt dependent binding strength should result in a salt-dependent maximum coverage because attaching more and more diblocks requires that the C_8 block stretches. Stretching of the C_8 block costs more energy which is not necessarily available when the electrostatic contribution of the binding energy is reduced by increasing salt concentrations. Indeed, we observe that at 80 mM NaCl, the maximum coverage for C_8-Sso7d is 0.016 ptn/nt, which is a factor of 4 lower than the maximum coverage of 0.064 ptn/nt at

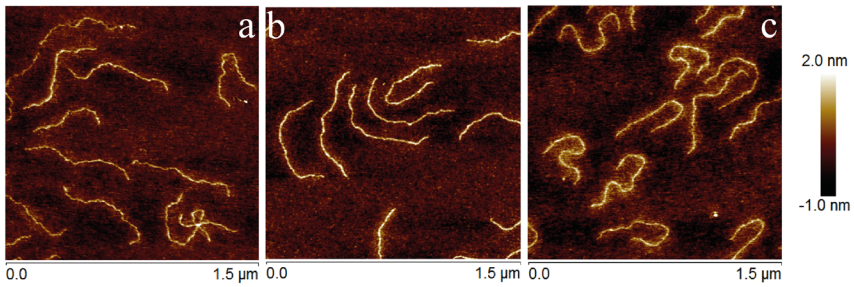

Figure 5.3: *AFM images of complexes of C_8-Sso7d with dsDNA. (a) 0.25 ptn/nt (theoretical full coverage), (b) 0.50 ptn/nt and (c) 0.75 ptn/nt. The samples were incubated in a 10 mM Tris-HCl solution of pH 7.6 for 24 hours prior to deposition onto the silica wafer.*

10 mM Tris-HCl.

Typical AFM images of 2000bp dsDNA fragments coated with various amounts of C_8-Sso7d diblock are shown in Figure 5.3(a-c). Figure 5.3(a) shows the DNA-C_8-Sso7d complexes at a protein to DNA ratio of 0.25 ptn/nt (if all proteins would be bound, this would correspond to the full coverage for the Sso7d binding domain), Figures 5.3(b) and (c) show AFM images of complexes at protein to DNA ratios of 0.50 and 0.75 ptn/nt respectively. From the AFM images we estimated both the contour lengths, l_c, and the persistence lengths, l_p, of C_8-Sso7d coated dsDNA. Results for 0.25, 0.50 and 0.75 ptn/nt are given in Table 5.1. As a control experiment we used bare DNA. Its contour length (l_c = 650 +/- 45) was close to the expected length of 680 nm, based on a contour length of 0.34 nm/bp. Also, the estimated persistence length was l_p = 51 +/- 6 nm, in agreement with the accepted value of 50 nm. While it is clear that with AFM on dried samples there are many possibilities for systematic errors, in view of the good result for the bare DNA control, we are confident that the method should at least give qualitatively correct results also for the complexes.

We find that when coating the dsDNA with the C_8-Sso7d diblock, the persistence length, l_p, increases to almost double the value for bare DNA, namely to about 100 nm. The increase in persistence length we observe is most likely caused by the dense brush of C_8 chains around the DNA, that induces the so-called main-chain stiffening effect first described by Fredrickson.[43] Similar stiffening effects were observed for the C_4K_{12} diblock.[19,21] In that case, an analysis of C_4K_{12} coated DNA confined in nanopores resulted in estimated persistence lengths of up to 250 nm. The

stiffening effect observed here is much less strong. As we have found from SLS, the Sso7d binding block is not strong enough to lead to the formation of a bottlebrush with a very high grafting density, and the lower grafting density of the side chains probably leads to a lower degree of main-chain stiffening. In our measurements we also find that there is a significant increase of the contour lengths of the complexes at intermediate protein concentrations (see Table 5.1), a phenomenon that was not found in our initial studies.[26] For now it is unclear whether the differences between the two sets of experiments are due to differences in the details of AFM imaging (and hence are in fact an artifact), or due to slightly different experimental conditions for the two sets of experiments.

Table 5.1: *The contour length of 2000bp dsDNA coated with C_8-Sso7d protein and the corresponding persistence length determined from AFM images (Figure 5.3) according to 2D-equilibrium fit*

sample	l_c	l_p
(-)	(nm)	(nm)
bare dsDNA	650 ± 45	51 ±6
dsDNA + C_8-Sso7d 0.25 ptn/nt	660 ± 34	87 ±15
dsDNA + C_8-Sso7d 0.50 ptn/nt	740 ± 70	111 ±13
dsDNA + C_8-Sso7d 0.75 ptn/nt	804 ± 46	69 ±4
dsDNA + C_8-Sso7d 2.50 ptn/nt	687 ± 31	89 ±29

The extent of stretching of the C_8 chains, as reflected by the diameter of the DNA complexes in solution, is strongly related to the degree of main-chain stiffening.[44] In order to determine the solution diameter of C_8-Sso7d coated dsDNA, we have performed small angle X-ray scattering (SAXS), for values of the magnitude q of the wavevector, in the range of $0.1 < q < 2$ nm^{-1}. Results for the scattering intensity versus the magnitude of the scattering wavevector are shown in Figure 5.4 for both the free C_8-Sso7d protein, and for its complexes with dsDNA. Data for the free proteins can be fitted with a polymer excluded volume model, which gives a radius of gyration of 6.9 nm. For the case of the complexes, we know that there will also be free protein in the solution. Therefore, in fitting the data for the complexes, we use a combined model consisting of a cylindrical rod (representing the complexes) plus the model for a polymer excluded volume for the free protein in solution. Parameters for the free proteins were taken from the fit of the protein-only data. We find that at large wavevectors, ($0.1 < q < 2$ nm^{-1}) most of the noticeable features of the scattering due to the

cylindrical rods are masked by the scattering of the free proteins. Only at low wavevectors ($0.1 < q < 0.3\ nm^{-1}$), the scattering due to the rods results in distinct differences with respect to the results for the free proteins. By fitting this low wavevector data, we can extract an estimated value for the diameter of the cylindrical rods, for which we find 16.8 nm. This is more than twice the gyration radius for the free protein. Hence, the C_8 chains decorating the dsDNA are indeed significantly stretched and form a true "bottlebrush" around the central DNA chain. The stretching that we find from SAXS is also consistent with our conclusion from SLS, that maximum coverage is not achieved since binding of C_8-Sso7d opposes stretching of the C_8 blocks.

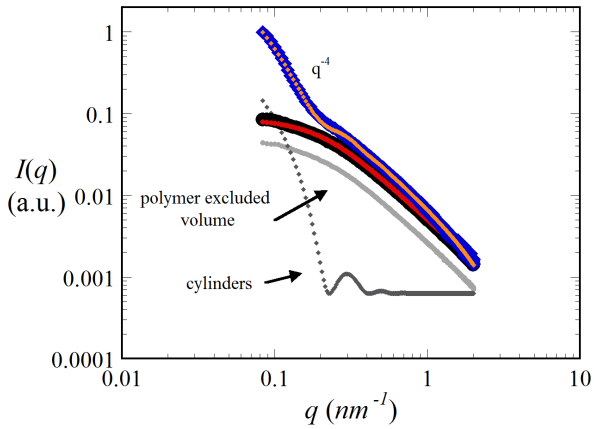

Figure 5.4: *SAXS spectra (scattered intensity I versus wavevector q) for DNA bottlebrushes and free protein polymers. The blue data points represent the DNA-bottlebrushes. The orange curve represents a combination fit for a "cylinder model" and a "polymer excluded volume". The black curve corresponds to free C_8-Sso7d protein polymer. The red curve is a fit for a polymer excluded volume. The intensity of the free C_8-Sso7d protein (black) was decreased by a factor of 10 to match the protein concentration of the DNA-C_8-Sso7d sample (blue). The two curves shown in gray represent the relative contributions to the total scattering of the fitted curve. These relative contributions were shifted horizontally for clarity reasons.*

5.3.2 Complexes with Alkaline Denatured dsDNA

In our initial studies on C_8-Sso7d, we found that binding of C_8-Sso7d to circular ssDNA (M13mp18 DNA) prevents hybridization of complementary stretches of ssDNA, whereas the C_4K_{12} diblock does not.[26] This is il-

lustrated in Figure 5.5. An AFM image of typical complexes of the M13 ssDNA with C_8-Sso7d are shown in Figure 5.5(a). This shows very little local hybridization. A few more branched M13 ssDNA coated with C_8-Sso7d complexes are shown in 5.5(b).

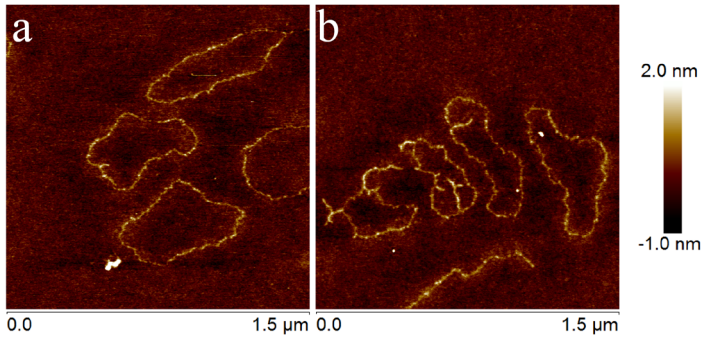

Figure 5.5: *AFM image of M13mp18 ssDNA coated with C_8-Sso7d (0.50 ptn/nt). (a) Typical AFM image of circular M13mp18 ssDNA complexes with C_8-Sso7d. (b) AFM image of more branched M13mp18 ssDNA-C_8-Sso7d complexes. The samples were incubated in a 10 mM Tris-HCl solution of pH 7.6 for 24 hours prior to deposition onto the silica wafer.*

For the M13 ssDNA, we have determined the amount of bound C_8-Sso7d in the same way as for dsDNA, using SLS. Results are shown in Figure 5.2, together with those for dsDNA. Clearly, the binding to the ssDNA is very similar to that for dsDNA, with maximum coverages for ssDNA and dsDNA that are very similar at both ionic strengths (10 mM and 80 mM Tris-HCl buffer).

Complementarity and the driving force for hybridization are of course even larger in the case of denatured dsDNA. This is the case we want to investigate next. We use alkaline denaturation and 2000bp linear dsDNA. The proteins are added when the DNA is still in its denatured form, at high *p*H. After denaturation and addition of the diblock protein polymer, the samples are washed extensively with the final *p*H 7.6 buffer using centrifugal filters. Complexes of alkaline denatured dsDNA were imaged using AFM. Results for different protein to DNA ratios are shown in Figure 5.6(a-c). There is a clear difference between the morphologies of these complexes and those for the non-denatured dsDNA (Figure 5.3). After the alkaline-denaturation procedure, complexes look in general more flexible. There seem to be two populations of complexes, for which the DNA molecules have, respectively, 'collapsed' and 'extended' configurations. The

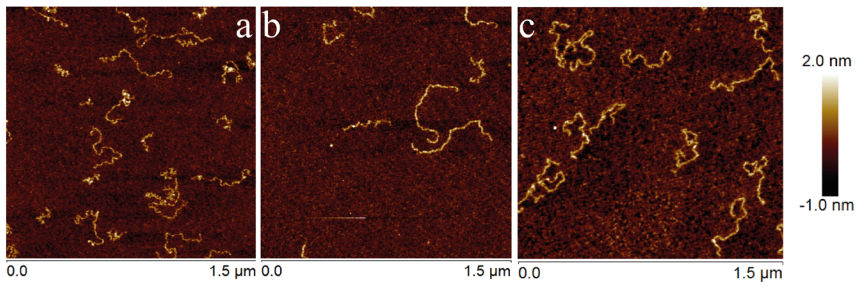

Figure 5.6: *AFM images of complexes of C_8-Sso7d with ssDNA. (a) 0.25 ptn/nt (theoretical full coverage), (b) 0.50 ptn/nt and (c) 0.75 ptn/nt. The C_8-Sso7d protein polymers were added to the DNA when the DNA was still in its denaturated state. After protein addition the samples were extensively washed with a 10 mM Tris-HCl buffer solution of pH 7.6. The samples were deposited on a silica wafer after 24 hours of incubation in a 10 mM Tris buffer.*

number of 'collapsed' complexes seems to decrease with increasing protein concentration, at the expense of the number of 'extended' complexes. At the lowest protein to DNA ratio (0.25 ptn/nt, Figure 5.6(a)), most complexes are 'collapsed' but at the highest protein to DNA ratio (0.75 ptn/nt, Figure 5.6(c)), there are only very few 'collapsed' objects left. The 'collapsed' configurations that we observe at the lowest protein coverages (0.25 prt/nt, Figure 5.6(a)) are similar to AFM images of bare ssDNA, such as those shown by Adamcik et al.,[45] except that the latter have a more branched structure, presumably due to local hybridization.

Table 5.2: *The contour length of 2000bp ssDNA coated with C_8-Sso7d protein and the corresponding persistence length determined from AFM images (Figure 5.6) according to 2D-equilibrium fit*

sample	l_c	l_p
(-)	(nm)	(nm)
bare dsDNA	650 ± 45	51 ±6
ssDNA + C_8-Sso7d 0.25 ptn/nt	659 ± 53	51 ±6
ssDNA + C_8-Sso7d 0.50 ptn/nt	704 ± 24	55 ±8
ssDNA + C_8-Sso7d 0.75 ptn/nt	645 ± 39	40 ±6

A remarkable observation is that we do not observe complexes that are partly 'collapsed' and partly 'extended'. This suggest that complex formation during the alkaline denaturation procedure is highly cooperative.

For the 'collapsed' complexes, that frequently are branched, it is not so clear how to perform a quantitative analysis of their shape and dimensions. We therefore focus on the 'extended' complexes, that are linear and for which we can determine a contour length l_c and a persistence length l_p. Results of this analysis are given in Table 5.2. It appears that the persistence length l_p of the 'extended' complexes is about 50 nm for all protein to DNA ratios. Note that ssDNA itself is extremely flexible, with a reported persistence length of l_p = 4.6 nm.[46] Contour lengths l_c of the 'extended' complexes were also quite independent of the protein to DNA ratio, and were close to the contour length of 680 nm, for a 2000bp dsDNA template, assuming a contour length of 0.34 nm per bp. Assuming for the moment that the DNA inside the 'extended' complexes is in a single stranded state, this means that the ssDNA should then be significantly, but not fully stretched, since in the latter case the contour length of the complexes should have exceeded that of the dsDNA.

If the DNA inside the complexes produced via the alkaline denaturation procedure is indeed in a single stranded state, it should be possible to digest the ssDNA using Mung Bean nuclease, a nuclease that is specific to ssDNA. Indeed, the Mung Bean nuclease rapidly (in 3 hours) degrades circular M13 ssDNA (compare lanes 4 and 5 of the gel in Figure 5.7(a). Also for M13 ssDNA coated with 0.25 ptn/nt of C_8-Sso7d, incubation for 3h with the Mung Bean nuclease leads to complete digestion. For the 2000bp linear dsDNA coated with 0.5 ptn/nt of C_8-Sso7d we find, as expected, that prolonged incubation with Mung Bean nuclease (96h) does not lead to digestion (compare lanes 3 and 4 of the gel in Figure 5.7(b). Somewhat surprisingly we find that the complexes prepared via the alkaline denaturation procedure can be digested by Mung Bean nuclease, but only after very long incubation times (96h, compare lanes 6 and 7 of the gel in Figure 5.7(b).

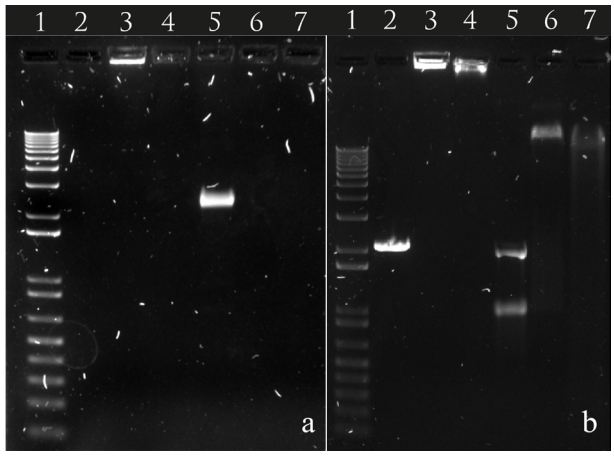

Figure 5.7: *Degradation of complexes of DNA and C_8-Sso7d by Mung Bean nuclease. (a) M13mp18 ssDNA in combination with C_8-Sso7d and or Mung Bean nuclease; lane 1: DNA ladder, lane 2: M13mp18 ssDNA coated with C_8-Sso7d (0.50 ptn/nt) in the presence of Mung Bean nuclease, lane 3: M13mp18 ssDNA coated with C_8-Sso7d (0.50 ptn/nt), lane 4: bare M13mp18 ssDNA in the presence of Mung Bean nuclease, lane 5: bare M13mp18 ssDNA. Samples were incubated for 3 hours at 37 °C. Image (b) uses linear 2000 NoLimits DNA complexes with C_8-Sso7d and or Mung Bean nuclease; lane 1: DNA ladder, lane 2: bare 2000 bp dsDNA, lane 3: 2000 bp dsDNA coated with C_8-Sso7d 0.50 ptn/nt, lane 4: 2000 bp dsDNA coated with C_8-Sso7d 0.50 ptn/nt and in the presence of Mung Bean nuclease, lane 5: denatured 2000 nt ssDNA and hybridized dsDNA (due to pH of agarose gel buffer), lane 6: 2000 nt ssDNA coated with C_8-Sso7d (0.50 ptn/nt), lane 7: complexes of 2000 nt ssDNA and C_8-Sso7d (0.50 ptn/nt). Samples were incubated for 96 hours at 37 °C with Mung Bean nuclease. Both gels consisted of 1% agarose gel and were run at 90 V.*

5.4 Concluding Remarks

Our results for the complexes of DNA with the C_8-Sso7d diblock protein polymer formed after the alkaline-denaturation procedure are somewhat ambiguous. Morphologies are clearly very different from those with non-denatured dsDNA, but for now it is unclear why there are two types of complexes. Combined with the fact that the complexes can be digested by Mung Bean nuclease, our results strongly suggest that the alkaline denaturation protocol does lead to complexes in which the two complementary parts of the ssDNA's are separately coated and protected from renaturation. It is not so clear why these complexes are so much more resistant to degradation by Mung Bean nuclease than the

complexes of C_8-Sso7d with circular M13 ssDNA. Possibly, during the alkaline incubation the Sso7d domain is in a denatured state.[47] During neutralization, the Sso7d domains may be bound to the DNA at a quite high density while renaturing, and this could possibly lead to incorrect refolding and/or aggregation of the Sso7d domains on the DNA template. Such an aggregation could explain the increased resistance against Mung Bean nuclease degration. Also, Sso7d aggregation on DNA could be a source of the cooperativity that is needed to explain why two rather different types of complexes coexist. Clearly, further work needs to be done to more definitely establish that in the complexes prepared via the alkaline denaturation route, the two complementary strands of the DNA are truly separated. Most likely this can be achieved using a FRET-based assay using 3' and 5'-fluorescently labeled DNAs.[48] Furthermore, the assumption that refolding during *p*H neutralization is problematic also suggest that it would be useful to explore other, possibly less extreme denaturation conditions. If it can definitely be established that the complexes prepared via the alkaline denaturation are single stranded, and if such complexes can be sequence specifically labelled with fluorescent probes, that could open up the possibility to stretch long ssDNA's e.g. in nanopores and use them for optical mapping.[20] For such an application, it would obviously be very important to better understand the molecular architecture of the complexes than we do now.

References

(1) Rodriguez-Cabello, J. C.; Reguera, J.; Girotti, A.; Arias, F. J.; Alonso, M. In *Ordered Polymeric Nanostructures at Surfaces*, Vancso, G., Ed.; Advances in Polymer Science, Vol. 200; Springer Berlin Heidelberg: 2006, pp 119–167.

(2) Lee, T. A. T.; Cooper, A.; Apkarian, R. P.; Conticello, V. P. *Adv. Mater.* **2000**, *12*, 1105–1110.

(3) MacEwan, S. R.; Chilkoti, A. *Peptide Science* **2010**, *94*, 60–77.

(4) Bracalello, A.; Santopietro, V.; Vassalli, M.; Marletta, G.; Gaudio, R. D.; Bochicchio, B.; Pepe, A. *Biomacromolecules* **2011**, *12*, 2957–2965.

(5) Werten, M. W. T.; Wisselink, W. H.; Jansen-van den Bosch, T. J.; de Bruin, E. C.; de Wolf, F. A. *Protein Eng.* **2001**, *14*, 447–454.

(6) Sanford, K.; Kumar, M. *Curr. Opin. Biotechnol.* **2005**, *16*, 416–421.

(7) Urry, D. W. *J. Phys. Chem. B* **1997**, *101*, 11007–11028.

(8) Prince, J. T.; McGrath, K. P.; DiGirolamo, C. M.; Kaplan, D. L. *Biochemistry* **1995**, *34*, 10879–10885.

(9) Anderson, J. P.; Cappello, J.; Martin, D. C. *Biopolymers* **1994**, *34*, 1049–1058.

(10) Rabotyagova, O. S.; Cebe, P.; Kaplan, D. L. *Biomacromolecules* **2009**, *10*, 229–236.

(11) Cappello, J.; Crissman, J. W.; Crissman, M.; Ferrari, F. A.; Textor, G.; Wallis, O.; Whitledge, J. R.; Zhou, X.; Burman, D.; Aukerman, L.; Stedronsky, E. R. *J. Controlled Release* **1998**, *53*, 105–117.

(12) Wlodarczyk-Biegun, M. K.; Werten, M. W. T.; de Wolf, F. A.; van den Beucken, J. J. J. P.; Leeuwenburgh, S. C. G.; Kamperman, M.; Cohen Stuart, M. A. *Acta Biomater.* **2014**, *10*, 3620–3629.

(13) Harada, A.; Kataoka, K. *Prog. Polym. Sci.* **2006**, *31*, 949–982.

(14) Yin, H.; Kanasty, R. L.; Eltoukhy, A. A.; Vegas, A. J.; Dorkin, J. R.; Anderson, D. G. *Nat. Rev. Genet.* **2014**, *15*, 541–555.

(15) DeRouchey, J.; Walker, G. F.; Wagner, E.; Rädner, J. O. *J. Phys. Chem. B* **2006**, *110*, 4548–4554.

(16) Wei, Z.; Ren, Y.; Williford, J.-M.; Qu, W.; Huang, K.; Ng, S.; Mao, H.-G.; Luijten, E. *ACS Biomater. Sci. Eng.* **2015**.

(17) Kakizawa, Y.; Kataoka, K. *Adv. Drug Deliv. Rev.* **2002**, *54*, 203–222.

(18) Hernandez-Garcia, A.; Kraft, D. J.; Janssen, A. F. J.; Bomans, P. H. H.; Sommerdijk, N. A. J. M.; Thies-Weesie, D. M. E.; Favretto, M. E.; Brock, R.; de Wolf, F. A.; Werten, M. W. T.; van der Schoot, P.; Cohen Stuart, M. A.; de Vries, R. *Nat. Nanotechnol.* **2014**, *9*, 698–702.

(19) Hernandez-Garcia, A.; Werten, M. W. T.; Cohen Stuart, M. M. A.; de Wolf, F. A.; de Vries, R. *Small* **2012**, *8*, 3491–3501.

(20) Zhang, C.; Hernandez-Garcia, A.; Jiang, K.; Gong, Z.; Guttula, D.; Ng, S. Y.; Malar, P. P.; van Kan, J. A.; Dai, L.; Doyle, P. S.; de Vries, R.; van der Maarel, J. R. C. *Nucleic Acids Res.* **2013**, 1–8.

(21) Storm, I. M.; Kornreich, M.; Hernandez-Garcia, A.; Voets, I. K.; Beck, R.; Cohen Stuart, M. A.; Leermakers, F. A. M.; de Vries, R. *J. Phys. Chem. B.* **2015**, *119*, 4084–4092.

(22) Choli, T.; Henning, P.; Wittmann-Liebold, B.; Reinhardt, R. *BBA - Gene Structure and Expression* **1988**, *950*, 193–203.

(23) Baumann, H.; Knapp, S.; Karshikoff, A.; Ladenstein, R.; Härd, T. *J. Mol. Biol.* **1995**, *247*, 840–846.

(24) Baumann, H.; Knapp, S.; Lundback, T.; Ladenstein, R.; Härd, T. *Nat. Struct. Mol. Biol.* **1994**, *1*, 808–818.

(25) Agback, P.; Baumann, H.; Knapp, S.; Ladenstein, R.; Härd, T. *Nat. Struct. Mol. Biol.* **1998**, *5*, 579–584.

(26) Hernandez-Garcia, A. Protein-based Polymers that Bind to DNA., Ph.D. Thesis, Physical Chemistry, Soft Matter, Wageningen University, and Research Centre, 2014.

(27) Levy-Sakin, M.; Ebenstein, Y. *Curr. Opin. Biotechnol.* **2013**, *24*, 690–698.

(28) Lam, E. T.; Hastie, A.; Lin, C.; Ehrlich, D.; Das, S. K.; Austin, M. D.; Deshpande, P.; Cao, H.; Nagarajan, N.; Xiao, M.; Kwok, P.-Y. *Nat. Biotechnol.* **2012**, *30*, 771–776.

(29) Neely, R. K.; Deen, J.; Hofkens, J. *Biopolymers* **2011**, *95*, 298–311.

(30) Dorfman, K. D.; King, S. B.; Olson, D. W.; Thomas, J. D. P.; Tree, D. R. *Chem. Rev.* **2013**, *113*, 2584–2667.

(31) Golinska, M. D.; de Wolf, F. A.; Cohen Stuart, M. M. A.; Hernandez-Garcia, A.; de Vries, R. *Soft Matter* **2013**, *9*, 6406–6411.

(32) Huang, N.; Vörös, J.; de Paul, S. M.; Textor, M.; Spencer, N. D. *Langmuir* **2002**, *18*, 220–230.

(33) Altgelt, K.; Hodge, A. J.; Schmitt, F. O. *Proc. Natl. Acad. Sci. U. S. A.* **1961**, *47*, 1914–1924.

(34) Lamour, G.; Kirkegaard, J. B.; Li, H.; Knowles, T. P. J.; Gsponer, J. *Source Code Biol. Med.* **2014**, *9*, 1–6.

(35) Benoit, H., *Comptes Rendus*; 245, 1957, pp 2244–2247.

(36) Hammouda, B. *Adv. Polym. Sci.* **1993**, *106*, 87–133.

(37) Guinier, A.; Fournet, G., *Small-Angle Scattering of X-Rays*; John Wiley and Sons, New York: 1955.

(38) Pedersen, J. S. *Advances in Colloid and Interface Science* **1997**, *70*, 171–210.

(39) Gao, Y.-G.; Su, S.-Y.; Robinson, H.; Padmanabhan, S.; Lim, L.; McCrary, B. S.; Edmondson, S. P.; Shriver, J. W.; Wang, A. H. J. *Nat. Struct. Mol. Biol.* **1998**, *5*, 782–786.

(40) Robinson, H.; Gao, Y. G.; McCrary, B. S.; Edmondson, S. P.; Shriver, J. W.; Wang, A. H. J. *Nature* **1998**, *392*, 202–205.

(41) Driessen, R. P. C.; Meng, H.; Suresh, G.; Shahapure, R.; Lanzani, G.; Priyakumar, U. D.; White, M. F.; Schiessel, H.; van Noort, J.; Dame, R. T. *Nucleic Acids Res.* **2013**, *41*, 196–205.

(42) McAfee, J. G.; Edmondson, S. P.; Zegar, I.; Shriver, J. W. *Biochemistry* **1996**, *35*, 4034–4045.

(43) Fredrickson, G. H. *Macromolecules* **1993**, *26*, 2825–2831.

(44) Feuz, L.; Leermakers, F. A. M.; Textor, M.; Borisov, O. V. *Macromolecules* **2005**, *38*, 8891–8901.

(45) Adamcik, J.; Klinov, D. V.; Witz, G.; Sekatskii, S. K.; Dietler, G. *FEBS Lett.* **2006**, *580*, 5671–5675.

(46) Rechendorff, K.; Witz, G.; Adamcik, J.; Dietler, G. *J. Chem. Phys.* **2009**, *131*.

(47) Behar, G.; Bellinzoni, M.; Maillasson, M.; Paillard-Laurance, L.; Alzari, P. M.; He, X.; Mouratou, B.; Pecorari, F. *Protein Eng. Des. Sel.* **2013**, *26*, 267–275.

(48) Bates, M.; Blosser, T. R.; Zhuang, X. *Phys. Rev. Lett.* **2005**, *94*.

6 General Discussion

6.1 Bottlebrushes: Flexible when Compressed

In this thesis, we have focused on the main-chain stiffening of molecular bottlebrushes. It has been known for decades that, repelling, rod-like particles possess the tendency to order in anisotropic phases at sufficiently high concentrations.[1] One therefore wonders whether bottlebrushes can order anisotropically too; once they are sufficiently stiff. A prominent early theory for molecular bottlebrushes by Fredrickson suggested that, in fact, also flexible chains can acquire this tendency when sufficiently long side chains are attached to it in a sufficiently high density.[2] Given the fact that quite some work has been done on molecular bottlebrushes, one would therefore expect that there are ample examples of liquid crystals formed by molecular bottlebrushes. In fact, only a few illustrations of liquid crystalline bottlebrush systems have been reported in the literature.[3] This puzzling observation indeed poses many questions, for example, one may ask questions regarding the applicability of Fredrickson's theory.

In this thesis, we have shown that in fact, bottlebrushes co-assembled from a DNA main-chain and flexible C_4K_{12} protein polymers side chains do show liquid crystalline behaviour, thus lending credibility to Fredrickson's theory. Motivated by our initial success with the liquid crystalline DNA-bottlebrushes, we started to explore other bottlebrush systems based on other protein polymers studied previously in our lab. Remarkably, none of these systems readily formed liquid crystals like our DNA-C_4K_{12} system did. By briefly presenting these "failed" experiments, we want to illustrate that conditions to find liquid crystals of bottlebrushes are not so general as suggested by Fredrickson, or by our "easy" initial success with the DNA-C_4K_{12} bottlebrushes.

In part this is due to effects outlined in **chapter 2** where we show that adding an increasingly dense bottlebrush to some main-chain initially decreases its effective aspect ratio (l_p/D). Only at very high grafting densities of very long side chains we find an increase of the effective aspect ratio. Only the latter conditions, that are hard to realize in most experiments, promote liquid crystallinity.

We discovered yet another reason in **chapter 3**: bottlebrushes become flexible when compressed. In this general discussion we provide some additional context to consider for why putting pressure on bottlebrushes is an interesting problem. We do so by zooming in on some examples of biological bottlebrushes. These invariably operate under pressure, and we believe a better understanding of the physical properties of bottlebrushes under pressure could also contribute to understanding, preventing and

curing diseases that relate to malfunctioning biological bottlebrushes.

6.2 Protein-Polymer Bottlebrushes that do not readily form Liquid Crystals

We first discuss three other protein polymers, used as side chains on a DNA backbone, and then discuss a case where a different main-chain was used, i.e. xanthan. The sample preparation procedure for the samples discussed next are exactly the same as for the samples described in the section "Preparation of Concentrated DNA-Protein Mixtures" of **chapter 2**. For all samples, the amount of protein polymer side chains was chosen in such a way that all the charges of the backbone would be compensated (stoichiometric amounts).

6.2.1 $C_2S^H_{24}C_2$ Protein Polymer as Side Chain

One of our attempts to make liquid crystalline samples with a DNA-protein polymer bottlebrush was by using $C_2S^H_{24}C_2$.[4–7] This protein polymer has two 200 aa random coiled stabilizing blocks (C_2) and a silk-based octapeptide $(GAGAGAGH)_n$ middle-block. When the *p*H is raised from acidic conditions (*p*H = 2...3) to (nearly) *p*H 6, these protein polymers self-assemble into very long and stiff fibrils while the histidine groups of the middle-block are still positively charged, see Figure 6.1(a). Hence combining positively charged $C_2S^H_{24}C_2$ fibrils with negatively charged DNA may be expected to lead to fibrils growing along the DNA. Interestingly, AFM images of DNA-$C_2S^H_{24}C_2$ complexes show two types of structures, see Figure 6.1(b).

Some objects clearly consist of DNA (DNA of 3000bp is approximately 1 μm in length). Other objects look much stiffer and do not have the correct length, expected when they would have DNA as the backbone molecule. Concentrated samples of the $C_2S^H_{24}C_2$ fibrils without the DNA template (such as shown in Figure 6.1(a)) are slightly birefringent when examined in a crossed-polarizer set-up. On the other hand, our concentrated samples of DNA-$C_2S^H_{24}C_2$ complexes were not birefringent. We assume that the majority of DNA-$C_2S^H_{24}C_2$ bottlebrushes observed in Figure 6.1(b) are too flexible for liquid crystalline behaviour, whereas the fiber-like bottlebrushes (pure $C_2S^H_{24}C_2$ fibers) do show some potential.

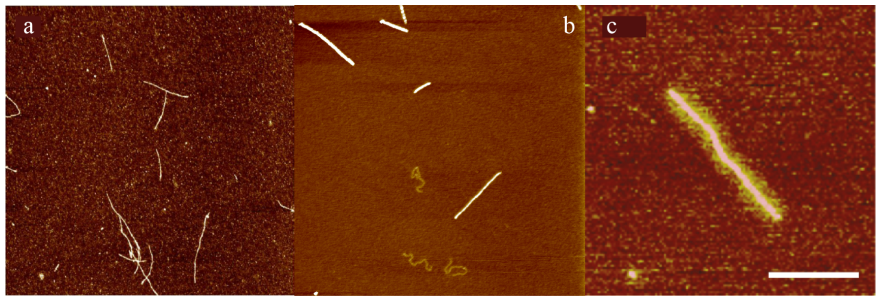

Figure 6.1: *AFM images of protein polymer complexes. Fibrils consisting of* $C_2S^{H}_{24}C_2$ *protein polymers (a), bottlebrush complexes consisting of DNA and* $C_2S^{H}_{24}C_2$ *protein polymers (b) and artificial virus-like particles consisting of DNA coated with* S^{Q}_{10} *protein polymer (c). Images are 5 × 5 µm (a,b) or have a scale bar of 300 nm (c). The AFM images from (a) and (c) were reproduced with permission from references.*[7,8]

6.2.2 $C_4S^{Q}_{10}K_{12}$ Protein Polymer as Side-Chain

Another interesting protein polymer that appeared as a promising side chain candidate for creating liquid crystalline bottlebrushes is the protein polymer $C_4S^{Q}_{10}K_{12}$ (from now on denoted as S^{Q}_{10}). The S^{Q}_{10} block is a self-assembling tenfold repetition of a GAGAGAGQ sequence.[8] This triblock protein polymer co-assembles with DNA into rod-shaped complexes reminescent of virus-like particles, see Figure 6.1(c). Since there are more than a few viruses that show liquid crystalline behaviour, we reasoned that the rod-like DNA-S^{Q}_{10} complexes might be suitable as well.[9–11] Unfortunately and surprisingly, concentrated mixtures of DNA and S^{Q}_{10}, when incubated sufficiently long to allow for rod formation, did not show any sign of anisotropy. Examining the physical appearance of the DNA-S^{Q}_{10} sample showed already a different texture as compared to the liquid crystalline DNA-C_4K_{12} samples. The liquid crystalline DNA-C_4K_{12} samples are very viscous solutions, whereas, the DNA-S^{Q}_{10} was almost solid-like. Possibly, during assembly in concentrated solutions, the S^{Q}_{10} self-assembling block is not only interacting with neighbours within the same bottlebrush (intra) but also with neighbouring protein polymers from different bottlebrushes (inter). Drying a droplet of a dilute solution of DNA-S^{Q}_{10} comlexes did not lead to viscous liquid crystalline samples either. Since the S^{Q}_{10} protein is identical to our C_4K_{12} protein polymer apart for the self-assembling block, S^{Q}_{10}, the differences that we observe are clearly caused by this block. Moreover, this S^{Q}_{10} protein polymer easily

aggregates (also in the dilute regime) and it is almost impossible to reverse this aggregation under biological conditions. Real viruses do not seem to experience this problem during the self-assembling process. The self-assembly mechanism of the capsid proteins of a virus is most likely slightly different and probably the interaction between the capsid proteins is more reversible than in our DNA-S^{Q}_{10} case.[12,13]

6.2.3 C_8-Sso7d Protein Polymer as Side Chain

The last case that we discuss is again a simple diblock protein polymer without a self-assembling block. The C_8-Sso7d (discussed in **chapter 5**) has a C_8 stabilizing block which is twice the size of the C_4 block that we used for our successful DNA-C_4K_{12} bottlebrush system.[14] In principle longer side chains (at fixed grafting density) should increase the main-chain stiffening effect of bottlebrushes and hence promote liquid crystallinity.

We initially expected the grafting density of the C_8-Sso7d protein polymer on DNA to be close to the maximum value based on the size of the binding site of the protein Sso7d (from the hyperthermophilic archaeabacteria *Sulfolobus solfataricus*), on DNA, that is, one protein per four base pairs.[15–17] However, we found that this expected maximum grafting density of one protein per 4 base pairs (0.25 ptn/nt) was never reached. Static light scattering experiments revealed a maximum coverage of at most 0.07 ptn/nt, meaning that we have two times longer but almost four times fewer side chains. In other words, the brush diameter has increased while the persistence length has decreased. Hence a smaller aspect ratio, l_p/D, is obtained and a system that is less likely to form liquid crystal phases. Unsurprisingly, the DNA-C_8-Sso7d bottlebrush complexes did not show anisotropic phase behaviour. Adding a large excess of C_8-Sso7d protein polymers might be expected to drive the binding equilibrium to the side of a higher grafting density, but it also leads to a large concentration of free, unbound C_8-Sso7d protein polymers. As we have shown in **chapters 3** and **4**, using self consistent field (SCF) calculations, these excess free polymer chains make matters worse: a semi-dilute background solution of free polymer chains results in a dramatic drop of the persistence length, l_p, and hence in even more flexible bottlebrush molecules.

6.2.4 Xanthan as the Main-Chain

Besides varying the protein polymer side chains grafted on the DNA main-chain, it is of course possible to use a different main-chain. The results in **chapter 2** already suggested that it would be very hard to stiffen a flexible main-chain using protein polymer side chains to the extent that the resulting bottlebrush would make liquid crystals. To achieve this, clearly a semi-flexible main-chain is required. Apart from DNA, there are many other negatively charged semi-flexible biopolymers. For example, the polysaccharide xanthan[18] is negatively charged and forms stiff triple helices, leading to lyotropic liquid crystalline behavior.[19] We found however, that the addition of C_4K_{12} protein polymer (leading to a screening of the xanthan charges and the formation of a polymer brush around the triple helical xanthan main-chain), did not affect the xanthan concentration at which the isotropic-nematic phase transition occurred. This observation can be explained by the rather large value of the persistence length of the xanthan triple-helix, which is reported to be about 370 nm,[20] as compared to 50 nm for DNA. Most likely, by attaching side chains, we reduced the electrostatic contributions to the persistence length by a (similar) contribution of induced persistence length. A similar case was discussed in **chapter 4**. Overall, the persistence length of the xanthan bottlebrush may have remained, at best, more or less constant. Using xanthan as a backbone for a potential model bottlebrush system is apparently not very helpful when it is not affected by attaching side chains.

6.2.5 C_4K_{12} Protein Polymers as a Side Chain for DNA

The examples of the C_8-Sso7d/DNA, C_4K_{12}/xanthan and C_4K_{12}/DNA complexes nicely illustrate the delicate balance between different effects that either promote or prevent the formation of liquid crystals. With some luck, we did strike a balance for the C_4K_{12}/DNA system where the addition of a bottlebrush did lead to a shift of the isotropic-nematic phase boundary, but not to a complete disappearance of liquid crystals. As emphasized in **chapter 2**, attaching the C_4K_{12} side chains actually reduced the aspect ratio of the DNA backbone. Bare DNA has an aspect ratio, l_p/D, of about 20 (l_p = 50 nm, D = 2.4 nm), whereas our bottlebrushes have an aspect ratio of almost 10 (l_p = 250 nm, D = 25 nm). However, for the C_4K_{12}/DNA system the reduction in aspect ratio was not so dramatic that the liquid crystalline ordering disappeared completely. This illustrates that conditions for obtaining liquid crystalline bottlebrush systems are not so

general as sometimes thought.[21] For the C_4K_{12}/DNA system, we were just in the right regime to still have liquid crystalline ordering. For a longer side chain at fixed binding strength (e.g. C_8K_{12}), we probably would have had a grafting density that was too low to attain liquid crystallinity. Similarly, for a main-chain more flexible than DNA, at the same density of grafted side chains, most likely, samples would not have been liquid crystalline either. In summary, it is much easier to make a bottlebrush system that does not form liquid crystals, than one that does.

6.3 Bottlebrushes under Pressure

In **chapters 3** and **4** we have found additional causes that reduce the stiffness of bottlebrushes: it appears that they become more flexible both in the presence of excess free polymer, and when compressed. Biological bottlebrushes very often operate at high (osmotic) pressures, therefore we now give a discussion of some biological bottlebrush systems.

6.3.1 Biological Bottlebrushes

Nature has examples of bottlebrushes that do and do not form liquid crystals. The biological bottlebrush aggrecan, a molecule that ensures the lubrication of the joints, is typically not in a liquid crystalline state.[22–24] The aggrecan molecules are highly branched with side chains having their own side chains, but apparently, this does not stiffen up the brush to such an extent that it forms ordered phases. On the other hand, neurofilaments are a good example of biological bottlebrushes that do form lyotropic liquid crystalline phases.[25–27] Neurofilaments contribute to the stability of neurons by forming a nematic gel that acts as a structural scaffold.[28,29] The core of neurofilaments is a semi-flexible chain that is self-assembled from alpha-helical protein subunits, and it is most likely the stiffness of the core of these filaments that causes them to exhibit liquid crystallinity.

A key feature that the aggrecans and the neurofilaments have in common is that they operate under external pressure. The aggrecan bottlebrush is an essential constituent of the synovial fluid; it is able to hold on to water even when large pressures are applied and maintains a constant viscosity. Neurofilaments align in long myelinated neuronal axons, ensuring stability and rigidity. Externally applied pressures are distributed over the entire nematic neurofilament network and thereby reduce the risk of damage. Deviations from the native neurofilament structure caused by non-native

subunit compositions, or changes in phosphorylation can result in neuronal diseases such as amyotrophic lateral sclerosis.[30–32]

6.3.2 Pressure induces Flexibility

The C_4K_{12}/DNA bottlebrush system initially investigated in **chapter 2**, turned out to have interesting and unexpected behaviour when an external osmotic pressure was applied (**chapter 3**). We expected higher osmotic pressures to lead to an increased alignment of the bottlebrushes. While this indeed was the case, we also found that the system with the largest protein polymers to DNA ratio had the lowest degree of liquid crystalline alignment. Using SCF calculations we identified the mechanism behind this unexpected observation: a large concentration of excess free (unbound) protein polymers in solution result in a drastic decrease of the bottlebrush persistence length and to a decrease of the brush diameter. This, in turn, leads to a reduction of the effective aspect ratio, and a reduction of the degree of liquid crystalline alignment. We believe that compression of molecular bottlebrushes should have a similar effect: in this case side chain (rather than free) polymers are being pushed into neighbouring side chains. This idea is illustrated schematically in Figure 6.2.

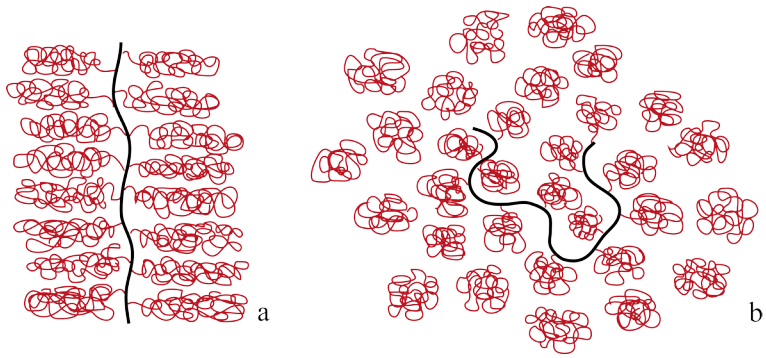

Figure 6.2: *Schematic representation of a single stiff molecular bottlebrush (a) and a flexible bottlebrush in a concentrated polymer solution (b).*

What would happen if one would compress our liquid crystalline sample of C_4K_{12}/DNA bottlebrushes even more? Most likely, the liquid crystalline behaviour will eventually disappear and we will have a concentrated isotropic bottlebrush system with a persistence length equal to that of the main-chain. Continued compression might lead to reappearance of a liquid crystalline phase, this time caused by the

semi-flexible DNA main-chain, when a DNA concentration is reached at which bare DNA exhibits an isotropic-nematic transition ($\sim$ 120 g/l for bare DNA[33]). Experimental data illustrating that bottlebrushes become more flexible upon compression are shown in Figure 6.3. The figure shows experimental plots of distances d between the DNA as a function of DNA concentration (Figure 6.3(a)), and distances d between the DNA as a function of osmotic pressure π (Figure 6.3(b)). The composition of the samples in the two scattering experiments was similar and therefore we would expect the isotropic-nematic phase transition to occur at roughly the same distance d between the DNA molecules. Instead we find that for the compressed bottlebrushes, the transition occurs at roughly 16 nm whereas, for the system in which we fixed the concentration rather than the pressure, the transition occurs at around $d = 30$ nm. The DNA concentration around the isotropic-nematic transition for the compressed sample is then roughly a factor four higher.

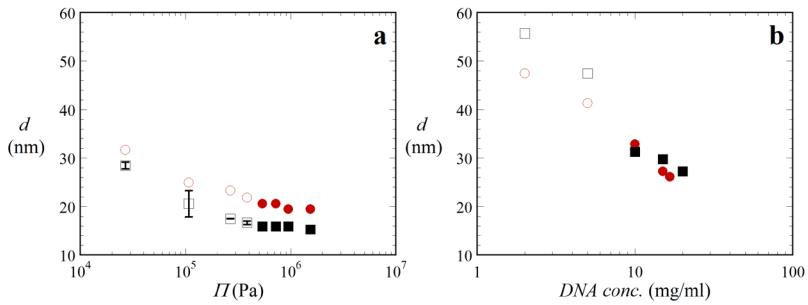

Figure 6.3: *Distances d determined from scattering techniques. In (a) the distances between the DNA backbone is plotted as a function of the DNA concentration. In (b) this distance is plotted as a function of the osmotic pressure π. The open symbols correspond to isotropic samples, whereas the closed symbols represent anisotropic samples. The circular red data points belong to samples with three times excess amounts of protein polymer (Γ = 30) and the squared black data points represent samples that have stoichiometric amounts of protein polymer (Γ = 10).*

6.3.3 Concluding Remarks and Future Directions

In this thesis, we have elucidated why bottlebrushes do not form liquid crystals so easily as might have been expected. We have found that one

reason is that free polymers or brush compression lead to more flexible brushes. The increase of flexibility for bottlebrushes under external pressure has implications for biological bottlebrushes. Bottlebrushes like aggrecan and the neurofilalaments are known to operate in an environment where they have to withstand large applied pressures.

What happens to the flexibility of aggrecan or neurofilaments under pressure is maybe not so different from what happens to the DNA-protein polymer bottlebrush system that we have studied here. We hope therefore, that better understanding of the induced stiffening of bottlebrushes might also prove useful for more applied research that focuses on solving problems with malfunctioning biological bottlebrushes. For example, aggrecan is one of the major constituents of cartilage in the joints. Osteoarthritis or degenerative arthritis is an example where lubrication of the joints provided by aggrecan is failing. Currently, treatment of osteoarthritis mainly consists of pain relief, and as yet there is no real cure. Possibly, the understanding of bottlebrush systems that we provide here could also contribute to a better understanding of the behaviour of aggrecan in joints, and possibly to better treatments for conditions such as osteoarthritis.

References

(1) Onsager, L. *Ann. N. Y. Acad. Sci.* **1949**, *51*, 627–659.

(2) Fredrickson, G. H. *Macromolecules* **1993**, *26*, 2825–2831.

(3) Wintermantel, M.; Fischer, K.; Gerle, M.; Ries, R.; Schmidt, M.; Kajiwara, K.; Urakawa, H.; Wataoka, I. *Angew. Chem. Int. Ed.* **1995**, *34*, 1472–1474.

(4) Martens, A. A.; Portale, G.; Werten, M. W. T.; de Vries, R. J.; Eggink, G.; Cohen Stuart, M. A.; de Wolf, F. A. *Macromolecules* **2009**, *42*, 1002–1009.

(5) Martens, A. A.; van der Gucht, J.; Eggink, G.; de Wolf, F. A.; Cohen Stuart, M. A. *Soft Matter* **2009**, *5*, 4191–4197.

(6) Beun, L. H.; Beaudoux, X. J.; Kleijn, J. M.; de Wolf, F.; Cohen Stuart, M. A. *ACS Nano* **2012**, *6*, 133–140.

(7) Beun, L. H.; Storm, I. M.; Werten, M. W.; de Wolf, F. A.; Cohen Stuart, M. A.; de Vries, R. *Biomacromolecules* **2014**, *15*, 3349–3357.

(8) Hernandez-Garcia, A.; Kraft, D. J.; Janssen, A. F. J.; Bomans, P. H. H.; Sommerdijk, N. A. J. M.; Thies-Weesie, D. M. E.; Favretto, M. E.; Brock, R.; de Wolf, F. A.; Werten, M. W. T.; van der Schoot, P.; Cohen Stuart, M. A.; de Vries, R. *Nat. Nanotechnol.* **2014**, *9*, 698–702.

(9) Lettinga, M. P.; Dogic, Z.; Wang, H.; Vermant, J. *Langmuir* **2005**, *21*, 8048–8057.

(10) Tang, J.; Fraden, S. *Liq. Cryst.* **1995**, *19*, 459–467.

(11) Fraden, S.; Maret, G.; Caspar, D. L. D. *Phys. Rev. E* **1993**, *48*, 2816–2837.

(12) Zlotnick, A. *J. Mol. Biol.* **1994**, *241*, 59–67.

(13) Perlmutter, J. D.; Hagan, M. F. *Annu. Rev. Phys. Chem.* **2015**, *66*, 217–239.

(14) Hernandez-Garcia, A. Protein-based Polymers that Bind to DNA., Ph.D. Thesis, Physical Chemistry, Soft Matter, Wageningen University, and Research Centre, 2014.

(15) Agback, P.; Baumann, H.; Knapp, S.; Ladenstein, R.; Härd, T. *Nat. Struct. Mol. Biol.* **1998**, *5*, 579–584.

(16) Gao, Y.-G.; Su, S.-Y.; Robinson, H.; Padmanabhan, S.; Lim, L.; McCrary, B. S.; Edmondson, S. P.; Shriver, J. W.; Wang, A. H. J. *Nat. Struct. Mol. Biol.* **1998**, *5*, 782–786.

(17) McAfee, J. G.; Edmondson, S. P.; Zegar, I.; Shriver, J. W. *Biochemistry* **1996**, *35*, 4034–4045.

(18) Pham, T. T. H.; Snijkers, F.; Storm, I. M.; de Wolf, F. A.; Cohen Stuart, M. A.; van der Gucht, J. *Int. J. Polymer. Mater* **2016**, *65*, 125–133.

(19) Livolant, F.; Bouligand, Y. *J. Phys.-Paris* **1986**, *47*, 1813–1827.

(20) Dumitriu, S., *Polysacharides - structural diversity and functional versatility*, 2nd; CRC Press, Taylor and Francis group: 2004, p 205.

(21) Feuz, L.; Leermakers, F. A. M.; Textor, M.; Borisov, O. V. *Macromolecules* **2005**, *38*, 8891–8901.

(22) Klein, J. *Polym. Adv. Technol.* **2012**, *23*, 729–735.

(23) Klein, J. *Science* **2009**, *323*, 47–48.

(24) Kiani, C.; Chen, L.; Wu, Y. J.; Yee, A. J.; Yang, B. B. *Cell Res.* **2002**, *12*, 19–32.

(25) Rammensee, S.; Janmey, P. A.; Bausch, A. R. *Eur. Biophys. J.* **2007**, *36*, 661–668.

(26) Beck, R.; Deek, J.; Safinya, C. R. *Biochem. Soc. Trans.* **2012**, *40*, 1027–1031.

(27) Hesse, H. C.; Beck, R.; Ding, C.; Jones, J. B.; Deek, J.; MacDonald, N. C.; Li, Y.; Safinya, C. R. *Langmuir* **2008**, *24*, 8397–8401.

(28) Janmey, P. A.; Leterrier, J.-F.; Herrmann, H. *Curr. Opin. Colloid Interface Sci.* **2003**, *8*, 40–47.

(29) Beck, R.; Deek, J.; Jones, J. B.; Safinya, C. R. *Nat. Mater.* **2009**, *9*, 40–46.

(30) Fuchs, E.; Cleveland, D. W. *Science* **1998**, *279*, 514–519.

(31) Miller, C. C. J.; Ackerley, S.; Brownlees, J.; Grierson, A. J.; Jacobsen, N. J. O.; Thornhill, P. *Cell. Mol. Life Sci. CMLS* **2002**, *59*, 323–330.

(32) Nguyen, M. D.; Shu, T.; Sanada, K.; Lariviere, R. C.; Tseng, H. C.; Park, S. K.; Julien, J. P.; Tsai, L. H. *Nat. Cell Biol.* **2004**, *6*, 595–608.

(33) Livolant, F.; Leforestier, A. *Prog. Polym. Sci.* **1996**, *21*, 1115–1164.

7 Summary

The physical and biological properties of molecular bottlebrushes have been a topic that has been widely discussed in the past two decades. Attaching a sufficient number of side chains to a (flexible) main-chain polymer molecule should force the side chains to stretch, which in turn will result in the so-called main-chain stiffening effect. According to early theories this main-chain stiffening effect should also be able to induce liquid crystalline behaviour for bottlebrush systems. However, only a few experimental bottlebrush systems have been reported in literature that actually do form lyotropic liquid crystals.

The system we presented in **chapter 2** is one of those few systems. The bottlebrushes we used are co-assembled; consisting of DNA as a main-chain which is coated with protein polymer (C_4K_{12}) side chains. The C_4K_{12} protein polymers consist of a 400 amino acid hydrophilic random coil block (C_4), with a block of 12 positively charged lysines (K_{12}) functioning as binding block. The interaction between the DNA backbone and the side chains are based on electrostatic interactions. The liquid crystalline behaviour of our DNA-bottlebrushes make it a good model system to learn more about liquid crystals of bottlebrushes in general.

One way to determine whether we had liquid crystalline samples or not was to use a simple crossed-polarizer set-up, checking for birefringence. We also used small angle X-ray scattering (SAXS) experiments to determine the distances between our liquid crystalline DNA-bottlebrushes and proved that these distances are in fact of the same order of magnitude as the diameter of the brush. In **chapter 2** we argued that attaching side chains to a backbone will increase the effective persistence length. However, we also argue that the thickness of the bottlebrushes will increase even more, such that the net result of attaching side chains is that the effective aspect ratio decreases. This decrease in aspect ratio, apparently, did not lead to the complete disappearance of the liquid crystalline phases. Indeed, SCF calculations showed that our samples were only just in the right regime to still show liquid crystalline behaviour.

Some well-known examples of bottlebrush polymer architecture in nature are aggrecan and neurofilaments. In their biological context, both function under externally applied (osmotic) pressures. Our DNA-bottlebrush systems, which are relatively simple compared to biological bottlebrushes, are a good model system to study the influence of (osmotic) pressure on bottlebrushes. In **chapter 3** we therefore equilibrated DNA-bottlebrushes against PEG solutions of varying weight percentages, corresponding to a series of known osmotic pressures. The compressed bottlebrush samples were investigated with SAXS to determine the

distances between the DNA backbones and to observe the phase behaviour (liquid crystalline or not). We decided on using two types of situations: a system that used only just enough of C_4K_{12} protein polymers to coat all the negative charges of DNA (stoichiometric amounts) and a system that has three times excess amounts of protein polymer. As might be expected, applying more osmotic pressure on our bottlebrush system decreases the internal distances between neighbouring backbone molecules. However, we noticed that the presence of excess amounts of protein polymer in the bulk disrupted the liquid crystalline ordering. SCF calculations were used to explain this phenomenon and we showed that increasing the bulk concentration of C_4 polymers leads to a reduction of both the brush diameter and the bottlebrush persistence length. This therefore leads to a smaller effective aspect ratio. As is well known, smaller effective aspect ratios oppose the tendency to form liquid crystals. In short, we conclude that high concentrations of free polymers make bottlebrushes more flexible, thus reducing their tendency to form liquid crystals. We also argued that compression of bottlebrushes (rather than adding free polymers) has a similar effect: in this case side chains are being compressed by the brush layers of neighbouring bottlebrushes rather than by free polymers, but the net result will be the same.

Inspired by the novel SCF predictions of **chapter 3**, in **chapter 4**, we do a more systematic study on the main-chain stiffening effect of co-assembled (rather than permanently grafted) molecular bottlebrushes. We start by introducing various numerical SCF models to describe different aspects of our system more accurately. We first compare two different co-assembled bottlebrush systems: one where binding is based on electrostatic interactions (in this case the binding strength decreases as more and more side chains bind) and one model with a constant adsorption affinity. We show that the electrostatic assembly tends to lead to a larger induced persistence length because for curved brushes, the side chains relocate themselves to the concave part of the backbone where the charge density is higher. In **chapter 4** we also followed up on the research performed in **chapter 3** on the effect of free polymers; we confirm that free polymers in solution also cause self-assembled bottlebrushes to become more flexible. Finally, in **chapter 4** we show that there is an optimum concentration of free polymers chains for the induced persistence length: a small excess amount of free polymer initially results in a higher grafting density and hence a higher persistence length. Adding more free polymer (typically more than the overlap concentration) leads to a drastic decrease of the induced persistence length.

In **chapter 5** we introduce a slightly different bottlebrush system. Again, DNA is used as a main-chain, but this time we used a slightly different protein polymer, C_8-Sso7d, as side chain molecules. This protein polymer has a hydrophilic random coil block (C_8) that has twice the length of the previously used C_4K_{12} protein polymer. As a binding block we use a small protein, Sso7d, that specifically binds to DNA but does not require a certain DNA sequence. Previously, it had been observed that this protein polymer prevents local (intrachain) hybridization of ssDNA (M13mp18). In **chapter 5** we investigate whether the protein is also able to prevent fully complementary pieces of ssDNA from hybridizing. We do so by alkaline denaturing dsDNA, coating the resulting ssDNA with the protein polymer and then going back to neutral *p*H (renaturation conditions). We find that the resulting complexes look very different from the complexes obtained with dsDNA. Both the complexes with the M13 DNA and the complexes prepared via the alkaline denaturation procedure can be digested using Mung Bean nuclease, indicating they are single stranded. However, degradation of the M13 DNA complexes is very fast, whereas that of the complexes prepared via the alkaline denaturation procedure is very slow. We proposed that during the alkaline denaturation process the Sso7d-block denatures and possibly refolds incorrectly in the presence of DNA when *p*H is brought back to neutral values, leading to possibly aggregated or incorrectly folded Sso7d proteins in the DNA.

In **chapter 6** (general discussion) we reflect on the implications of our results for understanding practically relevant bottlebrush systems (both liquid crystalline and isotropic), focusing on the remarkable effect that bottlebrushes appear to become flexible under pressure.

Samenvatting

De fysische en biologische eigenschappen van borstel polymeren zijn een veelbesproken onderwerp geweest in de afgelopen twee decennia. Het bevestigen van voldoende zijketens aan een (flexibele) hoofdketen zou moeten resulteren in het strekken van deze zijketens, wat daardoor resulteert in een verstijvend effect van de hoofdketen. Volgens de theorie zou dit effect tevens moeten leiden tot het ontstaan van vloeibaar kristallijn gedrag van deze borstel polymeren. Ondanks deze voorspellingen zijn, tot de dag van vandaag, maar een handjevol borstel systemen bekend die vloeibaar kristallijn gedrag vertonen.

Het moleculaire borstel system, dat we voor het eerst beschreven in **hoofdstuk 2**, is een van de weinige systemen dat vloeibaar kristallijn gedrag vertoond. Deze borstels zijn opgebouwd uit meerdere componenten; we gebruiken DNA als de hoofdketen en artificiële eiwit polymeren (C_4K_{12}) als zijketens. Deze C_4K_{12} polymeren bestaan uit 400 amino zuren, die een hydrofiele ongestructureerde kluwen vormen (C_4), met een bindingsblok, die bestaat uit 12 positief geladen lysines (K_{12}). De binding tussen de DNA keten en de eiwit polymeren is gebaseerd op elektrostatische interacties. Omdat ons systeem in staat is vloeibare kristallen te vormen, is het een uitermate geschikt systeem om het vloeibaar kristallijn gedrag van borstel polymeren in het algemeen te bestuderen.

Een manier om te achterhalen of het systeem vloeibaar kristallijn is, is door te kijken of het dubbelbrekend is wanneer het systeem tussen gekruiste-polarisatoren wordt gehouden. Een andere methode die wij hebben gebruikt om ons systeem te analyseren, is X-ray verstrooiing onder kleine hoek (SAXS). Deze metingen hebben we gebruikt om de onderlinge afstanden tussen de DNA ketens te achterhalen, die tevens gelijk zijn aan de diameter van de borstel. In **hoofdstuk 2** hebben we bediscussieerd dat het aanhechten van zijketens leidt tot een toename van de effectieve persistentie lengte van de borstel. Echter, we hebben ook vermeld dat de dikte van de borstel, in verhouding, meer toeneemt dan de persistentie lengte en dat hierdoor de aspect verhouding effectief afneemt. Deze afname van de aspect verhouding heeft klaarblijkelijk niet geresulteerd in een volledige verdwijning van de vloeibaar kristallijne fases. SCF berekeningen hebben laten zien dat ons systeem nog precies in het juiste gebied zit om vloeibaar kristallijn te zijn.

Een paar bekende voorbeelden van borstel polymeren in de natuur zijn aggrecan moleculen en neurofilamenten. Deze twee macromoleculen met borstel architectuur functioneren beide onder externe druk. Ons systeem, dat relatief simpel is vergeleken met deze biologische voorbeelden, is een ideaal systeem om de invloed van druk op borstel

polymeren te onderzoeken. In **hoofdstuk 3** hebben we onze DNA-borstels ge-equilibreerd tegen PEG oplossing van variërende massapercentage PEG, zodat we een serie PEG oplossingen hebben van variërende osmotische druk. De door osmotische druk samengeperste DNA-borstels zijn onderzocht met SAXS om de onderlinge DNA afstanden te achterhalen en informatie te krijgen over eventuele vloeibaar kristallijne fases. We hebben twee verschillende situaties bestudeert: een systeem dat precies genoeg eiwit polymeren (C_4K_{12}) heeft om alle negatieve ladingen van de DNA hoofdketen te compenseren en een systeem dat drie keer een overmaat van C_4K_{12} eiwit polymeren bevat. Zoals verwacht, een hogere druk veroorzaakt dat de borstels dichter op elkaar gedrukt worden. Echter, de aanwezigheid van een overmaat aan C_4K_{12} verstoort de vloeibaar kristallijne fases. We hebben SCF berekeningen gebruikt om dit fenomeen toe te lichten en daarmee hebben we laten zien dat een toename van de vrije (eiwit) polymeer (C_4) concentratie resulteert in een afname van de borstel dikte en persistentie lengte. Met als gevolg dat de aspect verhoudingen van het systeem ook afnemen. Een afname van de aspect verhoudingen staat erom bekend dat het de vorming van vloeibare kristallen tegengaat. We concluderen dat hoge concentraties van vrije polymeren, borstel polymeren flexibeler maken en daardoor de vorming van vloeibare kristallen tegengaat. Het samendrukken van polymeer borstels heeft mogelijk een vergelijkbaar effect: in dit geval worden de zijketens samengedrukt door naburige zijketens in plaats van vrije polymeren, maar het resultaat is vergelijkbaar.

Geïnspireerd door de recente SCF resultaten uit **hoofdstuk 3**, gaan we in **hoofdstuk 4** een meer systematische studie beschrijven over de verstijvings effecten van samengestelde polymeer borstels. Dit hoofdstuk begint met het introduceren van verschillende numerieke SCF modellen die verschillende aspecten van ons systeem nauwkeuriger kunnen beschrijven. We vergelijken, in eerste instantie, twee verschillende samengestelde borstel polymeer systemen. In het eerste systeem is de binding gebaseerd op elektrostatische interacties (in dit geval neemt de bindings energie af als meer en meer zijketens binden aan de hoofdketen) en in het tweede systeem hebben we een constante adsorptie energie. We laten zien dat de elektrostatische interactie een grotere geïnduceerde persistentie lengte teweeg brengt doordat zijketens zich kunnen herschikken en daardoor in de convex van de borstel gaan zitten, omdat daar de ladingsdichtheid groter is. In **hoofdstuk 4** gaan we ook nog even verder met de effecten van vrije polymeren op de stijfheid van borstel polymeren (**hoofdstuk 3**). Vrije (eiwitten) polymeren veroorzaken ook voor

samengestelde borstels dat ze flexibeler worden. In **hoofdstuk 4** hebben we tevens laten zien dat er een optimum concentratie voor vrij polymeer is voor de geïnduceerde persistentie lengte: een kleine overmaat aan vrij eiwit polymeer zal, in eerste instantie, resulteren in een hogere dichtheid van gebonden zijketens en dus een hogere persistentie lengte. Als meer vrij polymeer wordt toegevoegd (meer dan de overlap concentratie) zal dit leiden tot een dramatische afname de geïnduceerde persistentie lengte.

In **hoofdstuk 5** introduceren we enigszins andere polymeer borstels. DNA wordt wederom als de hoofdketen gebruikt, maar dit keer hebben we C_8-Sso7d eiwit polymeren als zijketens gebruikt. Dit eiwit heeft wederom een hydrofiele ongestructureerde kluwen (C_8) dat twee keer zo groot is als het voorheen gebruikte C_4K_{12} eiwit. Het bindings blok van dit polymeer eiwit is een klein eiwit, Sso7d, dat specifiek aan DNA bindt maar geen speciale DNA sequentie nodig heeft. Voorheen, hebben we gezien dat dit C_8-Sso7d polymeer eiwit lokale hybridisatie van ssDNA (M13mp18) tegengaat. In **hoofdstuk 5** bekijken we of C_8-Sso7d polymeer eiwitten ook kunnen verhinderen dat complementair ssDNA hybridiseert. We gaan te werk door dsDNA te denatureren door middel van een alkaline behandeling, vervolgens wordt het ssDNA gecoat met C_8-Sso7d eiwitten en ten slotte wordt de *p*H terug gebracht naar neutrale *p*H. De complexen die op deze manier ontstaan, hebben een ander voorkomen vergeleken met de complexen die verkregen zijn met dsDNA. Zowel de M13 DNA complexen als de complexen verkregen via alkaline denaturatie zijn afbreekbaar met "Mung Bean Nuclease", wat aantoont dat het DNA in beide gevallen ssDNA is. Echter, de afbraak van M13 ssDNA gaat snel, terwijl het afbraak proces van de alkaline gedenatureerde complexen vrij langzaam gaat. We hebben voorgelegd dat dit verschil veroorzaakt zou kunnen zijn doordat het alkaline denaturatie proces het Sso7d-blok ook heeft gedenatureerd en vervolgens incorrect is hervouwen in de aanwezigheid van DNA, toen de *p*H werd terug gebracht naar neutrale omstandigheden.

In **hoofdstuk 6** (discussie) reflecteren we op de implicaties die onze resultaten hebben op relevante polymeer borstel systemen (zowel vloeibaar kristallijn als isotrope systemen). In het bijzonder richten wij ons op het effect dat polymeer borstels flexibeler worden onder druk.

List of publications

This thesis:

Chapter 2: **Storm, I. M.**; Kornreich, M.; Hernandez-Garcia, A.; Voets, I. K.; Beck, R.; Cohen Stuart, M. A.; Leermakers, F. A. M.; de Vries, R. Liquid Crystals of Self-Assembled DNA Bottlebrushes *J. Phys. Chem. B* **2015**, *119*, 4084–4092.

Chapter 3: **Storm, I. M.**; Kornreich, M.; Voets, I. K.; Beck, R.; de Vries, R.; Cohen Stuart, M. A.; Leermakers, F. A. M. Loss of Bottlebrush Stiffness due to Free Polymers *In preparation*

Chapter 4: **Storm, I. M.**; Cohen Stuart, M. A.; Leermakers, F. A. M.; Electrostatic Stiffening and Induced Persistence Length for Co-Assembled Molecular Bottlebrushes *In preparation*

Chapter 5: **Storm, I. M.**; Leermakers, F. A. M.; Cohen Stuart, M. A.; de Vries, R. Inhibition of Hybridization of Complementary Single Stranded DNA by a Protein-Polymer Bottlebrush Coating *In preparation*

Other work:

Włodarczyk-Biegun, M. K.; Werten, M. W. T.; Posadowska, U.; **Storm, I. M.**; de Wolf, F. A.; van den Beucken, J. J. J. P.; Leeuwenburgh, S. C. G.; Cohen Stuart, M. A.; Kamperman, M. Nanofibrillar Hydrogel Scaffolds from Recombinant Protein-Based Polymers with Integrin- and Proteoglycan-Binding Domains *Submitted 2016*

Cingil, H. E.; **Storm, I. M.**; Yorulmaz, Y.; te Brake, D. W.; de Vries, R.; Cohen Stuart, M. A.; Sprakel, J. Monitoring Protein Capsid Assembly with a Conjugated Polymer Strain Sensor *J. Am. Chem. Soc.* **2015**, *137*, 9800-9803.

Pham, T. T. H.; Snijkers, F.; **Storm, I. M.**; de Wolf, F. A.; Cohen Stuart, M. A.; van der Gucht, J. Enhanced Properties of Xanthan Hydrogels through Electrostatic Crosslinking with a Biosynthetic Triblock Protein Polymer. *Int. J. Polymer. Mater.* **2015**, *65*, 125-133.

Beun, L. H.; **Storm, I. M.**; Werten, M. W. T.; de Wolf, F. A.; Cohen Stuart, M. A.; de Vries, R. From Micelles to Fibers: Balancing Self-Assembling and Random Coiling Domains in pH-Responsive Silk-Collagen-Like Protein-Based Polymers. *Biomacromolecules* **2014**, *15*, 3349-3357.

Acknowledgement

Dear reader, this is almost the end of my thesis. Although, for most of you, this chapter will be the start of this thesis and possibly the only chapter you will read. I do hope some of you will continue reading other chapters as well.

My PhD at Wageningen University started with an interview on the 5^{th} of December 2011. Beforehand, I already knew I never wanted to do a PhD in Wageningen because of the "geitenwollen sokken" people. An opinion I obtained somewhere during high school. Whether this impression is correct, I still do not know. I do remember that I immediately liked the people I met during that day of my job interview. So, I will start this chapter by thanking those people: Josie, Martien, Frans, Renko, Joris, Evan and Lennart. Thank you for making me decide to come to Wageningen.

Dear Frans, I am happy you were my supervisor. You were always willing to help with any kind of problem and always full of new ideas. Thank you for teaching me how to write and for being so very patient when explaining things, if necessary, over and over again. I am sure without you my PhD would have been much more frustrating. There is just one thing; you promised you would invite me for dinner as soon as I moved to Wageningen. I have been living in Wageningen for almost three years now but still no invitation...

Renko, we had some very challenging discussions. Nevertheless, I enjoyed most of our meetings. I am also very grateful that you "forced" me to give talks at conferences and convinced me to spend some time in Israel. My time in Tel-Aviv is definitely one of the most memorable moments of my PhD. Martien, I really appreciate you always remembered what I was working on regardless of your busy schedule. Thank you for your help in finishing my thesis during these last months.

In these past four years I spend, of course, many ours in my office. During my first two years Hélène and the last two years, Wolf and Marcel shared my office. Hélène, thank you for the many talks we had. Wolf, you talk so much during lunch but in the office you almost disappear in the

background noise of our office. That makes you excellent company for working very efficient, though. Luckily, Marcel is always willing to talk. Marcel, you are very cheerful which is, I find, kind of contagious. You are also very good at reminding me I have to finish something. If not for your never ending question "is je boekje nou al af?", I might have "forgotten" to finish my thesis. Wolf, thank you so much for giving me the LaTeX template of this thesis.

Hande, we started together and we finish together. We shared many good and bad moments. You and Eric were always willing to help and give advice. Hande, you are a wonderful person, especially when you smile. I am happy to have you as a friend. When you started talking about having a dog, I must admit, I did not think that was such a good idea. On the other hand, I never met a Pamuk before. She is the most adorable and fluffy dog I have ever seen. Seeing her in the late evenings or weekends would guaranteed cheer me up. Thank Pamuk for me for having such a positive effect on people. Hande and Marcel, I asked you to be my paranimphs because the two of you are the most likely to make me less nervous and possibly even make me smile on the day of my defence.

Wolf and Jacob, I have good memories of our trip to Hawaï even though we stayed on the rainy side of the island. Wolf, thank you for the wonderful hikes we did in Hawaï and Israel. Thao, Natalia, Wolf and Juan thank you for the great weekend in Boston. Natalia, I am happy we decided to go to New York together.

Apart from all the hard work in our lab we have quite some athletic people around. I was quite surprised when we won the We-Day in 2014. The winning team: Jasper, Aldrik, Lennart, Wolf, Duc, Merve, Diane, Joshua, Marcel, Sabine, Jan-Bart, Vittorio and myself. I think we should keep that "wisselbeker" so we have proof we really won.

On the other hand, finishing last in the Veluweloop is a different kind of achievement. Thanks everyone who joined in the years 2014 and 2015: Peter, Frans, Jasper, Nicole, Anita, Diane, Gosia's, Kamuran, Marcin, Marieke, Ula, Jan-Maarten, Jacob, Ties, Jeroen, Marleen. Lione and Jan-Bart your mental support was priceless. Anita, to be able to win the Veluweloop, I think, we need more people like you; who can manage to find a "short-cut" in the middle of the forest.

Special thanks to the crazy people who are willing to pay to run through the mud: Lione, Diane, Jasper, Joshua, Jan-Maarten, Jan-Bart, Gerben, Marleen, Maria and Jeroen.

Merve, my dear neighbour, you are such a sweetheart and kind person. I hope I can still stay your neighbour for a while and look after Mirmir when

you are not around. Although, Mirmir is not welcome in my home anymore, he eats my plants. Let me know whenever you are having something typically Turkish for dinner, I can help you eat it.

Gosia (with the husband, horse, dog and baby), I will miss your jokes and good spirit. I enjoyed our running events, the time we spend together during conferences and our talks. Unfortunately, you will have started your new job when I defend this thesis; I could have used your optimism on that day.

Sweet Lennart, I miss your sharp remarks at lunch. Thank you for all the help with AFM and for making some of my "failed" proteins useful. Thao, your help and advice about proteins and fermentations was extremely useful. But I especially remember your kindness when you looked after me when I got the flu during the California PhD trip. Rui, I probably should not say this but I actually liked most of your jokes. Maarten, you are full of surprises, I am glad I got to know you. Gosia B, I really appreciate your sense of humour and your ability to see the amusing part of things that are seemingly not funny at all. Sabine thank you for organizing the California PhD trip and Wolf, Gosia W, Natalia, Maarten, Hanne for organizing the UK PhD trip.

Hans, you always smile at me when I see you in the corridor and laugh when I am eating sandwiches. Thank you for reading and commenting on my Introduction and Discussion. Remco, you probably solved more of my problems than I remember. I am happy you were around to help me with the SAXS in Eindhoven and Grenoble.

Micha thank you for your warm welcome when I came to Tel-Aviv and your endless patience when helping me with my samples.

Marc, without your help I am sure the first couple of fermentations would have failed. It is surprising how during each of my fermentations something weird happened.

Ruben, your games were a great success during the Friday evenings, especially "the resistance" . This brings me immediately to Esio. Esio, you are a sweet guy and always very helpful. There was no need, however, to always accuse me of being a "spy". It was not always me.

Lione and Marcel, if all else fails we can always start our own "stukjes" production company.

To all other friends and colleagues at Fysko and Biont who made my time as a PhD student such a nice moment of my life: Stan, Julia, Anton, Camilla, Junyou, Aldrik from Biont and Mieke, Anton, Johan, Ties, Ilse, Joanne, Marco, Hanne, Kamuran and Gosia, Bert, Rene, Mara, Josie, Joris,

Hannie, Dirk, Huanhuan, Tingting, Christian, Ronald, Antsje, Kris, Aljosha, Pieter from Fysko. Leaving you will be a very sad moment for me.

Mark and Inger, thank you for your last minute corrections of my thesis and your friendship during the past several years. To my family and friends, thank you for all the nice memories and distracting me from my PhD worries.

Finally, I would like to thank both of my parents for their support and endless patience. Reinier, my very dear brother, thank you for everything. You are always willing to help with anything. It surprises me a little that even though, I am quite sure you did not really know what my PhD research was about, you always seem to know when I was wrong. At this moment you are still struggling with your PhD in Germany. I hope that next year, around this time, you will have finished your thesis.

About the author

Inge Storm was born on the 30^{th} of March 1988 in Woerden, The Netherlands. In 2006 she graduated from Lek en Linge in Culemborg. In the same year she started studying chemistry at Utrecht University. As part of the Bachelor programme she did a project on the phase separation between goethite and aluminium doped goethite at the Van 't Hoff Laboratory for Physical and Colloid Chemistry under supervision of Esther van den Poll and Gert-Jan Vroege. For her master thesis she did a project on the synthesis of disc-like polystyrene particles at the Soft Condensed Matter group under supervision of Johan Stiefelhagen and Alfons van Blaaderen. During her Master she did an internship at the Physical Chemistry group at Lund University in Sweden under supervision of Charlotte Gustavsson, Ola Karlsson and Lennart Piculell on the effect of cross-linking on the structure of polymer-surfactant systems.

In January 2012 she started as a PhD-candidate at the department of Physical Chemistry and Soft Matter at Wageningen University under supervision of Martien Cohen Stuart, Frans Leermakers and Renko de Vries. The project was funded by the European Research Counsel (ERC) Advanced Grant of Martien Cohen Stuart. The research about DNA-protein polymer bottlebrushes is described in this thesis.

Overview of completed training activities

Discipline specific		
Small Angle Scattering School	Delft	2012
Summer School 'Physical Chemistry of Biointerfaces'★	San Sebastian, Spain	2012
Summer School 'JCNS Laboratory Course - Neutron Scattering'	Jülich, Germany	2013
International Symposium on Polyelectrolytes★	Ein Gedi, Israel	2014
Dutch Polymer Days†	Lunteren	2014
Summer School 'X-ray and Neutron Scattering'†	Bombannes, France	2014
Gordon Research Conference 'Bio-inspired Materials'★	Maine, USA	2014
Dutch Soft Matter Meeting†	Leiden	2014
Dutch Polymer Days	Lunteren	2015
European Colloid and Interface Society†	Bordeaux, France	2015
General		
Presentation Skills (WGS)	Wageningen	2013
Scientific Writing (WGS)	Wageningen	2013
Voice and Presentation Skills Training (WGS)	Wageningen	2014
Efficient Writing Strategies (WGS)	Wageningen	2014
Career Orientation (WGS)	Wageningen	2014

Optionals

Colloid Science	Wageningen	2012
Advanced Soft Matter	Wageningen	2012
PhD-trip California† †	USA	2013
PhD-trip UK† † ⋆	UK	2015
Group meetings and colloquia	Wageningen	2012–2016

Notes: †oral presentation, ⋆poster presentation

The research described in this thesis was financially supported by the European Research Council Advanced Grant Bio-Mate (ERC-267254)

Cover design by Ingeborg Storm

Printed by GVO drukkers & vormgevers B.V., Ede